

## EDITORIAL BOARD

### Editor-in-Chief

I.V. Krivtsun E.O. Paton Electric Welding Institute, Kyiv, Ukraine

### Deputy Editor-in-Chief

S.V. Akhonin E.O. Paton Electric Welding Institute, Kyiv, Ukraine

### Deputy Editor-in-Chief

L.M. Lobanov E.O. Paton Electric Welding Institute, Kyiv, Ukraine

### Editorial Board Members

O.M. Berdnikova	E.O. Paton Electric Welding Institute, Kyiv, Ukraine
Chang Yunlong	School of Materials Science and Engineering, Shenyang University of Technology, Shenyang, China
V.V. Dmitrik	NTUU «Kharkiv Polytechnic Institute», Kharkiv, Ukraine
Dong Chunlin	China-Ukraine Institute of Welding of Guangdong Academy of Sciences, Guangzhou, China
M. Gasik	Aalto University Foundation, Finland
A. Gumenyuk	Bundesanstalt für Materialforschung und –prüfung (BAM), Berlin, Germany
V.V. Knysh	E.O. Paton Electric Welding Institute, Kyiv, Ukraine
V.M. Korzhyk	E.O. Paton Electric Welding Institute, Kyiv, Ukraine
V.V. Kvasnytskyi	NTUU «Igor Sikorsky Kyiv Polytechnic Institute», Kyiv, Ukraine
Yu.M. Lankin	E.O. Paton Electric Welding Institute, Kyiv, Ukraine
S.Yu. Maksymov	E.O. Paton Electric Welding Institute, Kyiv, Ukraine
Yupiter HP Manurung	Smart Manufacturing Research Institute, Universiti Teknologi MARA, Shah Alam, Malaysia
M.O. Pashchin	E.O. Paton Electric Welding Institute, Kyiv, Ukraine
Ya. Pilarczyk	Welding Institute, Gliwice, Poland
V.D. Poznyakov	E.O. Paton Electric Welding Institute, Kyiv, Ukraine
U. Reisgen	Welding and Joining Institute, Aachen, Germany
I.O. Ryabtsev	E.O. Paton Electric Welding Institute, Kyiv, Ukraine
V.M. Uchanin	Karpenko Physico-Mechanical Institute, Lviv, Ukraine
Yang Yongqiang	South China University of Technology, Guangzhou, China
<b>Executive Director</b>	O.T. Zelnichenko, International Association «Welding», Kyiv, Ukraine

### Address of Editorial Board

E.O. Paton Electric Welding Institute, 11 Kazymyr Malevych Str., 03150, Kyiv, Ukraine  
Tel./Fax: (38044) 205 23 90, E-mail: [journal@paton.kiev.ua](mailto:journal@paton.kiev.ua)  
<https://patonpublishinghouse.com/eng/journals/tpwj>

**State Registration Certificate** 24933-14873 ПП from 13.08.2021

ISSN 0957-798X, DOI: <http://dx.doi.org/10.37434/tpwj>

**Subscriptions**, 12 issues per year:

\$384 — annual subscription for the printed (hard copy) version, air postage and packaging included;

\$312 — annual subscription for the electronic version (sending issues in pdf format or providing access to IP addresses).

### Representative Office of «The Paton Welding Journal» in China:

China-Ukraine Institute of Welding, Guangdong Academy of Sciences

Address: Room 210, No. 363 Changxing Road, Tianhe, Guangzhou, 510650, China.

Zhang Yupeng, Tel: +86-20-61086791, E-mail: [patonjournal@gwi.gd.cn](mailto:patonjournal@gwi.gd.cn)

The content of the journal includes articles received from authors from around the world in the field of welding, metallurgy, material science and selectively includes translations into English of articles from the following journals, published in Ukrainian:

- Automatic Welding (<https://patonpublishinghouse.com/eng/journals/as>);
- Electrometallurgy Today (<https://patonpublishinghouse.com/eng/journals/sem>);
- Technical Diagnostics & Nondestructive Testing (<https://patonpublishinghouse.com/eng/journals/tdnk>).

## CONTENTS

### ORIGINAL ARTICLES

<b>O.A. Gaivoronskyi, V.D. Poznyakov, A.V. Zavdoveyev, A.V. Klapatyuk, A.M. Denysenko</b> PREVENTION OF COLD CRACKING IN ARMOUR STEEL WELDING* .....	3
<b>I.O. Ryabtsev, A.A. Babinets, M.O. Pashchyn, O.M. Syzonenko, I.O. Lentugov, I.I. Ryabtsev, T.G. Solomiichuk, A.S. Torpakov</b> INFLUENCE OF DIFFERENT TYPES OF MODIFIERS ON THE STRUCTURE AND PROPERTIES OF DEPOSITED METAL OF THE TYPE OF 25KH5MFS TOOL STEEL* .....	11
<b>L.I. Nyrkova, L.V. Goncharenko</b> ANALYSIS OF CAUSES OF FAILURE OF FIELD WELDED BUTT JOINTS OF MAIN PIPELINES AFTER LONG-TERM OPERATION* .....	15
<b>A.R. Gavryk, A.K. Tsaryuk, I.G. Osypenko, O.V. Lynnyk, O.V. Vavilov, O.G. Kantor</b> TECHNOLOGY OF MIG WELDING OF CHROMIUM STEEL OF MARTENSITIC GRADE CA-6NM* .....	22
<b>Yu.V. Orsa, V.M. Nesterenkov, V.I. Zagornikov, M.O. Rusynyk</b> USE OF ELECTRON BEAM WELDING FOR MANUFACTURE OF BLADE PACKAGES FOR COGENERATION STEAM TURBINES* .....	29
<b>O.M. Sabadash, S.V. Maksymova</b> FLUXLESS BRAZING OF ALUMINIUM ALLOYS BY BRAZING FILLER METAL of Al-Ge SYSTEM* .....	35
<b>Yu.O. Nykytenko, V.O. Shapovalov, V.V. Yakusha, O.M. Gnizdylo, O.V. Karuskevych</b> 3D TECHNOLOGY OF GROWING SINGLE-CRYSTAL INGOTS IN THE FORM OF HOLLOW TUNGSTEN CYLINDERS** .....	42
<b>V.N. Uchanin, G.G. Lutcenko, A.V. Opanasenko</b> AUTOMATED EDDY CURRENT INSPECTION SYSTEMS WITH SURFACE PROBE OF DOUBLE DIFFERENTIAL TYPE*** .....	48

\*Translated Article(s) from "Automatic Welding", No. 4, 2023.

\*\*Translated Article(s) from "Electrometallurgy Today", No. 2, 2023.

\*\*\*Translated Article(s) from "Technical Diagnostics & Nondestructive Testing", No. 2, 2023.

DOI: <https://doi.org/10.37434/tpwj2023.05.01>

# PREVENTION OF COLD CRACKING IN ARMOUR STEEL WELDING

**O.A. Gaivoronskyi, V.D. Poznyakov, A.V. Zavdoveyev, A.V. Klapatyuk, A.M. Denysenko**

E.O. Paton Electric Welding Institute of the NASU

11 Kazymyr Malevych Str., 03150, Kyiv, Ukraine

## ABSTRACT

The work presents the results of investigations of cold cracking susceptibility of welded joints on modern high hardness armour steels and gives recommendations on their prevention. Investigations were performed using a calculation method according to EN 1011-2:2001 — the Implant method to determine the delayed fracture resistance of the HAZ metal and rigid technological test in welding multilayer joints. It is found that in arc welding the joints of high hardness armour steels have a higher susceptibility to cold cracking in the HAZ metal. In welding with low-alloyed consumable of Sv-10GSMT type application of preheating allows avoiding them. The preheating temperature can be calculated by CET and PT indices in keeping with the armour steel composition. In the presence of steel raisers in the welded joints the calculated preheating temperature should be increased by 50–70 °C. The welded joints made with high-alloyed consumable of Sv-08Kh20N9G7T type have higher delayed fracture and cold cracking resistance. In manufacture of light armoured vehicles, it is recommended to select armour steel with carbon content of not more than 0.26 %. In welding such armour steel by low-alloyed consumables sufficiently high cold cracking resistance of welded joints is ensured, even in the presence of stress raisers, due to preheating up to the temperature of 150 °C, as well as in welding without preheating at application of high-alloyed consumables.

**KEYWORDS:** armour steel, high hardness steel, arc welding, welded joints, HAZ metal, cold cracks

## INTRODUCTION

In selection of high-strength alloyed steel for welded structure fabrication one of the important factors is its weldability, alongside a complex of mechanical and special properties. Weldability is understood as the possibility of producing high-quality joints, which satisfy the requirements to technological and service properties of the structure. Therefore, at development of technologies of welding such structures, it is first of all necessary to have sufficient information on the weldability of the steel, which determines the respective selection of the welding consumables and welding technology parameters. It is also known that the main problem in welding high-strength alloyed steels is prevention of cold cracking in the welded joints [1–4].

Formation and development of cold cracks in the welded joints depends on the structural-phase composition of metal in the HAZ and in the weld, content of diffusion-mobile hydrogen in the deposited metal and stress level in the welded joints. Here, the cracking susceptibility of the welded joints becomes higher with increase of the content of carbon and such alloying elements as nickel, chromium, manganese, molybdenum and vanadium in steel. The mechanism of cold crack initiation and development in the welded joints is of a delayed nature. It is usually explained by Zener–Stroh classical model, according to which microcrack initiation in a metal hardened structure takes place along the grain boundaries in the areas of dislocation accumulation. Further crack propaga-

tion, depending on the state of the metal structure and stress level, occurs both along the boundaries and through the body of the grains. Hydrogen, with which the HAZ metal is saturated during welding, promotes an increase in the level of the structure brittleness, and the destruction process runs more intensively [5–7].

Modern high hardness armour steels ( $HB \geq 5000$  MPa), which are used in manufacture of lightly armoured vehicles, belong to high-strength medium-carbon alloyed steels by the content of carbon and alloying elements (Table 1). It is known that the welded joints of this class of steels have an increased cold cracking susceptibility exactly in the HAZ metal. In welding such steels by low-alloyed consumables to prevent cold cracking, preheating with the temperature of up to 250 °C and thermal tempering of the welded joints after welding are usually performed. In welding by high-alloyed consumables no preheating is required. Here, selection of the technological solutions depends on a specific type of the welded structure and its purpose.

The objective of this work was a comprehensive comparative evaluation of the susceptibility of modern high hardness armour steels to cold cracking and issuing recommendations on their prevention.

## MATERIALS AND METHODS OF INVESTIGATION

High hardness armour steels of local and foreign production were used in investigations. Their chemical composition is given in Table 2.

**Table 1.** Chemical composition of modern high hardness armour steels

Armour steel	Weight fraction of elements, %												
	C	Si	Mn	Cr	Ni	Mo	Cu	V	Al	Ti	S	P	B
Grade 71 (Ukraine)	0.29– 0.36	1.20– 1.50	0.60– 1.0	1.50– 2.0	2.0– 2.40	0.45– 0.55	≤0.30	0.18– 0.25	0.015– 0.050	0.005– 0.025	≤0.003	≤0.012	–
Foreign steels	Specified maximum element content, %												
ARMSTAL 500 (Poland)	0.32	0.50	1.20	0.90	1.10	0.30	0.090	–	–	–	–	–	–
HB 500 MOD (Belgium)	0.30	0.80	1.60	1.0	1.0	0.50	0.023	–	–	–	0.010	0.025	0.005
Protection 500 (Finland)	0.30	0.70	1.70	1.5	0.80	0.50	0.026	0.020	–	–	0.015	0.030	0.004
ARMOX 500 (Sweden)	0.32	0.40	1.20	1.0	1.80	0.70	–	–	–	–	0.003	0.010	0.005
RAMOR 500 (Finland)	0.35	0.70	1.50	1.0	2.0	0.70	–	–	–	–	0.010	0.015	0.005

Weldability of steels was first evaluated by calculation methods by  $P_{CM}$  and CET values. In keeping with the recommendations of [1, 8] these values were calculated as follows:

$$P_{CM} = C + Si/30 + (Mn + Cr + Cu)/20 + Ni/60 + Mo/15 + V/10 + 5B, \% [1];$$

$$CET = C + (Mn + Mo)/10 + (Cr + Cu)/20 + Ni/40, \% [8].$$

Further on CET value and quantity of diffusible hydrogen in the weld metal were used to determine the preheating temperature, at which no cracks form in the welded joints:

$$PT = 697 \times CET + 160 \times \tanh(d/35) + 62 \times HD \times 0.35 + (53 \times CET - 32) \times Q - 328, \text{ }^\circ\text{C} [8],$$

where  $d$  is the metal thickness, mm;  $HD$  is the quantity of diffusible hydrogen in the deposited metal (determined by chromatographic method),  $\text{cm}^3/100 \text{ g}$ ;  $Q$  is the welding heat input,  $\text{kJ/mm}$ .

For quantitative evaluation of cold crack formation in the welded joints of armour steels, a recognized Implant method was used at HAZ metal testing for delayed fracture resistance [9, 10]. Samples-in-serts from the studied steel of 6.0 mm diameter with

and without a screw notch as a stress raiser were tested. Samples were inserted into a technological plate from high-strength steel, on which surfacing was performed. After metal cooling to the temperature of 30–50  $^\circ\text{C}$ , the samples were loaded by a constant force at axial tension. The results of these tests were used to determine the critical stresses ( $\sigma_{cr}$ ) and preheating temperature, at which sample failure did or did not occur within 24 hours. Maximal critical stresses, at which no delayed fracture occurred anymore under the defined welding conditions, was taken as the quantitative index of the cold cracking susceptibility of the HAZ metal.

Samples for the Implant method were welded by a mechanized process in the atmosphere of a mixture of shielding gases (82 % Ar + 18 %  $\text{CO}_2$ ) by high-alloyed and low-alloyed wires of the respective Sv-08Kh20N9G7T and Sv-10GSMT grades of 1.2 mm diameter. Welding was performed at the heat input of 8.6–9.0  $\text{kJ/cm}$ , the welding modes were as follows: welding current of 160–180 A, arc voltage of 26–28 V, welding speed of 12–15  $\text{m/h}$ .

For sound detection of cold cracks in welded joints of armour steels, the method of “rigid boxing”

**Table 2.** Chemical composition of the studied high hardness armour steels

Armour steel	Weight fraction of elements, %												
	C	Si	Mn	Cr	Ni	Mo	Cu	V	Al	Ti	S	P	B
Grade 71	0.31	1.16	0.74	1.66	2.26	0.30	0.080	0.202	0.040	0.024	0.010	0.016	–
ARMSTAL 500	0.29	0.24	0.89	0.74	1.03	0.23	0.090	0.060	0.019	0.037	0.005	0.009	0.002
HB 500 MOD	0.26	0.21	0.78	0.42	0.74	0.27	0.023	0.001	0.033	0.004	0.006	0.012	0.001
Protection 500	0.28	0.49	0.96	0.58	0.37	0.25	0.026	0.002	0.028	0.029	0.011	0.016	0.002
ARMOX 500	0.23	0.25	0.84	0.50	0.97	0.33	0.030	0.001	0.023	0.021	0.003	0.010	0.002
RAMOR 500	0.21	0.45	0.92	0.58	0.38	0.20	0.010	0.002	0.027	0.015	0.005	0.023	0.002

of a technological sample was used [11]. Control joints, which were first mounted on a rigid plate of 50–60 mm thickness and welded around the contour on it, had a stress raiser in the form of a blunting of up to 4 mm to produce a lack-of-penetration. The joints were welded by the same method, welding consumables and in the modes as at sample testing by the Implant method. Acoustic emission method was used for registering the moment of cold crack initiation and propagation during cooling of the control welded joints. After welding the samples were kept for three days, which was followed by cutting templates out of the control joints with their further visual examination to detect cracks.

### INVESTIGATION RESULTS AND THEIR DISCUSSION

The calculated estimate of weldability of high hardness armour steels which was determined by the preheating temperature (PT) to eliminate the probability of cold cracking in the joints, was performed on the base of analysis of the data on their chemical composition. Calculations were performed both for the maximal composition, declared in the normative documents (specifications, manufacturer's price-lists), and for the actual chemical composition of armour steels, which were provided for investigations. Results of calculation of  $P_{CM}$ , CET and PT values in armour steel welding by ferrite-pearlite materials, at which no cold cracks form in the welded joints, are given in Table 3. Here, it was taken into account that welding of the joints is performed on the thickness of 10 mm at the heat input of  $Q_w = 10$  kJ/cm, which is typical for armoured structures. Diffusible hydrogen content in the deposited metal was specified in the range of  $[H]_{dif} = 3\text{--}5$  cm<sup>3</sup>/100 g, the presence of which is typical in welding with low-alloyed wires.

Thus, it was previously determined that high hardness armour steels are characterized by poorer weld-

ability. At calculations by the maximal chemical composition,  $P_{CM}$  and CET values are higher than 0.50 and 0.54 %, respectively, which results in equally difficult conditions for welding all the steels to eliminate the probability of cold cracking in the welded joints. The temperature of their preheating in welding should be equal from 185 to 310 °C, depending on the steel and diffusible hydrogen content. This value is the highest for steel of grade 71, and the smallest for ARMSTAL 500 steel. It should be taken into account that the heating temperature of 230 °C corresponds to that of low-temperature tempering at armour steel hardening, exceeding which can lead to lowering of its hardness.

The  $P_{CM}$ , CET and PT values for actual chemical composition differ from those, which are characteristic for the maximal composition. They are significantly lower, particularly for foreign steels. They remain the highest for steel of grade 71, and the lowest for RAMOR 500 steel. Preheating temperature for steel of grade 71 decreases to 195–210 °C, and for RAMOR 500 steel, it does not exceed 80 °C. An essential lowering of PT values by more than 2 times is also characteristic for *HB 500 MOD*, *PROTECTION 500* and *ARMOX 500* steels. This is attributable to the fact that the actual chemical composition of armour foreign steels, which were studied, is lower than the declared one, as they are sparsely-alloyed. Here, the steels have sufficiently high hardness ( $HB \geq 5000$  MPa), which is achieved at application of special heat treatment methods. Lowering of the steel alloying level, from the viewpoint of improvement of their weldability is positive leverage. When welding the joints, however, it may lead to a significant lowering of armour steel hardness in the tempering zone of the HAZ metal.

The following stage of investigations was Implant testing of samples, in which the stress raiser was absent. It was established, first of all that in welding without preheating of the studied armour steels

**Table 3.** Calculated values of preheating temperature in welding of high hardness armour steels 10 mm thick

Armour steel	Steel chemical composition	$P_{CM}$ , %	CET, %	Preheating, PT, °C	
				3 cm <sup>3</sup> /100 g	5 cm <sup>3</sup> /100 g
Grade 71	Maximal	0.67	0.69	300	310
	Actual	0.55	0.56	195	210
ARMSTAL 500	Maximal	0.50	0.54	185	200
	Actual	0.43	0.47	130	150
<i>HB 500 MOD</i>	Maximal	0.53	0.59	235	255
	Actual	0.36	0.41	85	105
Protection 500	Maximal	0.55	0.61	240	260
	Actual	0.41	0.44	110	125
ARMOX 500	Maximal	0.55	0.61	240	260
	Actual	0.35	0.40	80	100
RAMOR 500	Maximal	0.60	0.65	280	290
	Actual	0.33	0.34	60	80

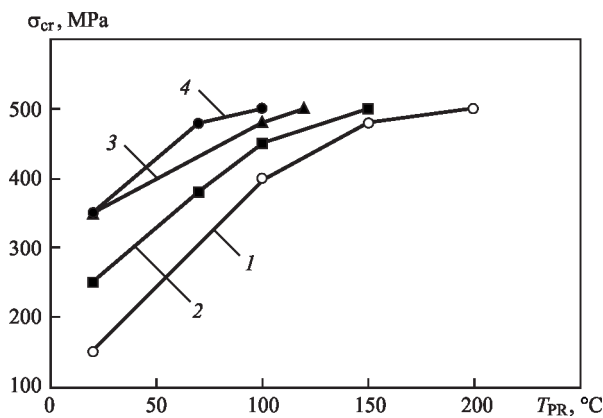


**Figure 1.** Delayed fracture resistance of armour steel HAZ metal in welding by Sv-10GSM wire (samples without stress raiser): 1 — steel of grade 71; 2 — ARMSTAL 500; 3 — Protection 500; 4 — HB 500 MOD

by high-alloyed wire of Sv-08Kh20N9G7T type no delayed fracture of the samples is observed, even at loads with up to 500 MPa stress level. At loads, when the stresses were higher than 500 MPa, the plastic deformation processes in the high-alloyed deposited metal became more active. It resulted in mechanical destruction exclusively through it. The rather high delayed fracture resistance of the HAZ metal in armour steel welding by high-alloyed wire is attributable to formation of predominantly tempering martensite in the hardening area, in which the dislocation density and structural stresses are practically 2 times lower than in welding with low-alloyed consumables [12, 13]. Therefore, at external loading such HAZ metal is more prone to microplastic deformation without microcrack formation.

Considering the obtained data in welding with high-alloyed wire, a stress of 500 MPa level was conditionally taken as the criterion, which should be reached in welding samples by low-alloyed wire due to preheating application. The generalized results of delayed fracture resistance testing of the HAZ metal of armour steel joints in welding with wire of Sv-10GSMT type, in the case of a dependences of critical breaking stresses on preheating temperature ( $T_{pr}$ ) are presented in Figure 1.

Critical breaking stresses in welding without preheating, which depending on the steel grade are equal to 150–350 MPa, are several times lower than the yield point of armour steel ( $\sigma_{0.2} \geq 1250$  MPa). The time of development of the delayed fracture process at sample loading with the stress level of 500 MPa is quite fast and it is equal to not more than 1–3 min. Preheating application promotes increase of delayed fracture resistance of the HAZ metal, which is related to formation of more ductile structures in the HAZ metal. Microcrack initiation and propagation time is significantly increased. So, for instance, in welding steel of grade 71 at preheating at the temperature of 100 °C, the time to fracture of the samples at such a loading level was equal to 1.5–2 h, at 150 °C it was already 4–6 h, and at 200 °C no delayed fracture of the samples was observed for 24 h.

Figure 2 shows typical surfaces of sample fracture through the HAZ metal in the case of armour steel of grade 71. As shown by special fractographic studies of the fracture surfaces, in welding without preheating, sample destruction during microcrack initiation and propagation occurs predominantly in the brittle mode by the boundaries and in the grain body (Figure 2, *a*). The ratio of brittle intergranular and intragranular fractures is equal to approximately 4/1. At application of preheating, the critical stresses are gradually increased. So, at preheating at the temperature of 100 °C the fraction of brittle intergranular fracture decreases to 30 % (Figure 2, *b*). At preheating at the temperature of 150 °C, the fracture can be characterized as a predominantly intragranular one with a small fraction of ductile fracture (Figure 2, *c*).

If we compare the data given in Table 3 and in Figure 1, one can see that the preheating temperature at sample testing, at which the critical stresses are equal to 500 MPa, is close to the calculated values for the mentioned steels at diffusible hydrogen content at the level of 3 cm<sup>3</sup>/100 g. Such a level of diffusible hydrogen is ensured in welding in a shielding gas mixture. Comparative studies showed that the preheating tem-

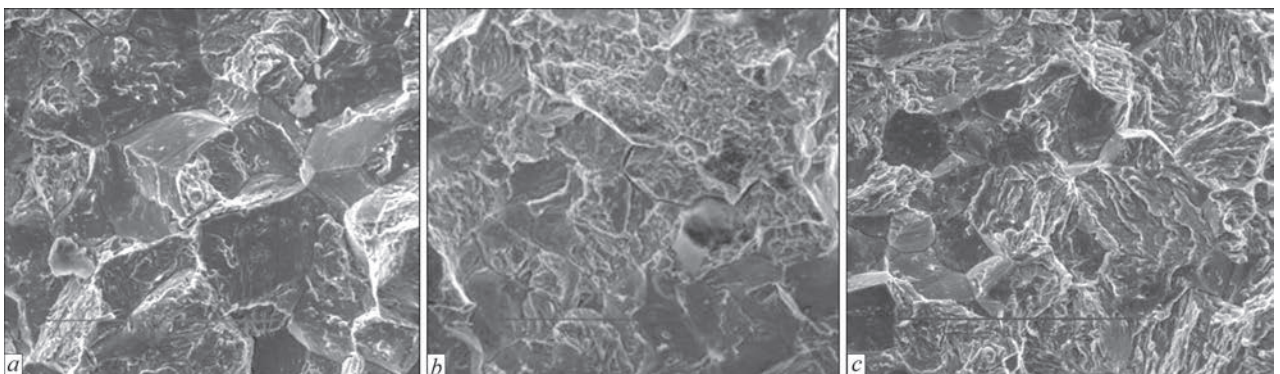


**Figure 2.** Characteristic fractures at delayed fracture of HAZ metal of steel 71 in welding with Sv-10GSMT wire ( $\times 800$ ): *a* —  $T_{pr} = 20$  °C; *b* — 100; *c* — 150

perature, at which according to calculated data cold cracks are absent in the welded joints, and according to Implant sample tests no delayed fracture takes place in the HAZ metal, for armour steel of grade 71 it is equal to 195 and 200 °C, for SMSTAL 500 steel — to 135 and 150 °C, for PROTECTION 500 — to 110 and 120 °C, for *HB* 500 MOD — to 85 and 100 °C, respectively. Thus, in welding joints of armour steels without any stress raisers, in order to eliminate the probability of cold crack formation in the welded joints, their preheating temperature can be determined by the calculation method by CET and PT indices.

It should be noted, however, that the presence of stress raisers in the welded joint can be incorporated in the design, if the joint is made without full penetration. These, for instance, can be fillet or overlap joints (DSTU EN ISO 9692-1). Stress raisers can also form in full penetration joints at violation of the welding technique or modes, when such individual defects as lack-of-penetration, lack-of-fusion, undercuts, etc. develop, as well as those, which could not be detected and removed promptly after welding. That is why Implant tests of the samples with a geometrical stress raiser were conducted. The generalized results of these tests are shown in Figure 3.

If we compare the data in Figure 1 and Figure 3, one can see that in welding Implant samples of armour steels with a geometrical stress raiser the processes of delayed fracture of the HAZ metal run more actively. In welding without preheating the critical stresses, which lead to delayed fracture, decrease to 50–150 MPa. Here, in order to each critical stresses at 500 MPa level, it is necessary to apply preheating at higher temperatures. So, for steel of grade 71 of the actual chemical composition the preheating temperature should already be not 200, but 250 °C, for steel of grade ARMSTAL 500 — not 150, but 200 °C, for PROTECTION 500 — not 120, but 180 °C, respectively. The same tendency of preheating temperature increase in the presence of a stress raiser is also characteristic for other armour steels. This is related to the fact that the stress raisers in armour steel welded joints significantly accelerate initiation and propagation of cracks in the HAZ metal. Therefore, in case of welding joints without complete penetration the calculated preheating temperature should be increased. As shown by Implant testing the preheating temperature of the welded joints should be increased approximately by 50–70 °C, compared to the calculated one, and the defects present in the welded joints must be detected and removed.

It should be also noted that at testing Implant samples with a geometrical stress raiser, which were welded by high-alloyed Sv-08Kh20N9G7T wire without preheating, a lowering of the level of critical

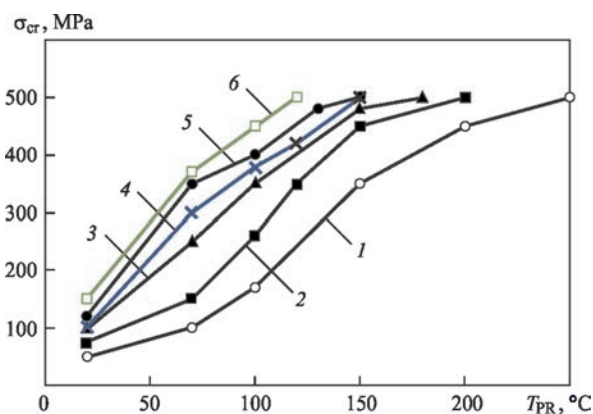


**Figure 3.** Delayed fracture resistance of armour steel HAZ metal in welding by Sv-10GSM wire (samples with a stress raiser): 1 — steel of grade 71; 2 — ARMSTAL 500; 3 — PROTECTION 500; 4 — *HB* 500 MOD; 5 — ARMOX 500; 6 — RAMOR 500

stresses of delayed fracture in the HAZ metal was also observed (Figure 4).

The above-given data show that the stress raiser has a significant influence on development of delayed fracture processes in the HAZ metal of armour steel joints, even at application of high-alloyed welding consumables. While no delayed fracture took place at testing of samples of all the mentioned steels without a geometrical concentrator, in its presence they already proceed actively. So, critical stresses, at which fracture is absent, for steel 71 decrease to 200 MPa, and for ARMSTAL 500, ARMOX 500 and PROTECTION 500 steels to 300–350 MPa. With this testing variant *HB* 500 MOD and RAMOR 500 steels were also tested. The critical stresses for them were higher and were equal to 400–450 MPa. For foreign armour steels of the specified composition, this is a rather high level of critical stresses, above 300 MPa, which can be sufficient for avoiding cold cracking in the root part of the welded joints in welding multilayer joints. It cannot be stated for steel of grade 71. Therefore, it was nec-

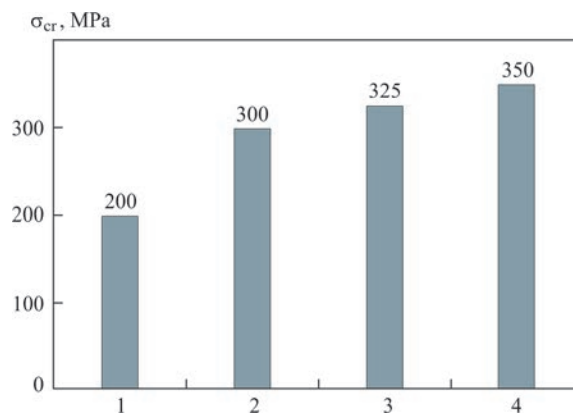


**Figure 4.** Influence of stress concentration on delayed fracture resistance of armour steel HAZ metal in welding by Sv-08Kh20N9G7T wire without preheating: 1 — steel of grade 71; 2 — ARMSTAL 500; 3 — ARMOX 500; 4 — PROTECTION 500

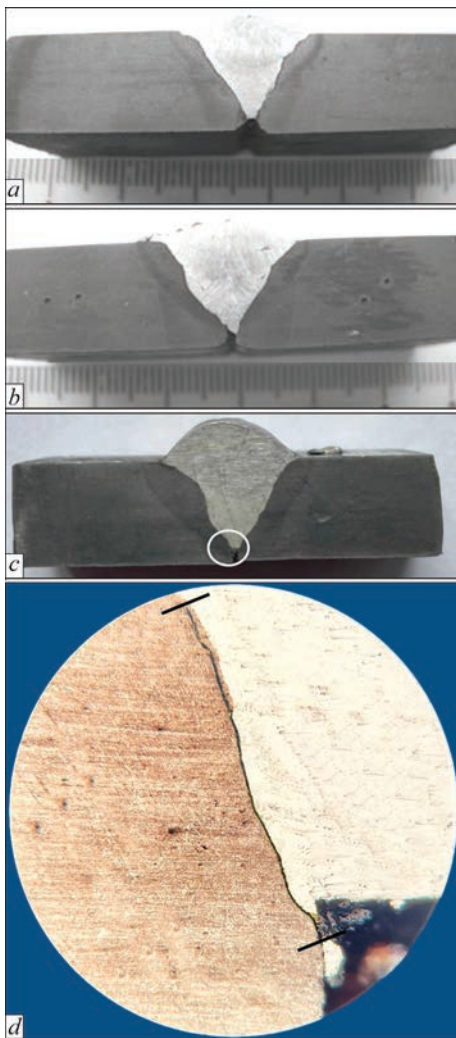


**Figure 5.** Macrosections of welded joints of “rigid boxing” technological samples of 10–12 mm armour steels made by Sv-08Kh20NG7T wire without preheating: *a* — HB 500 MOD; *b* — PROTECTION 500; *c* — grade 71; *d* — microcrack in the HAZ of the joint of grade 71 steel ( $\times 100$ )

essary to conduct additional studies with application of technological samples.

Making of “rigid boxing” technological samples confirms the conclusions based on the results of Implant tests. No cold cracks form in the joints in welding armour steels of the above-mentioned chemical

**Table 4.** Cold cracks in control joints of 10–12 mm armour steels in welding technological samples by Sv-10GSMT wire

Armour steel	Preheating temperature ( $T_{pr}$ ), °C				
	20	100	150	200	250
Grade 71	Yes	Yes	Yes	Yes	No
ARMSTAL 500	—>—	—>—	—>—	No	—
HB 500 MOD	—>—	—>—	No	—	—
PROTECTION 500	—>—	—>—	Yes	No	—
ARMOX 500	—>—	—>—	No	—	—
RAMOR 500	—>—	No	—	—	—

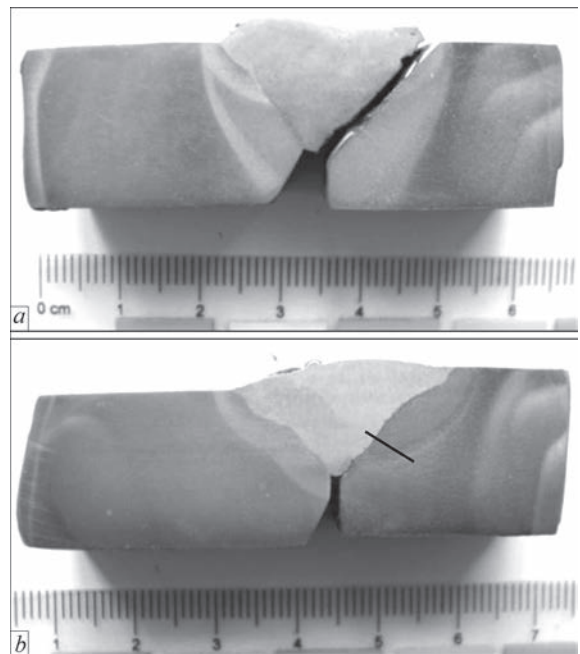


**Figure 6.** Cold cracks in welded joints of armour steel of grade 71 in welding by Sv-10GSMT wire: *a* — welding without preheating; *b* —  $T_{pr} = 150\text{ }^{\circ}\text{C}$

composition of foreign grades without preheating at application of high-alloyed Sv-08Kh20N9G7T wire (Figure 5, *a, b*). In welding armour steel of grade 71 no cold cracks were visually observed in the welded joint, either, at regular examination. However, after special etching of some sections and image magnification microcracks of up to 0.5 mm depth were detected. These are so-called “tears”, which formed in the joint HAZ in the stress raiser area (Figure 5, *d*). These cracks did not propagate any further, which is attributable to stress relaxation at crack formation and high enough ductile properties of the metal of the joint HAZ, which formed at application of a high-alloyed welding consumable. This, however, does not exclude the possibility of their development at external loads during the product service. In other cases, no such microcracks were revealed in welding foreign armour steels of the specified chemical composition. Still, however, welding of joints by a high-alloyed consumable without preheating of the local armour steel of grade 71 and foreign armour steels, which are close by carbon content to the composition of steel of grade 71, should be performed with full penetration.

Contrarily, in welding with Sv-10GSMT wire cold cracks actively propagate in the HAZ metal in the welded joints. Cold cracking in welded joints at this welding variant can only be avoided under the conditions, when the preheating temperature is from 100 up to 250 °C, depending on the steel grade. Table 4 gives the general results of welding the technological samples by Sv-10GSMT wire, and Figures 6, 7 show the typical microsections of welded joints.

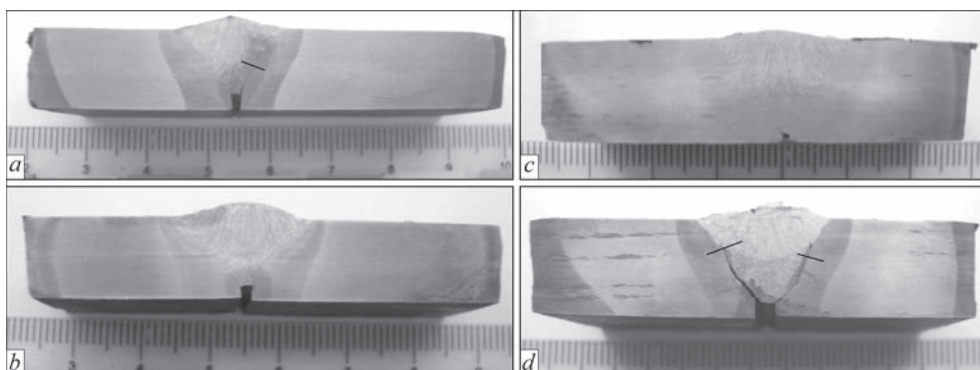


**Figure 7.** Macrosections of welded joints of foreign armour steels in welding by Sv-10GSMT wire: *a* — *HB 500 MOD* without preheating, cold cracks in the HAZ; *b* — *HB 500 MOD*,  $T_{pr} = 150\text{ }^{\circ}\text{C}$ ; no cracks; *c* — *PROTECTION 500*,  $T_{pr} = 200\text{ }^{\circ}\text{C}$ , no cracks; *d* — *ARMSTAL 500*,  $T_{pr} = 100\text{ }^{\circ}\text{C}$ , cold cracks in the HAZ

Initiation and propagation of cold cracks can be different, depending on the steel composition, which was determined by the acoustic emission method. So, in welding of armour steels of grades 71 and ARMSTAL 500 without preheating cold cracks intensively form already directly after welding of the first layer of the weld is over. The time of their development is up to one minute. In welding *HB 500 MOD*, *PROTECTION 500*, *ARMOX 500* and *RAMOR 500* steels cold cracks propagate slower in the HAZ metal of the joints, during 10 to 30 min. At application of preheating the destruction processes are decelerated, and at the temperature of  $150\text{ }^{\circ}\text{C}$ , the time of crack initiation and propagation in the welded joints of steels of grades 71 and ARMSTAL 500 is already equal to approximately one hour. This is attributable to the fact that at preheating the cooling rate decreases and the HAZ metal forms structures with a lower degree of hardening, the metal becomes more ductile and much more time is required for its destruction. It should be noted that obtained values of preheating temperature in welding control joints of “rigid boxing” technological samples, in which a lack-of-penetration was incorporated, and those derived by the results of testing samples with the geometrical stress raiser by the Implant method practically coincide.

One can also see from the results of investigations that the cold cracking susceptibility of welded joints of high hardness armour steels and value of preheating temperature for their prevention essentially depend on the steel chemical composition, namely carbon content. So, among the armour steels of the specified composition, considered by us, the highest carbon content, at the level of 0.28–0.30 % is found in steels of grades ARMSTAL 500, PROTECTION 500 and 71. Therefore, preheating temperature of the joints in their welding with low-alloyed consumables should be equal to  $200\text{--}250\text{ }^{\circ}\text{C}$ , respectively. In welding joints of steels of grades RAMOR 500, ARMOX 500 and *HB 500 MOD*, in which the carbon content

is on the level of 0.21–0.26 %, the preheating temperature is equal to  $100\text{--}150\text{ }^{\circ}\text{C}$ , respectively. If foreign armour steels are made with maximum admissible carbon content, i.e. increased to 0.30–0.35 %, as it is declared by the manufacturers’ specifications, then from the viewpoint of ensuring the cold cracking resistance of the welded joints it will be necessary to increase their preheating temperature to  $250\text{ }^{\circ}\text{C}$ , and higher. Here, it should be noted that this preheating temperature is higher than that of low-temperature tempering of the steel during its production, and it will certainly lead to lowering of armour steel hardness in the welded joint area. As a result, it will have a negative impact on the performance of products as a whole, which is unacceptable. Therefore, it is rational to limit the carbon content in armour steels to a level not higher than 0.26 %.

## CONCLUSIONS

1. In arc welding by low-alloyed consumables of Sv-10GSMT type, the joints of high hardness armour steels have a higher susceptibility to cold cracking in the HAZ metal. Application of preheating allows preventing them. Preheating temperature, at which no cold cracks initiate in the welded joints, can be calculated by CET and PT values, in keeping with the chemical composition of the armour steel. In the presence of incorporated stress raisers in the welded joints, the calculated preheating temperature should be increased by  $50\text{--}70\text{ }^{\circ}\text{C}$ .

2. Welded joints of high hardness armour steels of the studied composition were made by high-alloyed consumable of Sv-08Kh20N9G7T type. As a result of formation of more ductile hardening structures in the HAZ metal they have higher delayed fracture and cold cracking resistance. Presence of stress raisers in welding foreign armour steels activates the delayed fracture processes, but critical breaking stresses are rather high, more than 300 MPa. As a result, no microcracks in the HAZ metal or cold cracks in the joints

are formed. That is why, the joints of these steels can be welded without preheating by high-alloyed consumables, even in the presence of stress raisers.

3. In welded joints of local armour steel of grade 71 with carbon content of 0.31 % made by a high-alloyed consumable without preheating, presence of stress raisers significantly accelerates the delayed fracture processes, and microcracks form in the HAZ metal. Furtheron, these microcracks do not develop into a main cold crack. It is attributable to stress relaxation during their formation and sufficiently high ductile properties of the metal to hinder their propagation. This, however, does not exclude the possibility of their propagation at external loads during the product service. Therefore, it is rational to weld joints of armour steel of grade 71 by high-alloyed consumables with full penetration.

4. At selection of high hardness steel in manufacture of lightly-armoured vehicles preference should be given to steel with not more than 0.26 % carbon content. In welding such armour steel by low-alloyed consumables sufficiently high cold cracking resistance of the welded joints is ensured even in the presence of stress raisers, due to preheating up to the temperature of 150 °C, as well as in welding without preheating at application of high-alloyed consumables.

## REFERENCES

1. Makarov, E.L. (1981) *Cold cracks in welding of alloyed steels*. Moscow, Mashinostroenie [in Russian].
2. Efimenko, M.G., Radzivilova, N.O. (2003) *Physical metallurgy and heat treatment of welded joints*. Kharkiv, Kharkivska Drukarnya No. 16 [in Ukrainian].
3. Skulsky, V.Yu. (2009) Peculiarities of kinetics of delayed fracture of welded joints of hardening steels. *The Paton Welding J.*, **7**, 12–17.
4. Günen, A., Bayar, S., Karakaş, M.S. (2020) Effect of different arc welding processes on the metallurgical and mechanical properties of Ramor 500 armor steel. *J. of Engineering Materials and Technology*, **142**, 2.
5. Pokhodnya, I.K., Shvachko, I.V. (1997) Physical nature of hydrogen induced cold cracks in welded joints of structural steels. *Avtomatich. Svarka*, **5**, 3–12 [in Russian].
6. Gajvoronsky, A.A. (2013) Influence of diffusible hydrogen on delayed cracking resistance of high-carbon steel welded joints. *The Paton Welding J.*, **5**, 14–20.
7. Magudeeswaran, G., Balasubramanian, V., Reddy, G.M. (2008) Hydrogen induced cold cracking studies on armour grade high strength, quenched and tempered steel weldments. *Int. J. of Hydrogen Energy*, **33**(7), 1897–1908.
8. EN 1011-2:2001: *Recommendations for welding of metallic materials*.
9. Suzuki, H. (1980) *Cold Cracking and its Prevention in Steel Welding (III)*. DOC IIW IX-1157–80.
10. Magudeeswaran, G., Balasubramanian, V., Madhusudhan Reddy, G. (2008) Effect of welding consumables on hydrogen induced cracking of armour grade quenched and tempered steel welds. *Ironmaking & Steelmaking*, **33**(7), 549–560.
11. Poznyakov V.D., Shelyagin V.D., Zhdanov S.L. et al. (2015) Laser-arc welding of high-strength steels with yield strength of more than 700 MPa. *The Paton Welding*, **10**, 19–24.
12. Gaivoronskyi O.A., Poznyakov V.D., Berdnikova O.M. et al. (2020) Influence of low-temperature tempering on structure and properties of welded joints of high-strength steel 30Kh2N2MF. *The Paton Welding*, **6**, 20–26. DOI: <https://doi.org/10.37434/tpwj2020.06.04>
13. Magudeeswaran, G., Balasubramanian, V., Reddy, G.M. (2018) Metallurgical characteristics of armour steel welded joints used for combat vehicle construction. *Defence Technology*, **14**(5), 590–606.

## ORCID

O.A. Gaivoronskyi: 0000-0002-5922-5541,  
V.D. Poznyakov: 0000-0001-8581-3526,  
A.V. Zavdoveyev: 0000-0003-2811-0765,  
A.V. Klapatyuk: 0000-0002-8170-5322

## CONFLICT OF INTEREST

The Authors declare no conflict of interest

## CORRESPONDING AUTHOR

O.A. Gaivoronskyi  
E.O. Paton Electric Welding Institute of the NASU  
11 Kazymyr Malevych Str., 03150, Kyiv, Ukraine.  
E-mail: [paton39@ukr.net](mailto:paton39@ukr.net)

## SUGGESTED CITATION

O.A. Gaivoronskyi, V.D. Poznyakov,  
A.V. Zavdoveyev, A.V. Klapatyuk, A.M. Denysenko  
(2023) Prevention of cold cracking in armour steel  
welding. *The Paton Welding J.*, **5**, 3–10.

## JOURNAL HOME PAGE

<https://patonpublishinghouse.com/eng/journals/tpwj>

Received: 25.04.2023

Accepted: 29.06.2023

DOI: <https://doi.org/10.37434/tpwj2023.05.02>

# INFLUENCE OF DIFFERENT TYPES OF MODIFIERS ON THE STRUCTURE AND PROPERTIES OF DEPOSITED METAL OF THE TYPE OF 25Kh5MFS TOOL STEEL

I.O. Ryabtsev<sup>1</sup>, A.A. Babinets<sup>1</sup>, M.O. Pashchyn<sup>1</sup>, O.M. Syzonenko<sup>2</sup>, I.O. Lentugov<sup>1</sup>, I.I. Ryabtsev<sup>1</sup>, T.G. Solomiichuk<sup>1</sup>, A.S. Torpakov<sup>2</sup>

<sup>1</sup>E.O. Paton Electric Welding Institute of the NASU  
11 Kazymyr Malevych Str., 03150, Kyiv, Ukraine

<sup>2</sup>Institute of Pulse Processes and Technologies of the NASU  
43, a Bohoyavlenskyi Prosp., 54018, Mykolayiv, Ukraine

## ABSTRACT

Comparative analysis of the influence of modifying additives of boron or titanium carbides on the structure and properties of the metal deposited with PP-Np-25Kh5FMS flux-cored electrode wire was performed in this study. It is shown that addition of some modifier in the amount of 0.01 % does not have any significant influence on the deposited metal structure. Their influence on the structure differs to a certain extent. Boron modifying leads to an essential reduction of the crystallite dimensions, redistribution of nonmetallic inclusions and increase of metal microhardness. Unlike that, introducing titanium carbide microadditives into the weld pool influences the kinetics of metal solidification, which results in elimination of crystallite columnarity and metal structure transformation into the cellular one. It is shown that owing to the mentioned changes in the structure, the wear and heat resistance of the metal, deposited with application of both the types of modifiers, is increased. Obtained results can be used at selection of promising methods to improve the service properties of the surfaced parts, which operate under the conditions of thermal force loading and wear at metal friction against metal.

**KEYWORDS:** arc surfacing, modifying, microalloying, deposited metal, flux-cored wire, wear resistance, heat resistance, microstructure

## INTRODUCTION

It is known from technical literature that modifying or microalloying of steels and alloys, at which grain refinement, redistribution of nonmetallic inclusions, cleaning of the grain boundaries, etc., take place, allows significantly influencing the structure and service properties of these metals. Materials with microadditives of boron, tungsten, titanium, etc. are used for modifying [1–3]. Doping the steels and alloys with microadditives of these elements, usually leads to formation of a large number of crystallization centers and influences the ratio of crystal initiation and growth rates, which in its turn, has an impact on the metal mechanical properties. At the same time, control of the metal structure and properties by its modifying or microalloying has a rather limited use at surfacing [3].

Some works, aimed mainly at solving practical tasks, give examples of application of various types of modifiers, in order to improve the performance of parts, differing by service conditions, chemical composition, etc., so that it is difficult to compare such data even for one type of modifier [4–8]. Known are the good prospects of deposited metal modifying by microadditives of boron [9] and titanium carbides

[10], which were added to the deposited metal through the flux-cored wire charge.

The objective of this work is conducting comparative experimental evaluation of the effectiveness of application of modifying additives with boron or titanium carbides, added in equal quantities to the flux-cored wire charge, on the structure and service properties of the deposited metal of the type of heat-resistant tool steel 25Kh5FMS.

## EXPERIMENTAL MATERIALS AND PROCEDURES

Flux-cored wire for investigations was selected proceeding from that the flux-cored wire PP-Np-25Kh5FMS is rather widely used in manufacture and restoration of rolls of hot rolling mills, hot stamping dies, CCM rolls and similar parts, operating under the conditions of thermal cycling, in combination with wear at metal friction against metal, so that heat resistance and wear resistance are important for them. It is exactly deposited metal 25Kh5FMS, which is characterized by a high fatigue life under the conditions of thermal force loading and wear [11].

Deposited metal modifying was performed by using powders with the respective additives in the charge of flux-cored electrode wires. This method

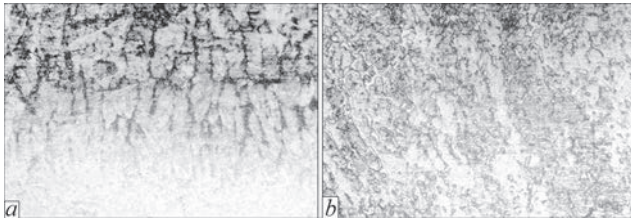


**Figure 1.** Microstructure ( $\times 320$ ) of 25Kh5FMS deposited metal without modifying additives near the fusion line (a) and in the deposited metal upper part (b)

is quite simple in terms of technology, and it can be applied with success in practice [9]. The flux-cored wire charge was calculated so as to obtain the same composition of modifying additives in the deposited metal at the level of 0.01 %. The initial charge materials used were FKkB-1 master alloy which contains 12 % boron, as well as powder of Ti–TiC system with  $\geq 23$  % carbide content, produced by titanium powder treatment by a high-voltage electric discharge in the hydrocarbon liquid [10]. The quantity and type of modifiers, added to the deposited metal, were selected proceeding from the earlier obtained data, in order to improve the deposited metal service properties and prevent crack initiation in it [9, 10].

Test samples were surfaced by flux-cored wires of 1.8 mm diameter using AN-26P flux. Plates from 40Kh steel were used as the base metal. Surfacing modes were as follows:  $I = 220$  A;  $U = 36$  V;  $v = 25$  m/h. Each sample was surfaced in five layers to avoid the impact of deposited and base metal mixing. Used for comparison were samples, surfaced by flux-cored wire PP-Np-25Kh5FMS of a standard composition without modifying additives.

Sample surface was prepared for metallographic studies by standard methods, which include stage-by-stage grinding of the sample surface, using diamond pastes of different dispersity and subsequent electrolytic etching in 20 % solution of chromic acid. Microstructural studies were performed in metallographic optical microscope MIM-7 with digital video ocular Sigeta MCMOS-3100 at  $\times 320$  magnification.

Service properties of the deposited metal were evaluated experimentally by two indices — heat resistance and wear resistance at higher temperature. Two parameters were compared to assess the deposited

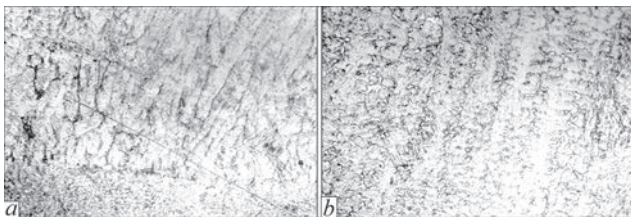


**Figure 2.** Microstructure ( $\times 320$ ) of 25Kh5FMS deposited metal with boron microadditives near the fusion line (a) and in the deposited metal upper part (b)

metal heat resistance: number of heating-cooling cycles up to appearance of a network of thermal cracks on the test sample surface and their propagation depth after all the samples reached 200 heating-cooling cycles. The temperature of the sample surface is equal to 650 °C at heating and to 60 °C at cooling.

Wear resistance at higher temperatures was assessed at metal friction against friction by the “shaft-plane” schematic. During testing the deposited surface of the test sample wears against the surface of a ring counter-body heated up to the temperature of 950 °C. The temperature of the sample surface in the zone of contact of the sample and the ring is equal to approximately 600 °C. Wear resistance was evaluated by the test sample weight loss before and after testing.

Samples from steel 45, hardened to *HRC* 48–52 were used as the reference samples at optimization of the testing modes. Derived values of heat and wear resistance for the reference samples were taken as the conventional unity. The procedures of investigation of the deposited metal service properties are described in greater detail in work [9].

## INVESTIGATION RESULTS AND THEIR DISCUSSION

Metallographic investigations of the surfaced samples (Figures 1–3) showed that application of both the types of modifiers leads to refinement of the deposited metal structure. So, the average size of unmodified metal crystallites in its central part is equal to 30–60  $\mu\text{m}$ , in the majority of them it is 40–45  $\mu\text{m}$ . In the metal modified by boron, the crystallite size in a similar area of the metal is equal from 20 to 40  $\mu\text{m}$ , and in the majority of them it is 20–25  $\mu\text{m}$ . In the metal modified by titanium carbides, the average crystallite size is equal to 20–50  $\mu\text{m}$ , in the majority of them it is 30–35  $\mu\text{m}$ .

Alongside the crystallite size, the structure of the deposited metal sample, containing microadditives of boron (Figure 2), differs little from that of an unmodified metal sample (Figure 1), and it consists of columnar crystallites, growing in the heat removal direction. An acicular martensitic structure is observed in the crystallite body, and light precipitates of residual austenite are found beyond their boundaries. Individual

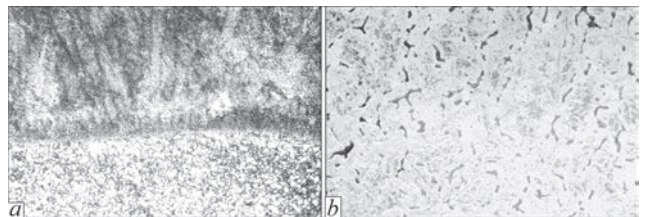


**Figure 3.** Microstructure ( $\times 320$ ) of 25Kh5FMS deposited metal with titanium carbide microadditives near the fusion line (a) and in the deposited metal upper part (b)

round-shaped precipitates are present in the crystallite body, which, obviously, are complex carboborides. Microhardness in this zone in a sample with boron microadditives is equal to  $HV1-6130-6420$  MPa, which is higher than that of a similar area of a sample without modifying additives ( $HV1-5720-6060$  MPa).

In a sample deposited by wire, containing a modifier of Ti–TiC system, the structure of the deposited metal upper layer consists of rather equilibrium cells, within which dark etching precipitates are observed (Figure 3). The microhardness of this area of the deposited metal is equal to  $HV1-5720-5850$  MPa. Influence of modifying TiC particles, compared to boron, is manifested not so much in crystallite refinement, but in transformation of the deposited metal structure from the columnar into the cellular one, and precipitation of complex compounds beyond the cast crystallites in the form of individual inclusions. Microhardness of the deposited metal, compared to an unmodified sample, practically does not change.

Investigations of the level of the surfaced sample contamination by nonmetallic inclusions in keeping with the procedure of GOST 1778–70 on polished unetched microsections showed that the highest contamination of the deposited metal, mainly by oxides, is observed in the sample without modifying additives: it corresponds to point No. 3a of “Point oxides” Table. Deposited metal samples, which were modified by boron additives, are cleaner compared to a sample without additives and their contamination corresponds to point No. 1a of the same Table. The lowest level of contamination by nonmetallic inclusions which is lower than point No. 1a, is observed in a sample, surfaced with application of a modifier of Ti–TiC system.

Investigations of service properties of surfaced samples showed that modifying of the deposited metal by boron allows improvement of its hardness from  $HRC 48-50$  to  $HRC 52-54$ . Hardness of the deposited metal, modified by Ti–TiC, practically did not change and is equal to  $HRC 48-52$ .

Results of experimental investigations of the deposited metal service properties are given in Figure 4, where the values of wear resistance at a higher temperature ( $\epsilon_{600}$ ), heat resistance by the number of cycles to crack initiation ( $N_q$ ) and their average length ( $N_d$ ) are given in relation to the respective characteristics of reference-samples made from steel 45, the values of which are taken as a unity.

As one can see from Figure 4, heat and wear resistance of samples of metal deposited by flux-cored wires with microadditives of both types, became higher. Thermal fatigue cracks in the modified metal of the surfaced samples initiate later, their average length and quantity is smaller than in the samples without

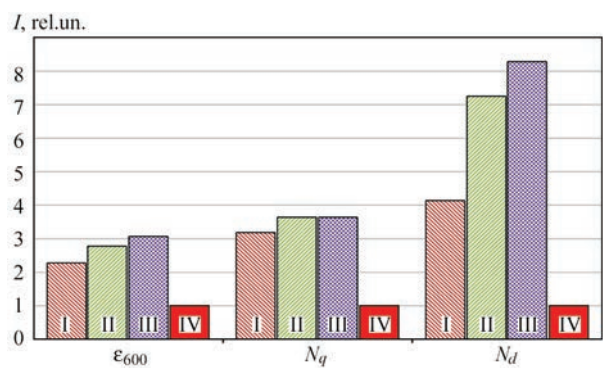


**Figure 4.** Relative wear resistance of 25Kh5FMS deposited metal at a higher temperature ( $\epsilon_{600}$ ), relative heat resistance by the number of cycles to crack initiation ( $N_q$ ) and their average length ( $N_d$ ): without modifying additives (I), with modifying additives of boron (II) and titanium carbides (III) relative to a reference-sample from steel 45 (IV), the values of which are taken to be a unity the modifying additives. It should be noted that evaluation of heat resistance, made by the average depth of crack propagation, turned out to be more accurate than evaluation by the number of cycles to formation of a ramified crack network. This is attributable to the fact that 25Kh5FMS steel is characterized by rather high heat resistance, and visual determination of the exact moment of appearance of a ramified network of cracks may be inaccurate. Positive impact of microadditives of both types on the deposited metal was found not only in a smaller loss of the surfaced sample weight, but also in reduction of the extent of wear of ring counter-bodies, contacting the studied samples, which means more favourable service conditions, which were in place in the friction pairs.

In general, increase of wear resistance of the deposited metal with modifying additives of both types is on approximately the same level, and it is equal from 22 to 34 %, compared to unmodified metal. Increase of heat resistance, assessed by the number of cycles to crack initiation, is equal to 20 % for both types of modifiers, and in the case of evaluation by the average crack depth, it is from 75 % at boron application and up to 200 % at titanium carbide application. As we can see, deposited metal modifying by microadditives of powder of Ti–TiC system has a more positive influence on its service properties.

In our opinion, a positive influence of modifying by boron microadditives on the deposited metal properties is attributable to several factors. First, boron is a more active deoxidizer, compared to silicon and manganese, and it has high surface activity. Due to that, boron is predominantly located on the crystal boundaries, which leads to redistribution of nonmetallic inclusions and their driving from the boundaries into the crystallite volume [6]. Secondly, deposited metal modifying by boron leads to increase of the crystallite microhardness, while the matrix microhardness re-

mains practically unchanged, which can be accounted for by increase in the density and ramification of boron-hardened crystallite boundaries.

Positive influence of microadditives of powder with titanium carbides on the properties of the deposited metal is obviously related, primarily, to the high melting temperature of these compounds ( $3260 \pm 150$  °C). Deposited metal modifying by these compounds leads to their effective transition from the flux-cored wire charge into the weld pool, due to their low dissolution in the weld pool, thus influencing the kinetics of the deposited metal solidification. It results in elimination of columnar crystallites and their refinement, which has a positive influence on the deposited metal performance.

## CONCLUSIONS

1. Introducing microadditives of boron or titanium carbides in equal quantity (0.01 %) into the deposited metal of the type of 25Kh5FMS tool steel has a different influence on its structure and leads to significant refinement of the crystallite sizes and a certain increase in the microhardness of its matrix in the first case, and to an essential change of its structure with transformation of the columnar structure into the cellular one without any major change in the crystallite sizes or microhardness in the second case.

2. Modifying by both the types of the studied additives has a positive effect on the deposited metal service properties. Here, application of powder, containing titanium carbides as a modifier, looks more promising, allowing increase of the deposited metal wear and heat resistance by 1.34 and 2.0 times, respectively.

## REFERENCES

1. Baker, T.N. (2016) Microalloyed steels. *Ironmaking & Steelmaking*, 43(4), 264–307. DOI: <https://doi.org/10.1179/1743281215Y.0000000063>
2. Baker, T.N. (2019) Titanium microalloyed steels. *Ironmaking & Steelmaking*, 46(1), 1–55. DOI: <https://doi.org/10.1080/03019233.2018.1446496>
3. Babinets, A.A., Ryabtsev, I.O. (2021) Influence of modification and microalloying on deposited metal structure and properties (Review). *The Paton Welding J.*, 10, 3–11. DOI: <https://doi.org/10.37434/as2021.10.01>
4. Gladkiy, P.V., Mikaelyan, G.S. (1992) *Microalloying and modification of wear-resistant deposited metal*. In: Surfacing. Technologies, Materials, Equipment. Kyiv, PWI, 33–36 [in Russian].
5. Stepnov, K.K., Matvienko, V.N., Oldakovsky, A.I. (2011) Modification of medium-chromium deposited metal. *The Paton Welding J.*, 8, 10–12.

6. Krivchikov, S.Yu. (2012) Modification by boron of deposited metal of white cast iron type. *The Paton Welding J.*, 6, 19–21.
7. Maksimov, S.Yu., Machulyak, V.V., Sheremeta, A.V. (2014) Investigation of influence of microalloying with titanium and boron of weld metal on its mechanical properties in underwater welding. *The Paton Welding J.*, 6–7, 76–79.
8. Syzonenko, O.M., Prokhorenko, S.V., Lypyan, E.V. et al. (2020) Pulsed discharge preparation of a modifier of Ti–TiC system and its influence on the structure and properties of the metal. *Materials Sci.*, 56(2), 232–239. DOI: <https://doi.org/10.1007/s11003-020-00421-1>
9. Babinets, A.A., Ryabtsev, I.O., Lentuygov, I.P., Bogaichuk, I.L. (2022) Influence of microalloying with boron on the structure and properties of deposited metal of the type of tool steel 25Kh5FMS. *The Paton Welding J.*, 6, 3–10. DOI: <https://doi.org/10.37434/as2022.06.01>
10. Lobanov, L.M., Syzonenko, O.M., Ryabtsev, I.O. et al. (2023) Improvement of technology of producing Ti–TiC modifiers and studying their impact on the structure of deposited metal of type 25Kh5FMS. *The Paton Welding J.*, 2, 3–9.
11. Ryabtsev, I.O., Knysh, V.V., Babinets, A.A., Solovei, S.O. (2022) *Fatigue life of deposited parts*. In: Monography. Kyiv, Interservice [in Ukrainian].

## ORCID

I.O. Ryabtsev: 0000-0001-7180-7782,  
A.A. Babinets: 0000-0003-4432-8879,  
M.O. Pashchyn: 0000-0002-2201-5137,  
O.M. Syzonenko: 0000-0002-8449-2481,  
I.O. Lentuygov: 0000-0001-8474-6819,  
I.I. Ryabtsev: 0000-0001-7550-1887,  
T.G. Solomiichuk: 0000-0001-7550-1887,  
A.S. Torpakov: 0000-0002-3038-8291

## CONFLICT OF INTEREST

The Authors declare no conflict of interest

## CORRESPONDING AUTHOR

I.O. Ryabtsev  
E.O. Paton Electric Welding Institute of the NASU  
11 Kazymyr Malevych Str., 03150, Kyiv, Ukraine.  
E-mail: ryabtsev39@gmail.com

## SUGGESTED CITATION

I.O. Ryabtsev, A.A. Babinets, M.O. Pashchyn, O.M. Syzonenko, I.O. Lentuygov, I.I. Ryabtsev, T.G. Solomiichuk, A.S. Torpakov (2023) Influence of different types of modifiers on the structure and properties of deposited metal of the type of 25Kh5MFS tool steel. *The Paton Welding J.*, 5, 11–14.

## JOURNAL HOME PAGE

<https://patonpublishinghouse.com/eng/journals/tpwj>

Received: 28.04.2023

Accepted: 29.06.2023

DOI: <https://doi.org/10.37434/tpwj2023.05.03>

# ANALYSIS OF CAUSES OF FAILURE OF FIELD WELDED BUTT JOINTS OF MAIN PIPELINES AFTER LONG-TERM OPERATION

**L.I. Nyrkova, L.V. Goncharenko**

E.O. Paton Electric Welding Institute of the NASU  
11 Kazymyr Malevych Str., 03150, Kyiv, Ukraine

## ABSTRACT

In the work on the examples of failure of four pipelines, the authors considered and analyzed the causes of failure of circumferential welded butt joints of main gas and oil pipelines with a long-term service life of 530–1420 mm diameter from low-alloy ferritic-perlitic steels of grades 17G1S, 17GS and 15GSTYu, constructed back at the end of the twentieth century. Technical experts assume that, as a rule, accidents are associated with the failure of circumferential butt welded joints produced in field conditions. Literature sources give quite limited reliable information about the causes of defect formation that lead to the failure of field welded joints. The authors show that even having provided satisfactory mechanical properties of steels and at the absence of deviations in the chemical composition of welded joints, depressurization of pipelines occurred due to weakening of the weld as a result of defect formation during operation or during construction and assembly works. The defects include pores, lacks of fusion, lacks of penetration, edge displacement, use of embedded elements, etc. that were not detected by non-destructive testing methods. The obtained results made it possible to adjust a set of technological recommendations on the requirements and rules for performing assembly and welding works during the construction and repair of main pipelines in Ukraine over the last 20 years.

**KEYWORDS:** main gas and oil pipelines, circumferential butt welds, welded joints, failure, technological defects, assembly and welding works, violations

## INTRODUCTION

More than 40 thousand km of functioning gas and oil pipelines, the life of which is 30–50 years, are operated on the territory of Ukraine. The statistic data presented in the scientific and technical literature, as well as own experience indicate that accidents occurring on the main pipelines are often associated with the failure of circumferential welds of butt joints. As a rule, based on statistics, the cases of their failure are attributed to the rejection in construction and assembly works.

The key factors that contribute to the failure of circumferential welds are the sizes of defects, inappropriate properties of pipe steels and welded joints. In particular, the presence of loads [1] should be noted, that arise for different causes: through sources of active external effect, for example, because of the soil shift, or loads that occur in the pipeline in the process of construction and operation, etc.

For example, in many cases, as a cause of arising critical defects in producing a circumferential weld, slag inclusions are considered that were not timely detected and removed [2, 3]. The failure was also facilitated by the detected crack of 10 mm length in the weld root. But these authors did not consider the causes of defect formation. In literary sources [4], the share of failures of the main pipelines associated with the mentioned factor is estimated in 22–25 %. Moreover, welding defects are approximately 13–19 %. In [5], the results of fatigue

studies have shown that in the presence of typical defects of welding in the circumferential weld, the pipeline service life may be more than 30 years. This approach may be the basis for analyzing the life and assessment of the reliability of the pipeline. The set of defects revealed by the method of non-destructive testing does not always allow finding the cause of their formation [6]. Therefore, it is important to determine the origin and causes of defect propagation in the welds to prevent their formation.

The aim of the work is to determine the probable causes for the formation of the most typical defects both at the stage of assembly as well as after a long-term operation, which led to failure during operation of gas and oil pipelines that were built at the end of the twentieth century.

## PROCEDURE OF EXPERIMENTS

The studies were conducted on the samples of field butt welded joints. The fragments of circumferential joints of gas and oil pipelines were cut out from the failed parts of gas and oil pipelines with a diameter of 530–1420 mm during their repair. In most cases, by that time there were the pipes made of typical low-carbon low-alloy and microalloy steels of grades 17GS, 17G1S and 15GSTYu. The quality of welded joint metal was determined by the method of visual-optic inspection and by the study of the macro- and micro-sections of welded joints. The sections were prepared by the standard procedure using pastes of different

**Table 1.** Mechanical properties of base metal of investigated pipes

Code	Steel grade	Pipe sizes, mm, features of steel production technology	$\sigma_y$ , MPa	$\sigma_p$ , MPa	$\delta_5$ , %	$KIC^{I-0}$ , J/cm <sup>2</sup>
1	17G1S	1020×14×10, normalized	460	568	30	90
2	17GS	720×7.5, hot-rolled	415	541	23	55
3	15GSTYu	1020×10.6, hot-rolled	416	592	27	109

**Table 2.** Chemical composition of base metal and metal of circumferential welds of investigated samples of welded joints

Steel grade	Zone of welded joint	Mass fraction of elements, %									
		C	Mn	Si	S	P	Al	Ni	Mo	Ti	Cr
17G1S	BM	0.16	1.32	0.47	0.023	0.016	N/D	0.06	N/D	N/D	0.04
	W	0.11	0.95	0.29	0.036	0.025	N/D	0.08	0.34	N/D	0.06
17GS	BM	0.18	1.09	0.49	0.029	0.023	0.006	0.09	N/D	–	0.054
	W	0.105	0.83	0.43	0.023	0.017	N/D	0.04	N/D	–	0.05
15GSTYu	BM	0.17	1.31	0.67	0.032	0.031	0.044	0.05	<0.03	0.14	0.07
	W	0.076	0.92	0.34	0.025	0.012	0.005	0.05	<0.03	0.12	0.06
17GS [8]	BM	0.14–0.20	1.0–1.4	0.4–0.6	≤0.0405	≤0.035	–	≤0.3	–	–	≤0.3
17G1S, TU 14-3-721	BM	0.15–0.20	1.15–1.60	0.4–0.6	≤0.035	≤0.030	–	≤0.3	–	–	≤0.3
15GSTYu ChMTU-156	BM	0.12–0.16	1.00–1.35	0.50–0.85	≤0.035	≤0.030	0.025–0.085	–	–	0.15–0.20	≤0.3

granularity. The mechanical properties of steels were determined on the machine of ZDM model according to GOST 6996. The chemical composition of steels and weld metal was determined by the spectral analysis in the DFS-36 spectrometer.

## RESULTS AND THEIR DISCUSSION

The authors considered and analyzed the four cases of the most characteristic failure of circumferential butt welded joints of pipelines that occurred during their operation. In the construction of such pipelines those grades of electrodes were used, which are recommended for arc welding of field joints according to VSN 006. Table 1 shows the mechanical properties

of the studied pipe samples. The chemical composition of the base metal and metal of the circumferential welds is given in Table 2.

### FEATURES OF MICROSTRUCTURE OF CIRCUMFERENTIAL BUTT WELDED JOINTS

Low-alloy steels in the normalized and hot-rolled state have a ferritic-perlitic structure with the grain size number 6, 7 and 8, and with a banded structure — not more than 2, Figures 1, 2, *a*.

The microstructure of metal of the studied circumferential welds on low-alloy ferritic-perlitic pipe steels 17G1S, 17GS and 15GSTYu is similar. The micro-

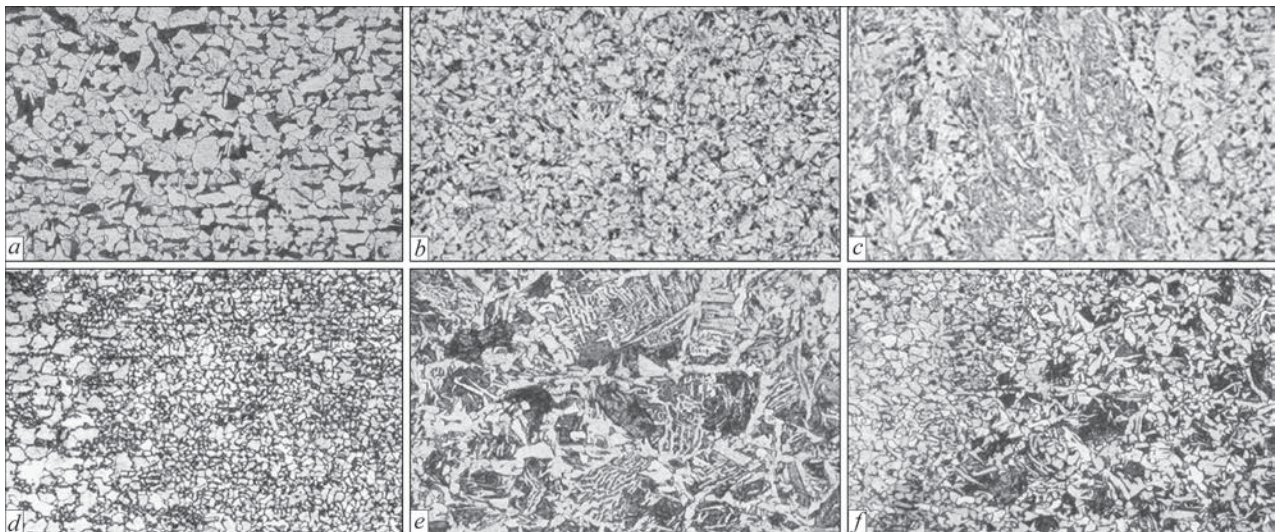


**Figure 1.** Metal microstructure of the circumferential welded joints of pipes of 17G1S steel, ×200: *a* — base metal; *b* — metal of root layer; *c* — metal of facing layer; *d* — zone of coarse grain of root layer; *e* — zone of coarse grain of facing layer; *f* — weld and zone of coarse grain of filling layer

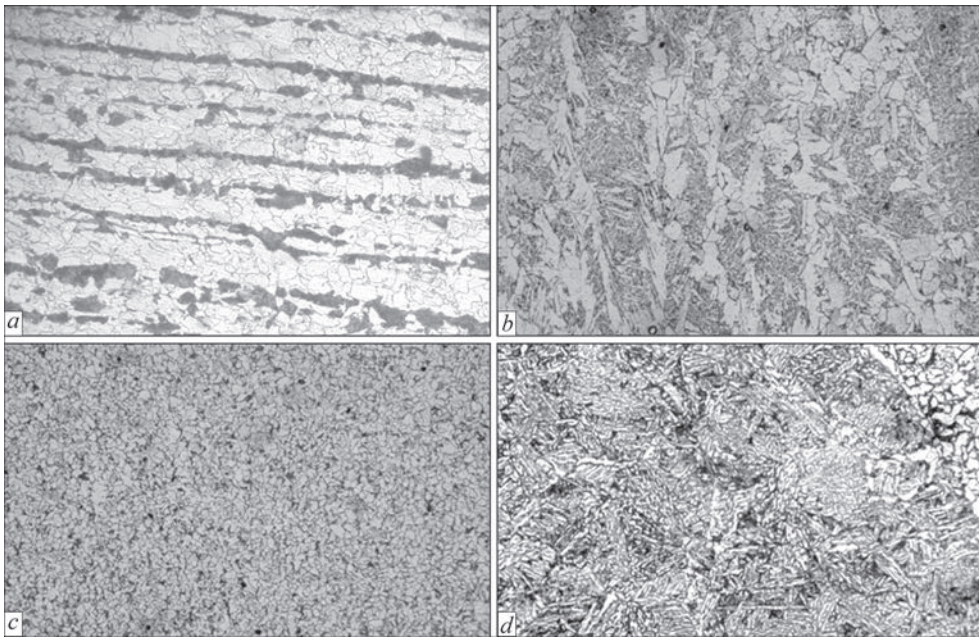


**Figure 2.** Metal microstructure of the circumferential weld of pipes of 15GSTYu steel: *a* — base metal; *b* — facing weld,  $\times 200$ ; *c* — root weld,  $\times 200$ ; *d* — zone of coarse grain of facing layer,  $\times 320$

structure of the metal of the root layer and filling layers, which are subjected to reheating while producing the subsequent layers, is mainly ferritic-perlitic with more equiaxial grains of ferrite (Figures 1, *b, d, 2, c, d*). A typical microstructure of metal of facing layers (Figures 1, 2) is a mixture of different forms of structural components of mainly polygonal ferrite, bainite, and smaller individual areas of Widmanstaetten and lamellar ferrite and pearlite. It should be noted that the change in the amount of impurities of alloy elements in steels and welds affects mainly the ratio of hypoeutectoid ferrite and intermediate decomposition structures that replace pearlite. Therefore, in the circumferential weld on the 15GSTYu steel (Figure 2), compared to the weld on the 17GS steel (Figure 1), the amount of bainite increases, and pearlite is almost absent, the amount of hypoeutectoid ferrite remains stable. The sample of the structure of the facing layer of circumferential joints of the pipe of 17GS and 15GSTYu steel is shown in Figure 1, *c* and Figure 2, *c*.

#### ANALYSIS OF CIRCUMFERENTIAL JOINTS OF GAS AND OIL PIPELINES WHICH FAILED DURING OPERATION

To determine the type of defects, the specialists were guided by the acting pipeline construction and modern standard documents of SNiP II-42 and VSN 006 [9, 10], according to which, the sizes and admissibility of defects were evaluated. According to the analysis of the features of defects, the probable causes of their formation were determined. In each considered case, the focus of failure was determined, the quality (defectness) of welded joints and properties of their metal were evaluated.

In the first case, the failure of the circumferential weld of the welded joint of the main gas pipeline, constructed approximately in 1987 from spirally-welded pipes of 17G1S steel, occurred mainly over the area of fusion of the circumferential weld with the base metal (Figure 3) at the area of about 3/4 perimeter of length of this butt. The root and filling layers of the circumferential joint are produced by manual arc welding, and the facing layer — by submerged arc welding. On the surface of the fracture, at one of the areas of failure, a large number of pores with a diameter of not more than 3 mm and with a depth of not more than 7 mm (Figure 3, *a, b*) were found. On the transverse macrosections of the samples from this area, deep pores (Figure 3, *b*) are seen, which spread to the metal of circumferential weld from the zone of its fusion with the base metal on the outer surface of the pipe. The pores are combined with a lack of fusion zone (300 mm long, 8 mm deep) of the filling and facing layers with the base metal, which led to weakening of the weld intersection. On the opposite side of the failure, a part of the unmolten edge is seen. Also, a displacement of the axis of the outer weld relative to the root by 3 mm is observed. In the specified area, lack of fusion of the root weld with the base metal (up to 3 mm deep) is observed. The total length of this defective area is approximately 350 mm, the depth does not exceed 7 mm. In other areas of the failure around the perimeter of the circumferential weld, only separate pores with a diameter of not more than 2 mm are present. The peculiarity of this joint of pipes with a circumferential weld is reduction in the hardness of the HAZ metal by  $50 HV_{49}$ , which is a consequence

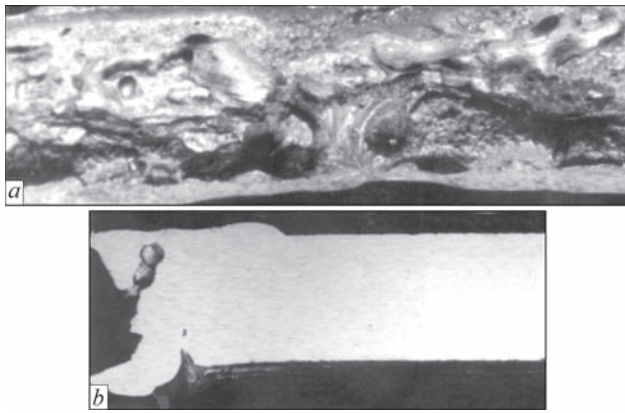


**Figure 3.** Appearance of fracture (*a*) and defects (*b*) in the metal of the failed weld of the gas pipeline of spirally-welded pipes with a diameter of 1020 mm of 17G1S steel: *a* — lack of fusion of 8 mm depth, pores of 7 mm; *b* — welds displacement, pores of 8 mm depth

of metal softening during welding. The width of the area of the strength decrease is 4–5 mm. The revealed metal softening in the case of welding of heat-treated pipes is a typical phenomenon and it did not cause failure of the investigated welded joint.

In view of the abovementioned, it can be assumed that the cause of the failure of the field welded joint of the gas pipeline from the spirally-welded pipes are defects of a circumferential weld formation in the form of elongated (about 300 mm) lack of fusion of the root and filling layers with one of the edges of the joint and pore clusters. These defects were formed during welding operations in the construction of the gas pipeline as a result of displacement of the mentioned layers relative to the butt of the joint edges and were not detected by non-destructive testing.

In the second case, on the main gas pipeline of 15GSTYu steel, the construction of which dates back to 1970, while performing diagnostic works, gas leakage was detected. The working pressure in this gas pipeline was 4.7 MPa. The gas pipeline is covered with bitumen-rubber insulation. At the upper part of the circumferential joint in the weld, a through crack-like

defect was revealed (Figure 4). The circumferential weld, produced by one-sided manual welding, joined a spirally-welded pipe with a size of 1020×10.6 mm of 15GSTYu steel with a 1020×9.5 mm pipe of the Kh60 steel. The detected defect is located along the weld at some displacement relative to its center. The length of the defect is approximately 250 mm. The edge preparation is insignificant (does not exceed 1 mm). The welded joint at a length of approximately 170 mm was produced with a significant edge displacement in the radial direction and with a wide gap of the edges (Figure 4, *c*). The edge displacement in this area is 6 mm, which is much higher than the allowable rate (not more than 3 mm). On the outer surface of the pipes in the defect area near the fusion line of the circumferential weld, traces of plastic deformation of the metal formed during the assembly of edges of the pipes with the purpose of their alignment for welding are observed.

At the fracture it is seen that the initial crack passes along the edge of the root layer and begins from the lack of fusion with one of the edges of the butt joint (Figure 4, *d*). The depth of the lack of fusion is approximately 3 mm. The back formation of the root layer of the weld is completely absent. The location of the crack coincides with the area of the metal flow in the zone of significant edge displacement (Figure 4, *c*). In the defect zone adjacent to the inner surface of the butt joint, there are pores and their clusters. The size of individual pores reaches 4 mm.

Taken into account the abovementioned, it can be stated that the cause of the failure of the circumferential weld of the specified main gas pipeline was a poor quality of assembly of edges of the circumferential welded joint (inadmissible sizes of radial displacement of welding edges and a wide gap), which led to the appearance of defects of formation (lacks of fusion, pores) in the root weld in the process of its welding, and subsequently provoked the occurrence

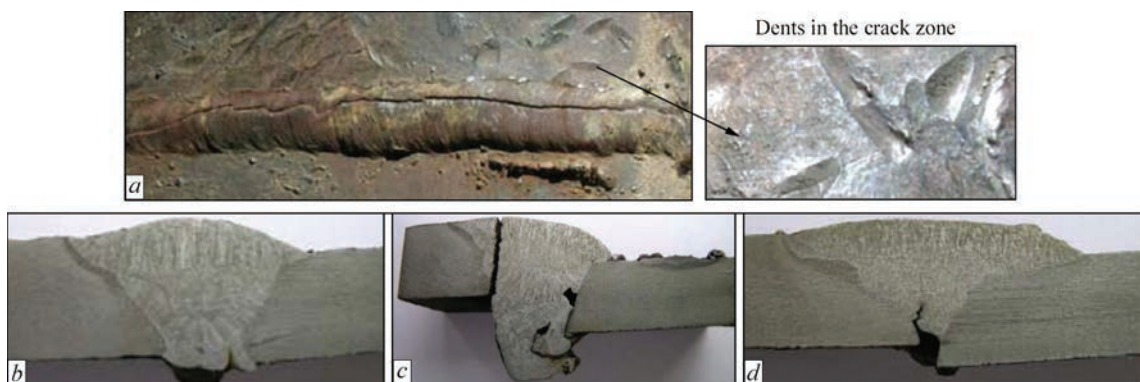


**Figure 4.** Defects in the circumferential weld of the pipeline with a diameter of 1020 mm from 15GSTYu steel and Kh60 steel: *a* — crack of ~250 mm long in the circumferential weld; *b* — macrosection of the circumferential weld outside the crack; *c* — macrosection of the circumferential weld in the crack zone, edge displacement of up to 6 mm, lack of fusion of edges; *d* — macrosection of the circumferential weld in the end part of the crack, lack of fusion and crack in the root layer, edge displacement of up to 3 mm

of a through crack. The formation and propagation of a crack was facilitated by local stresses, caused by attempts of a forced elimination of the inadmissible radial edge displacements. The crack surface is significantly damaged by corrosion indicating a long-term operation of a pipe with a defect.

Further, the failure of two circumferential welded joints of the oil pipeline with a diameter of 720 mm, built from pipes with a wall thickness of 7.4 mm of the strength class K54 was considered. In the first circumferential weld, a through crack-like defect of about 300 mm in length was revealed (Figure 5). In the crack zone, the exceeding sizes of the edges at a length of 600 mm were observed, which reached 7 mm, and a large gap between the edges of up to 10 mm at a length of 740 mm. In order to reduce the gap, contrary to standard documents, 2 rods with a diameter of 6 mm and a length of up to 150 mm were welded into the edge preparation (Figure 5, *b*). In the weld root, the formation of the inner weld is poor, here inadmissible lacks of penetration and lacks of fusion of the edges of up to 3 mm deep were found. In the second circumferential weld, in the fracture of the failed joint such defects as lacks of fusion and lacks of penetration on the side of the inner surface of the weld with a total length of about 100 mm were also detected. The minimum thickness of the deposited metal in the intersection between the outer surface and the area with defects (defect-free area) did not exceed 1 mm.

Therefore, the cause of oil leakage in the 3<sup>rd</sup> investigated case is the formation of defects in the welds of the circumferential joints as a result of improper performance of the welding process with a clear violation of rules of butt joint assembly, in particular, in the presence of a significant (up to 7 mm) excess of the edges and the gap (up to 10 mm) between them, as well as the use of additional embedded elements to fill the edge preparation. The occurrence of cracks in the circumferential welds was facilitated by the presence of inadmissible lacks of penetration in the weld root and lacks of fusion in them, caused by a low quality of assembly of the butt joint. The propagation of cracks and the formation of a through defect occurred, most probably, as a result of a variable load during the operation of the oil pipeline.

As for the 4<sup>th</sup> case, there non-structural embedded elements were detected to fill the excessive gap in the welded joint of the gas pipeline with a diameter of 1020 mm, built of the pipes made of coiled hot-rolled 15GSTYu steel. The detected through defect in the circumferential weld was oriented almost in the center of the weld and had a length of about 200 mm (Figure 6, *a*). The part of the weld of 700 mm long, which included also an area with a crack, the edge displacement of the pipes in a radial direction is pres-

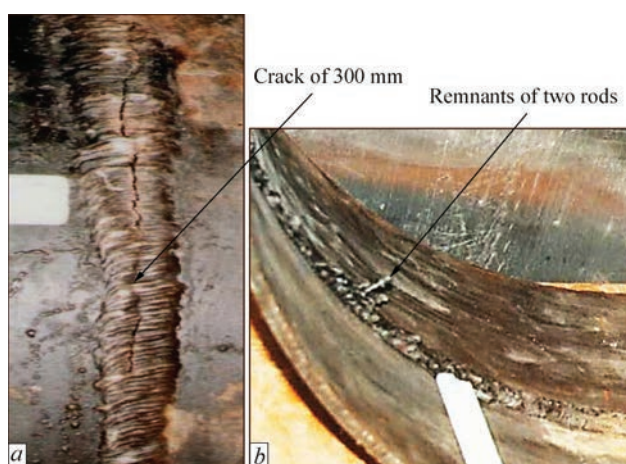


**Figure 5.** Circumferential joint of the oil pipeline with a diameter of 720 mm with a crack in the weld: *a* — on the side of the outer surface of the pipe; *b* — on the inner surface of the pipe

ent (Figure 6, *b*). The largest edge displacement (up to 5 mm) was recorded in the crack zone. Namely in the part of the crack, in the zone of the root layer, lacks of fusions of edges were observed, the depth of which reached 3.5 mm. On the inner side of the circumferential joint, there are areas of significant metal leakage (up to 7 mm in height).

The analysis of the chemical composition of the root layer metal in the crack zone revealed an excessively high content of vanadium, up to 1.7 % (usually, the content of vanadium in the welds in a low-alloy or a microalloy pipe steel does not exceed 0.1 %). This indicates that while producing the circumferential weld with a large edge displacement, metal billets were used to prevent metal leakage in this area, which led to a significant increase in the content of vanadium in the root layer and the occurrence of a hot crack in its center (Figure 6, *c*).

Taking into account the abovementioned, the cause of the failure of the circumferential butt weld-

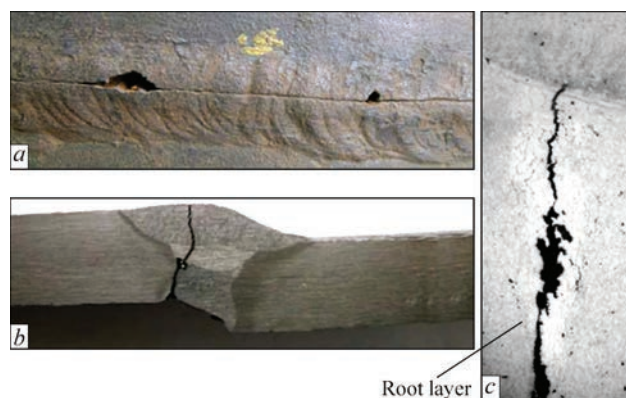


**Figure 6.** Crack in the circumferential welded joint of the pipeline with a diameter of 1020 mm from 15GSTYu steel: *a* — general appearance of the circumferential joint with a crack; *b* — crack in the weld, edge displacement in the area with a crack (up to 5 mm); *c* — anomalous structure of the metal of root and filling layers of the field joint (vanadium content is ~ 1.7 %), produced by manual welding in the crack zone

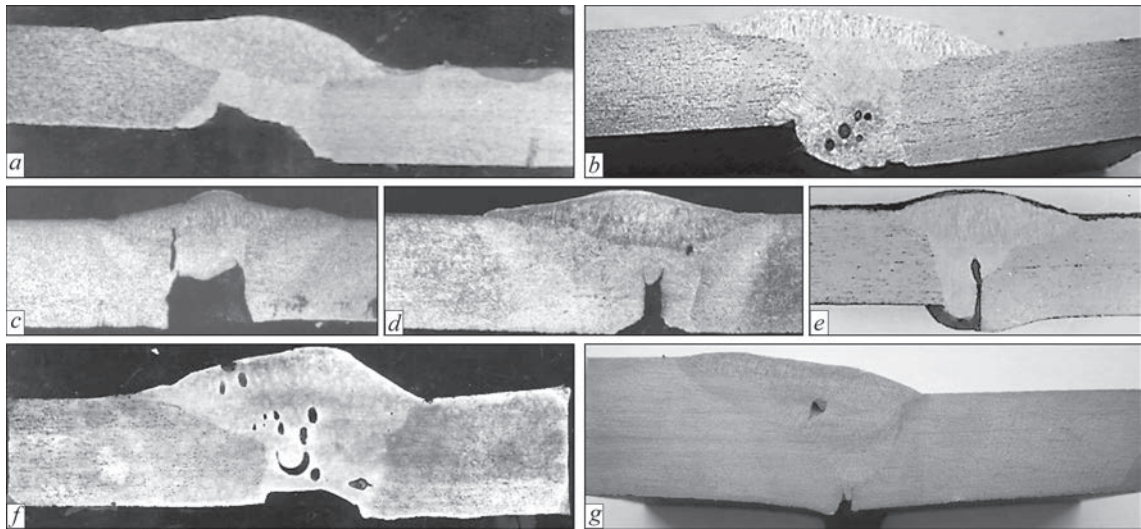


**Figure 7.** Defects in the circumferential welded joints of gas and oil pipelines of pipes with the sizes: *a* — 720×9mm of 17GS steel, edge displacement, wide gap, lack of filling the root part of the weld; *b* — 820×9 mm of 19G steel, edge displacement, wide gap, deformed ends of pipes, accumulation of pores; *c* — wide gap, lack of root layer, lack of fusion of the weld with the base metal; *d* — 720×7.5 mm of 17GS steel, lack of penetration in the root layer with a depth of 4 mm; *e* — 720×8mm of 16GB steel, edge displacement, lack of fusion (4 mm) in the root part of the weld; *f* — 720×9 mm of 19G steel, gap exceeding the standard, accumulation of pores; *g* — different thickness joint of 17G1S steel of 1020×10 and 1020×14 mm, deformed ends of pipes, lack of penetration in the root layer

ed joint of the gas pipeline, built from the pipes with a diameter of 1020 mm of the 15GSTYu steel, is a crack formed as a result of using additional foreign elements, gaps and excesses of edges during welding of the root layer, which are unacceptable according to standard documents. This led to a local enrichment (up to 1.7 %) of the root weld metal with vanadium and occurrence of a crack of hot origin. Thus, it can be assumed that during the operation of the gas pipeline, it gradually propagated in the filling and facing layers of the circumferential weld before the formation of a through defect. The formation of a through defect was largely facilitated by defects in the circumferential weld and disadvantages of edge assembly, first of all, excessive one, up to 5 mm, their exceeding and unacceptable gaps.

Thus, as to the conditions of arising, the revealed defects that led to the failure of gas and oil pipelines can be defined as defects of technological origin (i.e. they formed in the welded joints directly during the performance of assembly and welding works), to which, in the first turn, excessive radial edge displacements and the gap between them can be attributed, which led to the emergence of lacks of penetration, lacks of fusion, pores, cracks, cavities and other defects, including in the area of the root weld.

#### **ANALYSIS OF CIRCUMFERENTIAL WELDED JOINTS OF GAS AND OIL PIPELINES DEFECTS REVEALED DURING REPAIR**

The defects formed due to violation of the technological process of producing the circumferential weld

and propagated during operation. Typical defects are shown in Figure 7.

Most often, it was possible to identify the following defects: radial edge displacement (Figure 7, *a, b, e*), excessive gap between the edges (Figure 7, *a, b, f*), lack of penetration of the root layer (Figure 7, *a, c, d, e, f*), lacks of fusion of the root or intermediate layers (Figure 5, *e*), pores and slag inclusions (Figure 7, *b, f*), deformed ends of pipes (Figure 7, *g*). It should be noted that in most cases the revealed defects were formed as a result of poor performance of the operation of assembly of edges (their excessive displacement or gap) of adjacent pipes in the process of pipeline construction.

Above, it was stated that during the study of the failed circumferential welded joints of the pipelines, the evaluation of mechanical properties of the metal of the adjacent pipes and the joint itself, as well as its structural features was performed. We thoroughly assume that in all investigated cases the mechanical characteristics of the pipes and joints metal were in compliance with the determined standards, and the level of characteristics or structural features do not give reason to consider them the causes of the above-mentioned failures.

#### **CONCLUSIONS**

1. It was found out that defects of technological origin that caused the failure of the studied circumferential joints, occurred as a result of violation of the requirements to edge assembly (excessive radial displacements and gap between them), which led to cracking, lacks of penetration, lacks of fusion, pores, etc., first

of all, in the root layer of the circumferential weld. In some cases, the propagation of failure was also facilitated by local stresses that occurred during a cold method of eliminating unacceptable edges displacements during welding of pipes, in particular, while producing overlapped welds.

2. It was determined that in any of the investigated cases, the level of mechanical properties or structural characteristics of the metal of the circumferential welded joints produced using the welding technologies applied during the construction of gas and oil pipelines did not become the cause of their failure.

3. The obtained results made it possible to adjust a number of technological recommendations on the requirements and rules of performing assembly and welding works during the construction and repair of main pipelines in Ukraine over the last 20 years.

## REFERENCES

- Young, A., Andrews, R.M. (2020) Preventing girth weld failure in pipelines: Measurement of loads and application of assessment methods. In: Proc. of 13<sup>th</sup> Inter. Pipeline Conf., Virtual, Online, 28–30 September. DOI: <https://doi.org/10.1115/ipc2020-9551>.
- Cao, J., Ma, W., Pang, G. et al. (2021) Failure analysis on girth weld cracking of underground tee pipe. *Int. J. of Pressure Vessels and Piping*, **191**, 104371. DOI 10.1016/j.ijpvp.2021.104371.
- Xu, Y., Wu, M., Nie, et al. (2022) Performance inspection and defect cause analysis of girth weld of high steel grade pipeline. *J. of Physics: Conf. Series*, 2262(1), 012006. DOI: 10.1088/1742-6596/2262/1/012006.
- Chen, M.J., Dong, G., Jakobsen, R.A. et al. (2000) Assessment of pipeline girth weld defects. *Y. The Tenth International Offshore and Polar Eng. Conf. OnePetro*.
- Lihua, Q., Hui, F., Hui, Z. et al. (2018) Effect of welding defects on mechanical properties and fatigue life of girth welds of X80 steel pipe. *Pipeline Technology Conference*.
- Ma, W.F., Ren, J.J., Zhou, H.P. et al. (2019) Effect of type B steel sleeve rehabilitate girth weld defect on the microstructure and property of X80 pipeline. *Mat. Sci. Forum*, **944**, 854–861. DOI: 10.4028/www.scientific.net/MSF.944.854.
- GOST 5058–65: *Low-alloyed structural steel* [in Russian].
- ChMTU-156–68: *Provisional specifications for electric-welded pipes with a diameter of 1920 mm from 15GSTYu steel grade* [in Russian].
- SNiP III-42–80: *Construction norms and regulations. Main pipelines* [in Russian].
- VSN 006–89: *Construction of main and field pipelines. Welding* [in Russian].

## ORCID

L.I. Nyrkova: 0000-0003-3917-9063,

L.V. Goncharenko: 0000-0001-8371-2078

## CONFLICT OF INTEREST

The Authors declare no conflict of interest

## CORRESPONDING AUTHOR

L.I. Nyrkova

E.O. Paton Electric Welding Institute of the NASU

11 Kazymyr Malevych Str., 03150, Kyiv, Ukraine.

E-mail: lnyrkova@gmail.com

## SUGGESTED CITATION

L.I. Nyrkova, L.V. Goncharenko (2023) Analysis of causes of failure of field welded butt joints of main pipelines after long-term operation. *The Paton Welding J.*, **5**, 15–21.

## JOURNAL HOME PAGE

<https://patonpublishinghouse.com/eng/journals/tpwj>

Received: 06.04.2023

Accepted: 29.06.2023



## INTERNATIONAL CONFERENCE ON WELDING AND RELATED TECHNOLOGIES

7–10 October 2024, Kyiv, Ukraine

### KEY TOPICS

- Innovative Technologies, Materials and Equipment for Welding and Related Processes
- Strength and Stress-Strain States of Welded Joints and Structures
- Additive Technologies
- New Structural and Functional Materials, Nanomaterials, Composites
- Surface Engineering
- Mathematical Modeling of Welding and Related Processes
- Advanced Technologies of Special Electrometallurgy
- Non-Destructive Testing and Technical Diagnostics
- Materials and Technologies for Medicine and Ecology of Welding Production

E.O. Paton Electric Welding Institute of the NASU  
11, Kazymyr Malevych str., Kyiv, 03150, Ukraine  
Tel.: (38044) 205-23-13, 205-22-89, Fax: (38044) 528-04-86  
E-mail: [office@paton.kiev.ua](mailto:office@paton.kiev.ua), [www.paton.kiev.ua](http://www.paton.kiev.ua)



## TECHNOLOGY OF MIG WELDING OF CHROMIUM STEEL OF MARTENSITIC GRADE CA-6NM

A.R. Gavryk<sup>1</sup>, A.K. Tsaryuk<sup>1</sup>, I.G. Osypenko<sup>1</sup>, O.V. Lynnyk<sup>2</sup>, O.V. Vavilov<sup>2</sup>, O.G. Kantor<sup>2</sup>

<sup>1</sup>E.O. Paton Electric Welding Institute of the NAS of Ukraine

11 Kazymyr Malevych Str., 03150, Kyiv, Ukraine. E-mail: [tsaryuk@paton.kiev.ua](mailto:tsaryuk@paton.kiev.ua)

<sup>2</sup>JSC “Ukrainian Energy Machines”

199 Moskovsky Prosp., 61037, Kharkiv, Ukraine. E-mail: [office@ukrenergymachines.com](mailto:office@ukrenergymachines.com)

### ABSTRACT

The weldability of the martensitic steel CA-6NM was investigated and the fundamental technology of its mechanized welding in a mixture of shielding gases was developed according to the requirements for the manufacture of critical parts and assemblies of the hydroturbine equipment, as well as rewelding of casting defects. According to the strength level of the steel, the welding wire Thermanit 13/04 Si of a solid cross-section with a diameter of 1.2 mm and one of the variants of the shielding mixture Mix 1 (82 % Ar + 18 % CO<sub>2</sub>) were selected and comprehensively investigated according to EN 12072/G 134 (Germany). It was established that in order to prevent the formation of cold cracks in welded joints, it is necessary to perform welding of this steel with preheating and concurrent heating up to 150–200 °C and a mandatory postweld tempering at the temperature of 600 °C. The developed technology provides a significant improvement in mechanical properties of welded joints and weld metal (by 30–35 % higher than that specified by the requirements to the level of values for base metal of chromium steel CA-6NM). Certification of the technology was carried out and recommendations for its use in production at JSC “Ukrainian Energy Machines” were worked out.

**KEYWORDS:** mechanized welding, martensitic steel class, mixture of shielding gases, diffusible hydrogen, cold cracks, mechanical properties, structure

### INTRODUCTION

In Ukraine critical parts and welded components of hydroturbine equipment, exposed to intensive cavitation, corrosion and abrasive wear in service are manufactured using chromium steels, both of local grades 06Kh13N4MD, 06Kh12N3D, and foreign grades, in particular CA-6NM steel (03Kh13N5M) [1]. A feature of manufacturing such components of hydraulic radial-axial turbines is a great diversity of individual types of parts and welded structures, which are to be joined and which include, for instance joining stamped or cast blades, rolled and cast rims to make the impeller, as well as rewelding possible casting defects in parts of a large weight of up to 50 t. At the same time, manufacturing cast-welded structures requires a technology of joining to other steel grades of the same class (06Kh12N3DL, 06Kh12N4ML) under the conditions of large thicknesses and considerable rigidity of the parts. Here, it is necessary to preserve high mechanical properties of welded joints of these steel grades, and to focus on the requirements of CA-6NM steel. At present, at manufacture of welded parts and components of hydroturbine equipment from chromium steels of martensitic class, in particular, for rewelding casting defects, “Ukrainian Energy Machines” JSC, mainly, uses coated-electrode manual electric arc and mechanized CO<sub>2</sub> welding, which have

a number of drawbacks [2–4]. Taking into account the welding-technological properties, mechanized welding, for instance in a mixture with shielding gases (Ar + CO<sub>2</sub>), has significant advantages, compared to the above processes [5, 6]. In welding in a gas mixture of 82 % Ar + 18 % CO<sub>2</sub> the region of welding modes with short-circuiting of the arc gap is absent (just the region of drop transfer and jet transfer is observed). Here, electrode metal losses for burning-out and spatter are reduced, weld formation quality is improved, resistance to pore formation and technological strength are increased, labour consumption in the joint cleaning from spatter is reduced, and there is a real possibility for improving the values of welded joint mechanical properties.

Therefore, development and introduction of mechanized welding in a shielding gas mixture in manufacture of components of hydroturbine equipment from chromium martensitic steel and rewelding casting defects is an urgent task. In this connection, the objective of this work was investigation and development of scientifically substantiated principles of the technology of mechanized welding of CA-6NM steel in a mixture of shielding gases, which allow improvement of the technological strength, in particular cold cracking resistance of welded joints and ensuring their high service properties.

**Table 1.** Chemical composition of the studied steels, wt.%

Steel grade	C	Si	Mn	Cr	Ni	Mo	S	P	Other elements
							Not more than		
06Kh12N3D steel to TU 1081425-86	≤ 0.06	≤ 0.3	≤ 0.06	12.0–13.5	2.8–3.2	–	0.025	0.025	Cu–0.50–1.10 W+V
CA-6NM steel in as-delivered condition (PWI data)	0.037	0.20	0.43	11.81	3.9	0.47	0.016	0.017	–

## EXPERIMENTAL MATERIALS AND PROCEDURES

Chemical composition of chromium steels of steels of grades 06Kh12N3D and CA-6NM, considered in this work, is given in Table 1.

Selection of welding wire was based on its matching the chemical composition of the base metal, i.e. the possibility of its application for martensitic class steels with 13 % chromium. Alongside having a matching composition, the welding wire in mechanized welding should satisfy the requirements of equivalent strength by the mechanical properties — ensuring equivalent strength by all the indices with the material being welded.

Proceeding from analysis of the market of supply of welding consumables, 1.2 mm solid wire of Thermanit 13/04 Si grade of Thyssen (Germany) was selected. Chemical composition of the wire is given in Table 2. Previous evaluation of its welding-technological properties in mechanized welding in gas mixture Mix 1 showed the high stability in welding in all the positions in space with excellent weld formation, slight spatter and absence of any type of defects. Results of studying the chemical composition in the 7<sup>th</sup>

layer of the deposited metal are given in Table 2. As we can see, it is characterized by a low content of such impurities as sulphur and phosphorus, and it is close to CA-6NM steel composition.

Requirements of GTI-407–2018 Instructions [1] to the mechanical properties of base metal and weld metal are given in Table 3.

The following investigation procedures were used during performance of this work:

- alcohol procedure of investigation of “pencil test” sample, produced by pouring the weld pool into a detachable copper mould [7] to determine the diffusible hydrogen concentration in the deposited metal (applied in shipbuilding);

- procedure of restored melting of the sample in the flow of high-purity carrier-gas to determine the concentration of residual gases in the cast sample metal;

- procedure for determination of the equivalent of impurities in the weld meal [8], for evaluation of simultaneous influence of the concentration of oxygen, sulphur and phosphorus  $[P_E] = [O] + 0.8 [S] + 0.7 [P]$ , where [O], [S], [P] are the concentrations of oxygen, sulphur and phosphorus;

**Table 2.** Chemical composition of the wire and deposited metal, wt.%

Object of study	C	Si	Mn	Cr	Ni	Mo	S	P	Other elements
Thermanit 13/04 Si wire EN 12072/G 13/4	0.03	0.8	0.7	13.0	4.7	0.5	–	–	–
Metal deposited by Thermanit 13/04S wire (PWI data)	0.03	0.36	0.36	12.0	3.8	0.27	0.010	0.005	–

**Table 3.** Requirements to mechanical properties of the base and deposited metal

Object of study	Ultimate strength $\sigma_U$ , MPa	Yield point $\sigma_Y$ , MPa	Relative elongation $\delta$ , %	Reduction in area $\psi$ , %	Impact toughness J/cm <sup>2</sup> at 20 °C		Hardness, HB
					KCU	KCV	
06Kh12N3D steel (for comparison)	690	540	14.0	30.0	59	49	187–275
CA-6NM steel	755	550	15.0	35.0	≥ 50	–	–
Deposited metal (Thermanit 13/04 Si wire to EN 15971*)	800	≥ 680	≥ 15	–	–	≥ 50	250

\*After high-temperature tempering for 600 °C for 8 h.

- procedure of quantitative evaluation of cold cracking susceptibility of the welded joints (Implant method), which envisages evaluation of the strength properties at delayed fracture of samples-inserts [9];
- procedure of qualitative evaluation of cold cracking susceptibility of welded joints [10];
- metallographic investigations of welded joint microstructure were conducted using optical light microscope Neophot-32 with connected to it optical module based on a digital photcamera of Olympus C-5060 type for photorecording of images of the microstructures and nonmetallic inclusions;
- procedure of etching welded joint macrosections in 30 % water solution of iron chloride ( $\text{FeCl}_3$ );
- electrolytic etching of microsections in 10 % aqueous solution (distilled water) of chromic acid. Etching mode was as follows: 12–15 V voltage, 10–15 s etching time. Microstructure is revealed with re-polishing of the section surface on cloth with chromium oxide powder deposition on it;
- determination of welded joint metal hardness in TP-5 instrument.

## INVESTIGATION RESULTS AND THEIR DISCUSSION

Ensuring minimal gas saturation of the weld metal is one of the most important welding-technological properties of welding consumables. Diffusion-mobile oxygen has a particularly noticeable influence on the technological strength of the metal of the weld and HAZ. Concentration  $H_d$  of diffusion-mobile hydrogen was determined in the weld metal deposited with the studied wire. It was established that average value of  $H_d$  is on a very low level ( $<0.1 \text{ cm}^3/100 \text{ g}$  of the deposited metal). Special attention was also given to oxygen content in the deposited metal, as in the base metal it determines the volume fraction of nonmetallic inclusions, and in the deposited metal it is one of the key factors of weld metal impact toughness. Results of investigation of weld metal saturation by such gases as oxygen, nitrogen and residual hydrogen are given in Table 4. They show that gas content in the deposited metal is practically the same at different welding processes and it satisfies the specified requirements.

Impurities (sulphur, phosphorus and oxygen) are known to have a negative influence on the ductile properties and impact toughness of the weld metal. The notion of impurity equivalent [ $P_E$ ] was introduced by the procedure in work [8]. Introduction of the notion of impurity equivalent allows reducing the multiple correlation to two variables and comparing the embrittlement of the weld metal in the form of oxide inclusions, sulphur and phosphorus, despite the existing differences in the behaviour of these impurities. It was found that a significant ductility drop is observed at [ $P_E$ ]  $\geq 0.08 \%$  with a simultaneous increase in ultimate tensile strength [8]. At calculation of oxygen and sulphur and phosphorus content in the metal deposited with Thermanit 13/04 Si wire in shielding gas mixture Mix 1, [ $P_E$ ] is equal to 0.07%. This is indicative of significant loss of sulphur and phosphorus as a result of such an active impact of oxygen, which allows obtaining an admissible value of  $P_E$  at application of mechanized welding by the mentioned welding wire. Thus, chemical composition of weld metal, its concentration of diffusible hydrogen and content of gases ( $\text{O}_2$ ,  $\text{N}_2$  and H) fully meet the specified requirements and should promote high crack resistance and the required level of mechanical properties of welded joints of CA-6NM steel (Table 3).

Weldability of martensitic class steels with chromium fraction of 13% is characterized by a higher cold cracking susceptibility of the joints. The determinant role in this phenomenon is attributed to martensitic transformation, and increased content of hydrogen and carbon [13]. As a result of thermal cycle of welding, steels of martensitic class undergo hardening, HAZ metal becomes harder, stronger and more brittle [14]. To eliminate the possibility of cold cracking, the authors of works [15–16] recommend minimizing the content of carbon and nitrogen in the base and filler material, here the weld should have not more than 10 %  $\delta$ -ferrite. This is promoted by nickel content increased to 4–5 %. Maximal content of carbon and nitrogen in the base metal and welding consumables can be limited to the level of 0.02–0.03 %, and that of manganese and silicon usually is not more than 0.6–0.7 %. Optimal content of nickel of not more

**Table 4.** Content of residual gases in the deposited metal

Deposited metal	[O], wt.%	[N], wt.%	[H], ml/100 g Me
In a mixture of 82 % Ar +18 % $\text{CO}_2$ in welding with Thermanit 13/04 Si wire	0.059	0.043	2.46
In welding in 100 % $\text{CO}_2$ [11]	0.063–0.078	0.021	1.1
Manual welding by 4 mm TSL-20M electrodes [11]	0.0307	0.012	1.4
Automatic submerged-arc welding with AN-43M flux [12]	0.054	0.0138	1.6

than 5 % [17] also increases the content of highly ductile components in the welded joint structure.

For hardenable steels it is rational to evaluate the cooling cycle in the range from 500 to 300 °C, which reflects the thermokinetic features of austenite transformation in the martensite-bainite region. Also highly important for technological strength are the conditions of HAZ metal cooling after completion of phase transformation from ~200 to 100 °C. Delayed cooling at these temperatures ensures development of diffusion processes, with which the low-temperature tempering of martensite and atomic hydrogen escaping from the zone of possible cracking are associated.

Determination of actual cooling rates of the HAZ metal in the specified ranges was of interest when studying the delayed fracture susceptibility of CA-6NM steel. To assess the cold cracking susceptibility of CA-6NM steel and to determine the required preheating temperature at mechanized welding with 1.2 mm wire of Thermanit 13/04 Si grade in gas mixture Mix 1 a number of Implant tests were conducted at different preheating temperatures (100, 150, 200 and 250 °C) and without preheating, as well as at different level of loading of the samples-inserts. Welding was performed by a single stringer weld (bead) in the following mode:  $I_w = 180\text{--}200$  A,  $U_a = 24\text{--}26$  V, gas flow rate of 1000 l/h.

The cooling rate of the insert HAZ metal was determined by the thermal cycle (TC), welding characteristics were recorded to  $T = 100$  °C. Cooling rate in the ranges of  $T = 600\text{--}500$ ;  $500\text{--}300$  and  $200\text{--}100$  °C, which are denoted  $w_{6/5}$ ,  $w_{5/3}$  and  $w_{2/1}$ , was determined by calculation-graphic method by TC curve. Two to three curves from different TC, derived at one and the same heating temperature were processed in a similar way, and the obtained values were used to determine the average value of the cooling rate.

Results of evaluation of the delayed cracking susceptibility of welded joints of CA-6 NM steel are given in Figure 1. One can determine from the graph that absence of cold cracking susceptibility in mechanized

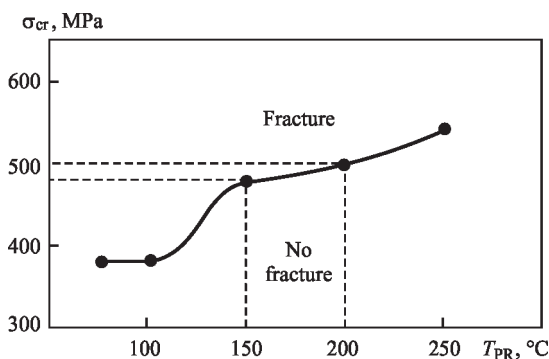


**Figure 1.** Curve of critical breaking stress for CA-6NM steel, depending on preheating temperature

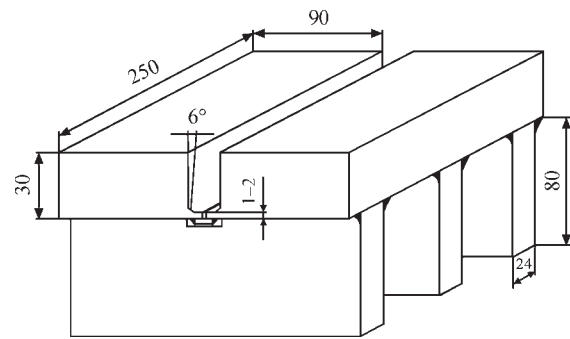


**Figure 2.** Rigid sample for making butt welded joint of CA-6NM steel

welding by wire of Thermanit 13/04 Si grade in gas mixture Mix 1 is provided by preheating the base metal up to the temperature of 150 °C. It is found that the level of critical stress above the yield limit is ensured at preheating to 150–200 °C. Thus, welding should be performed after preheating at the level of 150–200 °C.

Qualitative evaluation of cold cracking susceptibility of the welded joints was performed by welding the first root pass in a rigid butt joint (Figure 2) at preheating temperatures, the optimal value of which was determined by the Implant method. Such a temperature was taken to be the value of 150 °C.

After cooling to room temperatures and soaking for 48 h the welded rigid samples were cut into transverse templates. The surfaces of welded joints were studied for crack initiation. Preheating of welded joints above 150 °C allows preventing cracklike defects.

## EXPERIMENTAL-INDUSTRIAL VERIFICATION OF INVESTIGATION RESULTS

Butt samples of  $200 \times 300 \times 30$  and  $200 \times 300 \times 40$  mm size were prepared and welded, in order to study the structure and mechanical properties of weld metal in welded joints of CA-6NM steel made by mechanized welding in a shielding gas mixture. Figure 3 shows the shape of edge preparation for gas-shielded semi-automatic welding with dimensions, corresponding to type TP-6 according to DSTU EN 9692-1:2014.

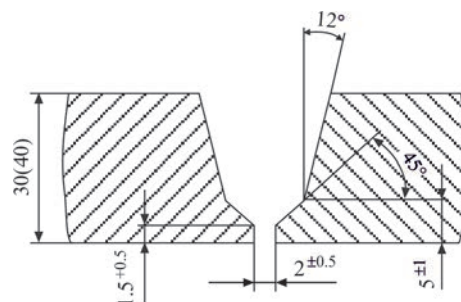


**Figure 3.** Shape of edge preparation of a joint of CA-6NM steel for mechanized welding

**Table 5.** Results of mechanical testing

Object of study	$\sigma_r$ , MPa	$\sigma_y$ , MPa	$\delta$ , %	$\psi$ , %	Impact toughness, J/cm <sup>2</sup> at 20 °C		Bend angle, deg	Hardness, HB
					KCU	KCV**		
Weld*	870.2–884.1	710.5–725.2	15.5–15.9	56.8–60.1	86.7–89.6–98.8	68.7–78.5–80.7	–	235–250
Welded joint*	814.3–827.7	–	–	–	–	–	130	–

\*After high-temperature tempering at 600 °C, for 4 hours.  
\*\*At –40 °C KCV is equal to 53.9–59.7–59.9.

Welding the test butt joint was performed with preheating and concurrent heating up to the temperature of 150 °C. Mode of welding the root pass was as follows:  $I_w = 120–140$  A,  $U_a = 19–22$  V, shielding gas flow rate was 600 l/h. To fill up the groove the mode parameters were increased:  $I_w = 180–200$  A,  $U_a = 24–26$  V, gas flow rate was up to 1000 l/h. Welding was followed by heat treatment of the butt joint in the form of tempering at the temperature of 600 °C for four hours, with further cutting up of the samples into templates, from which samples were prepared for mechanical testing. When studying the mechanical properties of the weld metal, static tensile tests were conducted on samples, cut out of the weld metal along the weld. When studying the welded joints, the samples were cut out across the weld with the sample middle located on the fusion line. For static bending at normal temperature, the bending angle of welded joint samples should be not lower than that of the base metal. Weld metal testing for impact bending of samples with a round notch (KCU) was conducted at room temperature. Impact bend testing of samples with a sharp notch (KCV) was performed in the temperature range from +10 to –40 °C. Results of mechanical testing of the metal of the weld and welded joint of CA-6NM steel are given in Table 5.

Thus, mechanical characteristics of the metal of the weld and welded joint of CA-6NM steel, made by mechanized welding in a shielding gas mixture Mix 1, using Thermanit 13/04 Si wire, fully meet the requirements to welded joints of CA-6NM steel (see Table 3).



**Figure 4.** Macrosection of CA-6NM steel welded joint

Metallographic investigations were performed in order to evaluate the quality of base metal, welded joints and weld metal, as well as structural changes,

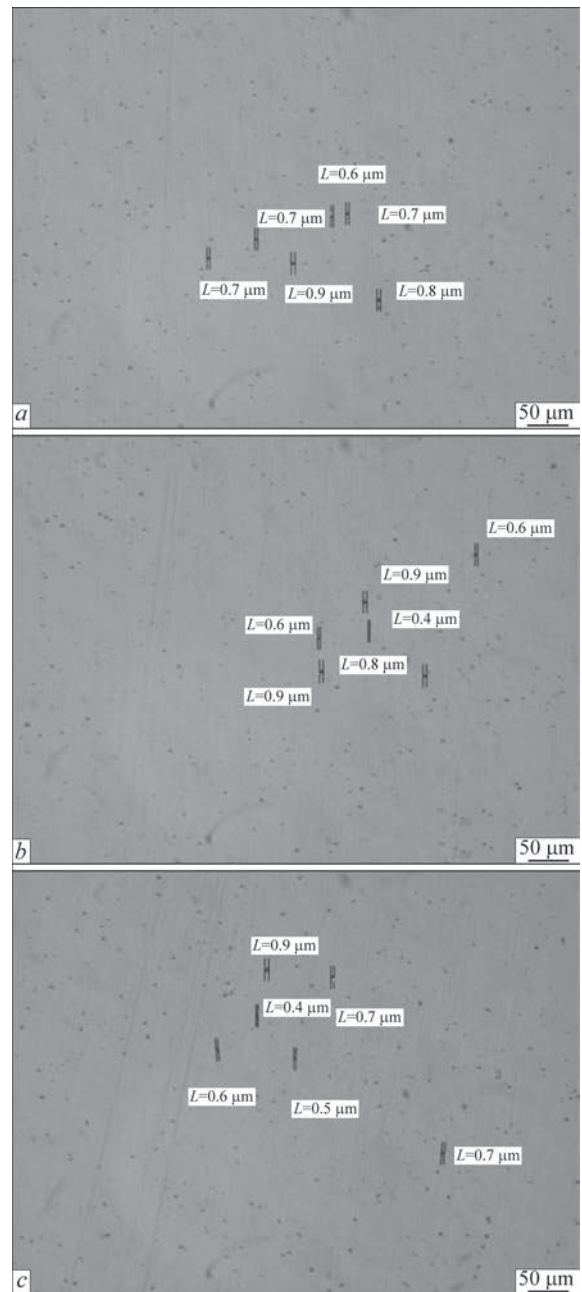


**Figure 5.** Nonmetallic inclusions and their size in the metal of the weld made by Thermanit 13/04 Si wire in shielding gas mixture Mix 1: a — weld upper part, ×1000; b — weld middle part, ×1000; c — lower (root) part of the weld

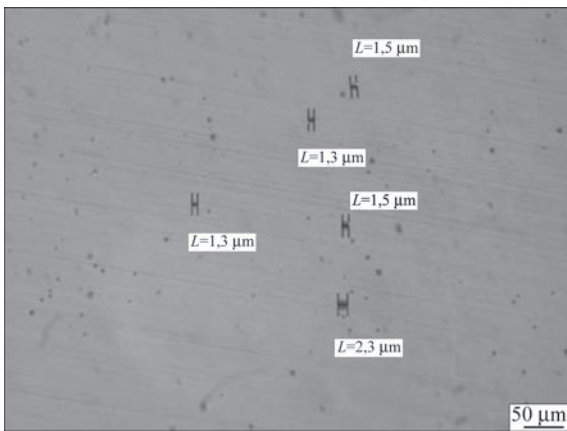


**Figure 6.** Nonmetallic inclusions and their size in the metal of the weld made by FOX CN 13/4 electrodes

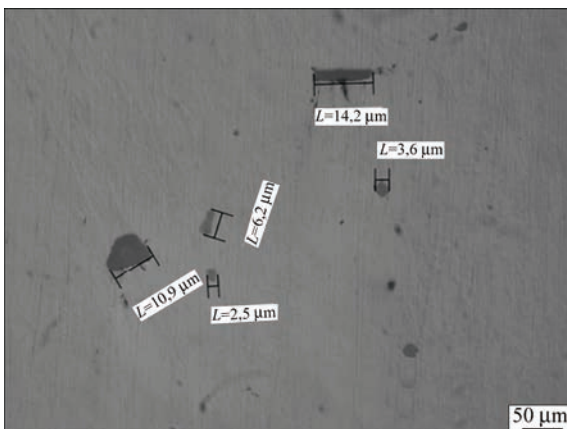


**Figure 7.** Nonmetallic inclusions and their size in CA-6 NM steel resulting from the process of welding and heat treatment. Macrosection of the full cross-section of the welded joint after heat treatment is shown in Figure 4.

For microanalysis, microsections were cut out of the welded joints after heat treatment, to study the microstructure.

Microstructures of the weld, HAZ and base metal were investigated.

As one can see from the given images in Figure 5, distribution of nonmetallic inclusions in the weld metal is rather uniform. They are isolated and fine oxides and silicates of 0.5–0.9  $\mu\text{m}$  size. For comparison, Figure 6 shows nonmetallic inclusions in the metal of the weld, made by manual arc welding by FOX CN 13/14 electrodes (BOHLER), which are oxides and silicates of 1.3–2.3  $\mu\text{m}$  size.

Nonmetallic inclusions in the base metal of CA-6NM steel shown in Figure 7, are individual oxides of 1.0–2.5  $\mu\text{m}$  size and oxysulphides of 4–15  $\mu\text{m}$  size.

Structural features of different areas of the welded joint of CA-6NM steel are considered in the condition after welding and tempering at 600  $^{\circ}\text{C}$  for four hours. The weld metal in the upper, middle and lower parts has bainitic-martensitic structure. HAZ structure of CA-6NM steel in the upper, medium and lower parts

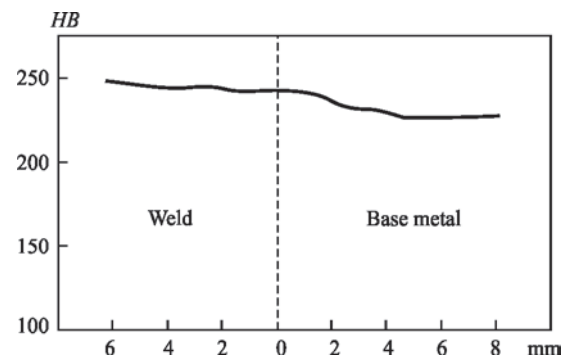


**Figure 8.** Hardness distribution in the welded joint of CA-6NM steel

consists of bainite and martensite with inclusions of grain-boundary ferrite. Base metal structure at a distance from the weld is bainitic-martensitic with precipitates of grain-boundary ferrite. Hardness distribution in the welded joint of CA-6NM steel in the condition after heat-treatment is shown in Figure 8.

Thus, proceeding from the conducted metallographic investigations it was shown that in the metal of the weld deposited by the mechanized process in gas mixture Mix 1 by Thermanit 13/04 Si wire such defects as pores, lacks of penetration, slag inclusions or cracks were absent. It was also shown that the nature of nonmetallic inclusion distribution in the deposited metal in welding in Mix 1 mixture is uniform, compared to the metal deposited with FOX CN 13/4 electrodes. Here, the size of the inclusions is smaller, which has a positive impact on the weld mechanical properties. The weld metal structure is rather homogeneous, it consists of bainite and martensite, which completely corresponds to this class of materials. In the condition after tempering at 600  $^{\circ}\text{C}$  for four hours the weld metal hardness is in the range of 240–250 HB. The HAZ structure is characteristic for CA-6NM steel (bainite + martensite) with individual precipitates of grain-boundary ferrite and its hardness is in the range of 230–240 HB. The hardness of weld and HAZ metal meets the requirements to welded joints of CA-6NM steel.

Results of the performed investigations were used for certification of the proposed technology of mechanized welding of CA-6NM steel in shielding gas mixture Mix 1. Certification showed the real possibility of application of this technology for welding and re-welding the casting defects in the parts and components of hydroturbine equipment.

## CONCLUSIONS

Weldability of CA-6NM martensitic steel was studied and basic technology was developed of its mechanized welding in a mixture of shielding gases, in keeping with the requirements to manufacturing critical parts and components of hydroturbine equipment,

as well as rewelding the casting defects. In keeping with the steel strength level, 1.2 mm solid welding wire Thermanit 13/04 Si to EN 12072/G 134 (Germany) and one of the variants of shielding mixture Mix 1 (82 % Ar + 18 % CO<sub>2</sub>) were selected and comprehensively studied. The rationality of application of preheating and concurrent heating up to the temperature of 150–200 °C and performance of postweld heat treatment – tempering at the temperature of 600 °C for welded joints of CA-6NM chromium steel was substantiated. The developed technology of MIG welding allows a significant improvement of technological strength and mechanical properties of welded joints by 30–35 % of the level of requirements to the values for base metal of CA-6NM chromium steel. Technology certification was conducted, and recommendations were developed as to its application in production at “Ukrainian Energy Machines” JSC.

## REFERENCES

- (2018) Instruction GTI-407-2018: *Hydraulic turbines. technical requirements on quality of producing the cast welded wheels of radial-flow turbines*. Kharkov, Turboatom [in Russian].
- Volichenko, N.P., Tsebrenko, E.K. (2009) Welding in turbine construction of Ukraine. *Svarshchik*, **2**, 66 [in Russian].
- Paton, B.E. (2013) Research and developments of the E.O. Paton Electric Welding Institute for nowadays power engineering. *The Paton Welding J.*, **10–11**, 14–22.
- Tsaryuk, A.K., Levchenko, E.V., Grishin, M.M. et al. (2020) Welding in power engineering industry of Ukraine. *The Paton Welding J.*, **3**, 19–24. DOI: <https://doi.org/10.37434/tpwj2020.03.03>
- Rimsky, S.T. (2006) *Guide on mechanized shielded-gas welding*. Kyiv, Ekotekhnologiya [in Russian].
- Kononenko, V.Ya. (2007) *Shielded-gas consumable and non-consumable electrode welding*. Kyiv, Niko-Print [in Russian].
- Kozlov, R.A. (1986) *Welding of heat-resistant steels*. Leningrad, Mashinostroenie [in Russian].
- Potapov, N.M. (1976) *Principles of flux selection in welding of steels*. Moscow, Mashinostroenie [in Russian].
- Sawhill, J.M., Dix, A.W., Savage, W.F. (1974) Modified implant test for studying delayed cracking. *Welding J.*, **12**, 554–560.
- Kasatkin, B.S., Musiyachenko, V.F. (1970) *High-strength low-alloyed steels for welded structures*. Kyiv, Tekhnika [in Russian].
- Anokhov, A.E., Zemskova, M.S. et al. (1974) Verification of serviceability of butt joints of pipelines made by semiautomatic CO<sub>2</sub>-welding. *The Paton Welding J.*, **8**, 43–46.
- Tsaryuk, A.K., Ivanenko, V.D., Kozlovets, O.N. (1995) Influence of welding material purity on properties of weld metal of heat-resistant steel 15Kh1M1F joints. *The Paton Welding J.*, **5**, 45–46 [in Russian].
- Bilmes, P.D., Llorente, C., Perez Ipina, J. (2000) Toughness and microstructure of 13Cr4NiMo high-strength steel welds. *J. Mater. Eng. and Performance*, **9(6)**, 609–615.
- Casas, W.J.P., Henke, S.L., Novicki, N. (2009) Fracture toughness of CA6NM alloy, quenched and tempered, and of its welded joint without PWHT. *Welding Inter.*, **23(3)**, 166–172.
- Rymkevich, A.I. (1980) Welding of low-alloyed 13 % chromium steel for producing of uniform and dissimilar joints. *Svaroch. Proizvodstvo*, **9**, 1–12 [in Russian].
- Rymkevich, A.I. (1986) Selection of electrodes for welding of high-strength corrosion-resistant steels. *Avtomatich. Svarka*, **6**, 57–60 [in Russian].
- Bilmes, P.D. et al. (2009) Microstructure, heat treatment and pitting corrosion of 13CrNiMo plate and weld metals. *Corrosion Sci.*, **51(4)**, 876–81.

## ORCID

A.R. Gavryk: 0000-0002-0793-2754,  
A.K. Tsaryuk: 0000-0002-5762-5584,  
I.G. Osypenko: 0000-0002-9969-7375

## CONFLICT OF INTEREST

The Authors declare no conflict of interest

## CORRESPONDING AUTHOR

A.K. Tsaryuk  
E.O. Paton Electric Welding Institute of the NASU  
11 Kazymyr Malevych Str., 03150, Kyiv, Ukraine.  
E-mail: [tsaryuk@paton.kiev.ua](mailto:tsaryuk@paton.kiev.ua)

## SUGGESTED CITATION

A.R. Gavryk, A.K. Tsaryuk, I.G. Osypenko, O.V. Lynnyk, O.V. Vavilov, O.G. Kantor (2023) Technology of MIG welding of chromium steel of martensitic grade CA-6NM. *The Paton Welding J.*, **5**, 22–28.

## JOURNAL HOME PAGE

<https://patonpublishinghouse.com/eng/journals/tpwj>

Received: 11.04.2023

Accepted: 29.06.2023

### Save the Date!



“SCHWEISSEN & SCHNEIDEN”, the world’s leading international trade fair for joining, cutting, and surfacing, will take place on September 11–15, 2023 at the Messe Essen Conference Center.



Visit Paton Welding Institute in Hall 8 at Stand 8B29.1 and check out our new and proven solutions for welding and allied technologies.

DOI: <https://doi.org/10.37434/tpwj2023.05.05>

# USE OF ELECTRON BEAM WELDING FOR MANUFACTURE OF BLADE PACKAGES FOR COGENERATION STEAM TURBINES

**Yu.V. Orsa, V.M. Nesterenkov, V.I. Zagornikov, M.O. Rusynyk**

E.O. Paton Electric Welding Institute of the NASU  
11 Kazymyr Malevych Str., 03150, Kyiv, Ukraine

## ABSTRACT

Industrial technology for manufacture of steam turbine blade packages from heat-resistant high-alloy steel of martensitic grade 18Kh11MNFB-Sh was offered. A technological process was introduced into the experimental production, which allowed solving the problem of welding blade packages of 120 mm thickness. The technological equipment was developed, required for positioning package parts in the process of assembly and welding. The results of experimental studies of weldability of heat-resistant steel of martensitic grade by electron beam were presented. It was determined that preheating of blade packages up to 200–250 °C using the defocused electron beam in the vacuum chamber allows obtaining higher ductile properties of welded joints. The required parameters of heat treatment modes after welding were indicated in order to remove inner stresses and provide the necessary mechanical properties of a product.

**KEYWORDS:** blade package, heat-resistant steel, electron beam welding, heat treatment

## INTRODUCTION

Working blades are one of the most critical parts of the steam turbine, which largely determine its reliability and service life. They are subjected to tensile and bending stresses, caused by the action of centrifugal forces, as well as forces that occur as a result of a change in the direction of gas movement in the channels between the blades. In order to increase the vibration reliability of the turbine, its working blades in a quantity from 2 to 5 pieces are joined by welding in packages. It is obvious that the presence of any defects in welded joints located in the tail part of the package creates difficulties during its attachment to the turbine rotor and is unacceptable. This article considers blades of the first stage of the rotor with an all-milled profile, butt welded in a package along the bandage and tail parts. In the world practice of steam turbine construction, for several decades welding of working blades in packages has been used, including electron beam welding [1]. The use of electric arc welding is associated with surfacing of a large volume of metal, which leads to significant residual deformations of steam channels of blade systems. Instead of electric arc welding, which produces relatively massive (volumetric) welds and creates problems of shape deformation of welded products, electron beam welding (EBW) is used, which provides a weld of a better quality without the effect of buckling. A high vacuum in the electron beam chamber contributes to a high metallurgical cleanliness of the welding pool due to its intensive degassing.

In modern steam turbine units operating at high pressures and temperatures of up to 600 °C, in the manufacture of blade packages, high chromium heat-resistant martensitic grades 15Kh11MF-Sh, 18Kh11MNFB-Sh and 20Kh12VNMF-Sh are widely used. Their welding is associated with known difficulties in providing the necessary physical-mechanical and service properties of welded joints. Welding of the mentioned steels is featured by a tendency to delayed failure and softening in the near-weld zone, hot cracking, as well as unstable formation of electron beam welds with a depth of more than 60 mm which is accompanied by the formation of root defects and cavities [2].

In the known works [1, 3], the use of electron beam welding of blade packages was limited to the total thickness of the tail part of 50–60 mm. The design of modern steam turbines requires joining blade packages with the thickness of the tail part of up to 120 mm. Thus, the development of EBW technology for thick-walled structures of heat-resistant high-chromium steel is a relevant and demanded task in industry. The aim of the work was to optimize the technology of welding blade packages of heat-resistant high-chromium steel of martensitic grade 18Kh11MFB-Sh of 120 mm thickness.

## MATERIALS AND EQUIPMENT USED IN THE MANUFACTURE OF STEAM TURBINE BLADE PACKAGES

In the work, an example of welding a blade package of heat-resistant high-alloy chromium steel of grade 18Kh11MFB-Sh (EP-291) was considered. It is used

**Table 1.** Chemical composition of 18Kh11MNFb-Sh steel, wt.%

C	Si	Mn	Ni	S	P	Cr	Mo	Nb	V
0.15–0.21	Not more than 0.6	0.6–1.0	0.5–1.0	Not more than 0.025	Not more than 0.03	10–11.5	0.8–1.1	0.2–0.45	0.2–0.4

for the manufacture of working and nozzle blades of steam turbines at an steam operating temperature of up to 600 °C. The chemical composition of steel is presented in Table 1.

It is known that steel of this grade is hard-to-weld, has a martensitic grade and requires a preheating. In order to provide the necessary service properties, the produced welded joints are subjected to mandatory heat treatment (high tempering).

Preliminary quality testing was carried out with the help of the UDM-3M flaw defector at frequencies of 2.5 and 5.0 MHz. The microstructure was examined with the help of the NEOPHOT-32 metallographic microscope at a magnification of 20–400. Photos of revealed structures were obtained with the help of the digital camera OLYMPUS C-500.

The microstructure was examined on the sections of 23 mm thick. The Vickers's hardness was measured in the M-400 LECO hardness tester at a load of 1 kg.

### TECHNOLOGICAL PROCESS OF ELECTRON BEAM WELDING OF A BLADE PACKAGE

Practicing the modes of EBW of heat-resistant high-alloy chromium steel of grade 18Kh11MFB-Sh was carried out on the plates with a thickness of 23 and 120 mm thick, which simulate the welded joint of the bandage and tail parts of the blade package. The works were performed in the laboratory installation of the type UL-209 designed by the PWI with a computer control of all parameters and systems. The installation UL-209 is equipped with the power complex on the base of ELA-60/30 and an electron beam

gun that moves inside the vacuum chamber along the linear coordinates  $X, Y, Z$ . At an accelerating voltage  $U_{acc} = 60$  kV, electron beam gun with a metal tungsten cathode of 3 mm diameter provides an electron beam current range of  $I_b = 0–500$  mA and the performance of technological beam scanning in the process of EBW (circle, ellipse, stroke) with an amplitude of 0–5 mm. The accuracy of electron beam gun positioning is at least 0.1 mm. The electron beam focusing on the surface of a welded product, its alignment with the butt and visualization of the EBW process while producing technological tacks is carried out by means of the RASTR system in the secondary-emission image. At the same time, the accuracy of alignment of at least 0.1 mm and 5 times magnification of a monitored object are provided.

The quality of the welds was evaluated by the uniformity of facial bead formation and the presence of inner defects in the weld, which was determined by studying macro- and microsections. For blade packages of each type and sizes, the specialized assembly and welding equipment (Figure 1) was developed.

Blade package 7 is mounted in the body of the equipment 1 and fixed in it with the help of embedded tabs 2 and clamping bolts 4. An accurate positioning of the package in the body of the equipment is carried out by means of the adjustable rest 5 and clamping devices 3.

The design of the equipment provides the vertical arrangement of the butt plane for both the bandage as well as for the tail parts of the blade package assembled for welding. To fix each body of the equipment on the working Table 1 of the welding installation

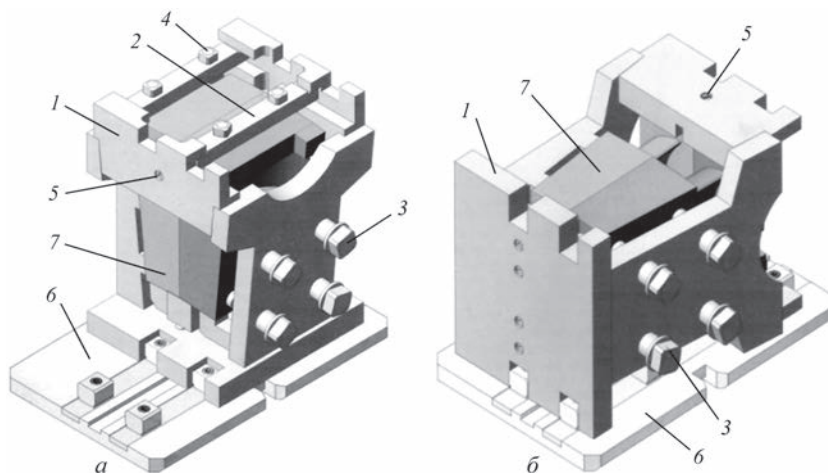


**Figure 1.** Blade packages as-assembled: *a* — position for welding bandage part of the package; *b* — position for welding tail part of the package

UL-209 in a set position, transitional supporting plate 6 is used.

The process of welding the bandage part of the package runs at the vertical arrangement of the body (Figure 1, *a*). To join the tail part of the blade package, EBW technology with two welds on both sides of this part of the package was offered. Welding was carried out in such a way that the second weld overlapped the first one in the root part by 15–20 % in depth. This technological technique provided joining the parts of 120 mm thick with a relatively small input of thermal energy. And this, in turn, allowed eliminating significant distortion of welded products and minimizing tolerances for their mechanical treatment.

The welding of a thick-walled tail part of the package was performed at the horizontal arrangement of the equipment body (Figure 1, *b*). In order to provide high-quality welded joints when using double-sided welding of the tail part of the package, special attention was paid to producing welds with the rounding in the root and absence of root defects.

To prevent the formation of discontinuities in the metal of the root part, the welds in the cross-section should have the maximum possible radius of rounding the root  $r_w$ . The rate of cooling the metal at the weld root at the moment of crystallization is [5]:

$$\frac{dT}{dt} \Big|_{T=T_m} \approx -\eta_T \frac{aT_m}{r_w^2},$$

where  $a$  is the thermal diffusivity coefficient;  $\eta$  is the thermal efficiency;  $T$  is the temperature;  $T_m$  is the metal temperature at the time of crystallization;  $r_w$  is the root radius.

The higher  $r_w$ , the slower the walls of the vapor-gas channel cool down and the molten metal fills the root part of the weld better without the formation of defects in the form of voids and lacks of fusion. To obtain the required radius at the root of the weld, an electron beam scanning in a circle with a diameter of 1.2 mm was used [5, 6]. In a one cycle of pumping-out of the vacuum chamber of the installation, a simultaneous EBW of up to 12 pieces of assembled blade packages (Figure 2) can be performed.

At the first stage, welding along the butt of the bandage part of the package is performed, at the second — of the tail part on both sides is performed. Input and output of welding current is carried out on technological (run-off) tabs that are removed at a further mechanical treatment of the package.

### FEATURES OF EBW OF STEAM TURBINE BLADE PACKAGES TABS

The EBW technology with the use of a scanned electron beam for the local preheating of the welded joint

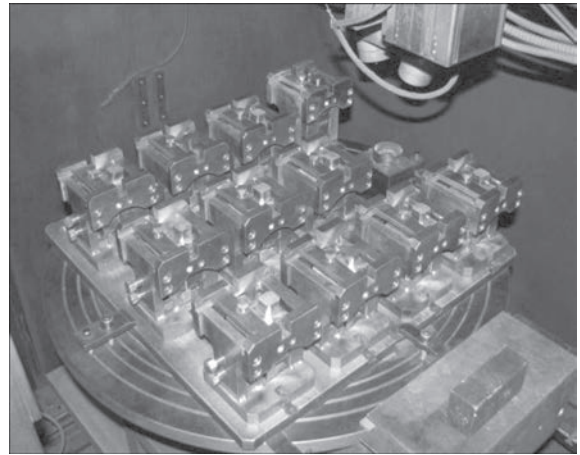


**Figure 2.** Set of blade packages as-assembled before EBW

zone was proposed. When preheating, the combination of a defocused beam and its oscillation was used.

It is known that while changing the focusing current, the concentration of the electron beam changes. This can expand its diameter and improve the stability of the channel in the welding pool, which promotes the stability in the formation of welds. It was experimentally determined that in EBW of blade packages of a large thickness, the electron beam focus should locate in the region of a middle penetration depth. This provides the formation of penetrations of up to 70 mm deep without inner defects arising (Figure 3). The location of the beam focus in the lower third of the weld or at the level of the root led to the appearance of root defects.

Welding of the tail part of the package of up to 120 mm thick is performed on two sides by opposed welds. Moreover, each of the welds provides penetration of up to 60 % of the total thickness of the tail part. Here, the size of the overlapping is about 12–18 mm.

The macrosection with the penetration by opposed welds on the specimen with a total thickness of 120 mm is shown in Figure 4.

In order to prevent softening of the welded joint metal at the area of high tempering, the welding speeds should be set within 3–5 mm/s. It is known that the

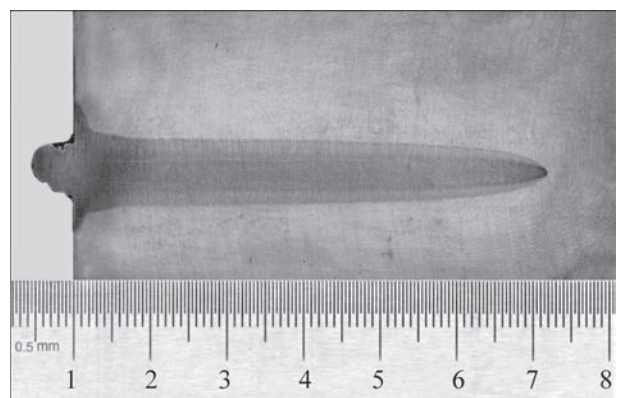


**Figure 3.** Macrosection of defect-free penetration of 70 mm depth

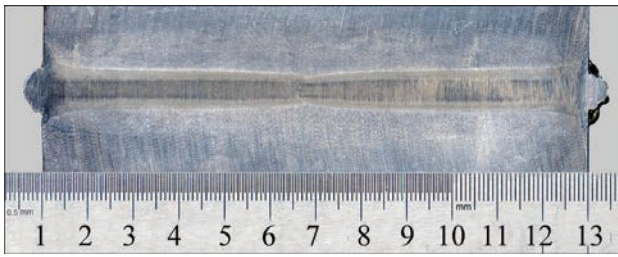


**Figure 4.** Macrosection with penetration by opposed welds of tail part of the blade package with a thickness of 120 mm

width of the softening zone and the degree of softening increases with an increase in the thickness of the welded metal, since the duration of its stay at a temperature of high tempering at a level of 740–760 °C increases. Therefore, the EBW mode should provide the structure of fine acicular martensite at a thickness of 120 mm, which is favorable in terms of increasing ductility.

In EBW of the tail part of the package with a penetration depth of 70 mm, the optimal frequency of a circular scanning  $f$  is 100–300 Hz at a diameter of 1.2 mm. The use of such scanning at a rate of 4 mm/s leads to the formation of the structure of equiaxial crystallites of about 200  $\mu\text{m}$  wide around the weld axis. An increase in the width of the equiaxial crystallites zone to the mentioned sizes prevents the formation of hot cracks and the probability of brittle fracture [7]. Each of the opposed welds was produced at an electron beam current of 320 mA at a welding speed of 4 mm/s.

According to the STP 735.104.-78, in welding of bandage flanges with almost through penetration, the formation of a reverse bead is not admitted. This requirement is performed when the beam focusing at the level of the root part of the butt joint and the electron beam current are at 95 mA for the fixed welding speed of 5 mm/s (Figure 5).

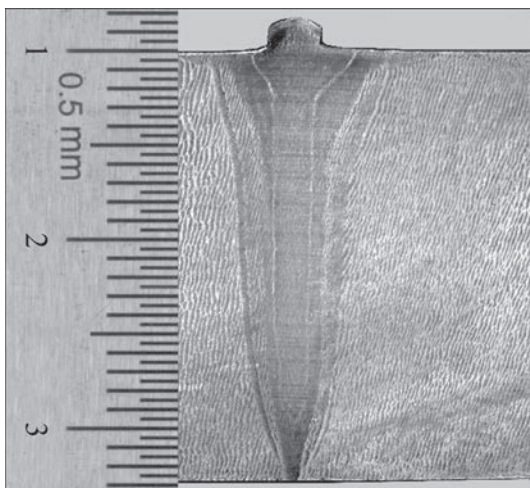


**Figure 5.** Macrosection of welded joint, produced on the simulator specimen of the bandage part of the package of 23 mm

## METALLOGRAPHIC EXAMINATIONS OF WELDED JOINTS OF 18Kh11MNFB-Sh STEEL

The examinations showed that at insufficient preheating (not more than 100–150 °C), in the welded joint metal cracks may form (Figure 6).

Taking into account the need in providing a margin of the technological strength in the development of EBW technology, the temperature of preheating the welded joint zone was determined at a level of 200–250 °C. The preheating temperature was controlled by an optical pyrometer with an error of not more than 1.2 %. The results of the examinations showed that preheating to a higher temperature does not benefit and may cause a reduction in the impact toughness and long-term strength of the welded joint. This can be explained by the fact that in welding of blade packages with a subsequent overlapping of several welds, the introduced preheating  $T > 300$  °C reduces the cooling rate in the range of 890–500 °C and shifts the transformation into the bainitic region [8, 9]. The latter is unacceptable since the  $\gamma$ - $\alpha$  transformation occurs with the formation of a coarse-acicular structure of bainite, with low ductile properties of strength. Therefore, the use of preheating temperature higher than  $T > 300$  °C is accompanied by softening to 10 % at the zone width of not more than 0.2–0.6 mm, which is associated with crystallite growth and is accompanied by a decrease in a long-term strength of the welded joint.

For metallographic examinations, two specimens of the welded joint were used. One specimen was in a state without heat treatment (HT) after welding. The second was after performing HT. The degree of strengthening or softening was determined as a percentage of the values of hardness of the base metal outside the heat-affected zone. The dependence of the weld shape on the EBW parameters was studied on the transverse macrosections cut out from the specimens after welding.

The visual inspection and microscope examination at a slight magnification revealed that the metal of the



**Figure 6.** Crack in the welded joint metal produced on 18Kh11MNFB-Sh steel,  $\times 100$

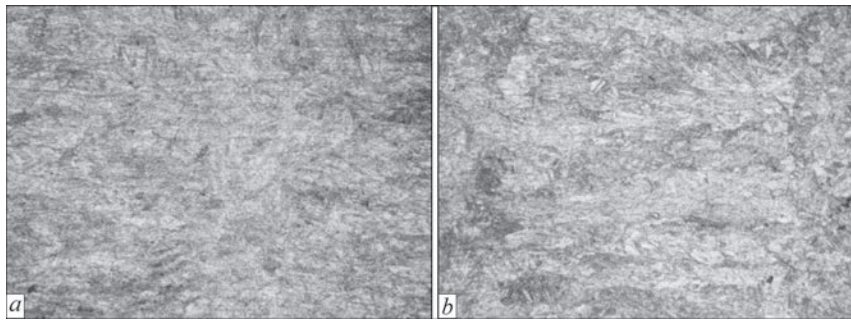


**Figure 7.** Macrostructure ( $\times 200$ ) of a central part of the weld: *a* — without HT; *b* — with HT

specimen weld without heat treatment has a dense structure without visible defects (pores, cracks). The HAZ is symmetric relative to the weld axis. At the root of the weld, the width of HAZ is about 0.5 mm. Further, closer to the upper part of the weld, it gradually grows to 2 mm. Columnar crystallites in the weld grow from the fusion line to the center of the weld at a direct angle to the fusion line, where they collide in the central part of the weld and form a small area of the cellular cast structure of 0.2 mm wide. At the upper part of the weld, the crystallites diverge in a fan shape from the upper edge of the weld. Microstructure of the specimen weld without heat treatment represents a mixture of fine-acicular martensite, a minimum amount of  $\delta$ -ferrite (about 1–1.5 %), carbides and intermetallics, the composition of which can only be determined by an electron microscope. The maximum hardness was observed on the fusion line and reached 453  $HV_1$ .

HAZ is represented by a dispersed sorbitic structure with the precipitates of carbides and intermetallics (Figure 7, *a*). Microstructure of the base metal (BM) represents a ferritic matrix with the precipitates of carbides and intermetallics.

The specimen that was subjected to heat treatment after welding has a microstructure of the weld, which is composed of tempered martensite with the hardness  $HV_1$ –343–363  $\text{kgf/mm}^2$ , also with a small amount of  $\delta$ -ferrite (1.0–1.5 %), carbides and intermetallics (Figure 7, *b*). The HAZ microstructure consists of sorbite, carbides and intermetallics. The BM structure after

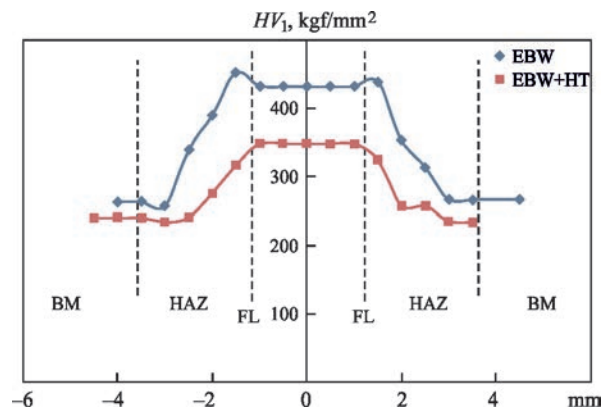


**Figure 8.** Diagram of hardness distribution in the welded joint of 18Kh11MNFb-Sh steel

heat treatment has not undergone significant changes and represents a ferritic base with the precipitates of carbides and intermetallics.

Taking into account an increased tendency to brittle fracture of heat-resistant martensitic steels after welding, the blade packages after EBW are subjected to heat treatment to relieve inner stresses and form the structure with the necessary mechanical properties.

The tempering mode for blade packages was as follows: electric furnace temperature during loading -  $T \leq 200$  °C. The heating was staged with a holding at a temperature: 1 st. — 200 °C — 2 h; 2 st. — 400 °C — 2 h; 3 st. — 600 °C — 2 h, 30 min. The tempering temperature was 680–700 °C, holding — 4.5 h.

The comparative measurements of hardness of welded joints of 18Kh11MNFb-Sh steel in the state af-

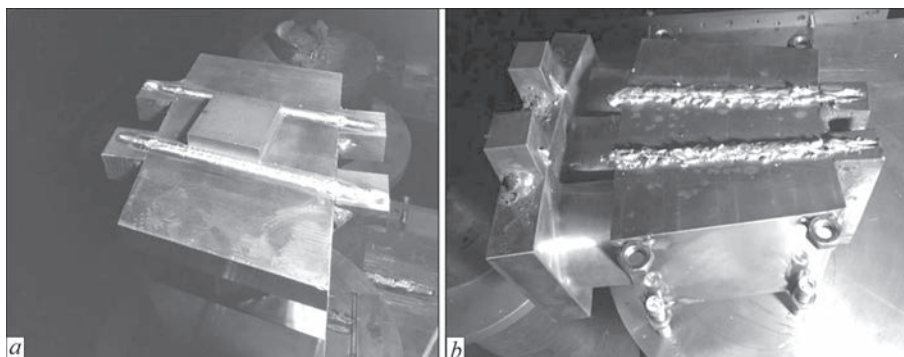


**Figure 9.** Appearance of the blade package with the tail part thickness of 120 mm, produced with the help of EBW: *a* — appearance of the bandage part of the package; *b* — appearance of the tail part of the package

ter EBW and subsequent high tempering were carried out (Figure 8).

The choice of the optimal heat treatment mode was carried out based on the results of the measurements of hardness of welded joints (in the weld and HAZ metal). After performing high tempering, the difference in the hardness of the weld metal with the base metal did not exceed 20 %, the maximum hardness of the weld metal did not exceed 350 HV1. At the same time, softening of the HAZ metal was not observed.

After receiving the optimal modes of both EBW as well as heat treatment, an experimental batch of thick-walled experimental packages of working and lock turbine blades was manufactured (Figure 9).

## CONCLUSIONS

1. The optimal thermal cycle in EBW of high-chromium martensitic steel of grade 18Kh11MNFB-Sh is provided during welding with preheating at rates of 3–5 mm/s, which makes it possible to obtain higher ductile properties of welded joints. The preheating temperature of the welded joint zone before EBW at 200–250 °C was determined.

2. The proposed and experimentally proven method of double-sided welding of steam turbine blade packages with a tail part thickness of 120 mm from 18Kh11MNFB-Sh steel allows preventing softening and formation of cold cracks and root defects in the weld zone, practically providing the equal strength of a produced welded joint.

3. The results of optimization EBW technology for thick-walled structures from heat-resistant high-alloy chromium steel allow recommending it for industrial production of modern steam turbine packages. The developed assembly and welding devices and welding technology were used in the manufacture of an experimental and industrial batch of packages of working and lock blades in the amount of 76 pieces at the order of JSC “Poltava Turbomechanical Plant”.

## REFERENCES

- Kheifets, M.L., Borodavko, V.I., Pynkin, A.M. et al. (2018) Technological process of electron beam welding of steam turbine blade package. *Naukoyomkie Tekhnologii v Mashinostroenii*, **3**, 9–13 [in Russian].
- Shorshorov, M.Kh. (1965) Physical metallurgy of welding of steels and titanium alloys. Moscow, Nauka [in Russian].
- Borodavko, V.I., Vabishchevich, P.A., Gretskeyi, N.L. et al. (2017) Application of electron beam welding in producing of steam turbine blade package. *Inzhener-Mekhanik*, **75**(2), 27–30 [in Russian].
- Nesterenkov, V.M., Nazarenko, O.K., Akopyants, K.S. (1998) Closing of circumferential welds of thick steels. In: *Proc. of 6<sup>th</sup> Int. Conf. on Welding and Melting by Electron and Laser Beams, Cisffel 6 (France, Toulon, 15–19 June 1998)*, 623–630.
- Nesterenkov, V.M., Kravchuk, L.A. (1981) Selection of parameters of circular beam rotation. *Avtomatich. Svarka*, **10**, 25–28 [in Russian].
- Nesterenkov, V.M. (2003) Application of scanning electron beam for welding to prevent root defects in thick steels. *The Paton Welding J.*, **9**, 5–10.
- Golikhov, I.V., Maslenkov, S.B. (1977) *Dendritic segregation in steels and alloys*. Moscow, Metallurgiya [in Russian].
- Shilov, G.A. (1984) *Electron beam welding of large-sized blade packages from high-chromium martensitic steels*: Thesis for Cand. of Tech. Sci. Degree. Kyiv [in Russian].
- Shilov, G.A., Sidorsky, N.A. (1978) Influence of welding parameters and electron beam focusing on formation of vertical welds in welding without backing. *Avtomatich. Svarka*, **11**, 37–40 [in Russian].

## ORCID

Yu.V. Orsa: 0000-0002-1208-4171,  
V.M. Nesterenkov: 0000-0002-7973-1986,  
V.I. Zagornikov: 0000-0003-0456-173X,  
M.O. Rusynuk: 0000-0002-7591-7169

## CONFLICT OF INTEREST

The Authors declare no conflict of interest

## CORRESPONDING AUTHOR

Yu.V. Orsa  
E.O. Paton Electric Welding Institute of the NASU  
11 Kazymyr Malevych Str., 03150, Kyiv, Ukraine.  
E-mail: orsa@technobeam.com.ua

## SUGGESTED CITATION

Yu.V. Orsa, V.M. Nesterenkov, V.I. Zagornikov, M.O. Rusynuk (2023) Use of electron beam welding for manufacture of blade packages for cogeneration steam turbines. *The Paton Welding J.*, **5**, 29–34.

## JOURNAL HOME PAGE

<https://patonpublishinghouse.com/eng/journals/tpwj>

Received: 20.04.2023

Accepted: 29.06.2023

DOI: <https://doi.org/10.37434/tpwj2023.05.06>

# FLUXLESS BRAZING OF ALUMINIUM ALLOYS BY BRAZING FILLER METAL OF Al–Ge SYSTEM

O.M. Sabadash, S.V. Maksymova

E.O. Paton Electric Welding Institute of the NASU

11 Kazymyr Malevykh Str., 03150, Kyiv, Ukraine

## ABSTRACT

The paper gives the results of investigations on fluxless brazing of AD1M, AMts (Al–Mn), AD31 (Al–Mg–Si) aluminium alloys (Al–Mg–Si) with application of Al–25Ge–5Si–5Cu–1.5Mn–0.15Ti brazing filler metal at the temperature of  $550 \pm 5$  °C in the atmosphere of high-purity nitrogen. The results of high-temperature differential thermal analysis were used to determine the solidus and liquidus temperatures of the brazing filler metal. Thermal effects on the derived thermal curve are indicative of the presence of three phases, which correlates with the results of X-ray microprobe analysis. It is shown that the brazing filler metal structure in the initial state is formed by two solid solutions, based on  $\alpha$ -Al and  $\beta$ -GeSi and eutectics. Mechanical testing revealed that the short-term strength of the brazed joints is higher than that of the base metal, and fracture occurs in AD1M alloy. Shear strength of brazed joint of AMts alloy is  $\tau_t = 82$  MPa. Application of steplike cooling of AD31 alloy brazed joint with soaking at the temperature of 500 °C promotes increase of shear strength from 84 to 102 MPa.

**KEYWORDS:** fluxless brazing, aluminium alloy, germanium brazing filler metal, nitrogen, brazed joint, shear strength

## INTRODUCTION

Brazing with aluminium brazing filler metals is used for simultaneous joining of parts and assemblies of multilayer thin-walled ( $\leq 1$  mm thickness) structure from aluminium alloys of 1000 (Al), 3000 (Al–Mn), 6000 (Al–Mg–Si) series with the aim to provide corresponding technical characteristics (strength, precision size, temperature and heat conductivity) in operation.

The main problem of manufacture of brazed structures is violation of integrity of aluminium thin-walled parts due to interaction with brazing filler metal under conditions of high-temperature heating. Existing technological processes of brazing of separate assemblies, in particular, slot antennas from aluminium alloy AMTs (A3003) with brazing filler metal of Al–Si system by means of deepening in a melt from chloride compounds [1, 2] and wave guides in dry furnace air using brazing filler metal Al–Si in form of powder mixture with flux of KCl–LiCl [3, 4] system are ecologically dangerous because of significant evaporations of toxic compounds and require considerable expenses for utilization of flux and its corrosion-active residues.

Development of brazing sheets of base metal with thin surface layer of brazing filler metals of Al–Si [5] and Al–Si–Mg [5–7] systems promoted development of furnace brazing of heat exchangers from aluminium alloys of 1000 and 3000 series in controlled medium (vacuum, purified nitrogen). Formation of joint of Al-alloy at brazing temperature 600–620 °C in vacuum differs by Si diffusion in multilayer material and balance of rates of Mg evaporation in open and closed

zones of radiator [8–10]. A disadvantage of this method is impossibility of application of corrosion-resistant coatings that contain anode protector-zinc directed on electrochemical protection of base metal by decrease of potential [10, 11].

There is information on application of aluminium brazing sheets with modified layer “brazing filler metal Al–Si–coating” [12] at furnace brazing of structures of aluminium alloys of 1000 and 3000 series in temperature interval 600–620 °C in purified nitrogen ( $p_{O_2} < 700$  Pa,  $T_{dew} = -50$  °C). In “brazing filler metal–Al–Si–coating–base metal” system the successful formation of brazed joint depends on alloying. Additives of lithium [13] and bismuth [14] reduce surface tension of brazing filler metal at the interface with base metal; multilayer electrochemical coatings from nickel [15], zinc, tin [16] in combination with non-corrosive flux KF–AlF<sub>3</sub>, which actively cleans the surface, provide high capillary properties of brazing filler metal [17, 18] and improve wetting of base metal with brazing filler metal. Microadditives of Bi and Mg in Al–10Si brazing filler metal promote quality filling of a gap in atmosphere of nitrogen of ultra-high purity ( $p_{O_2} = 10^{-25}$  Pa) [19].

Aluminium brazing filler metals of Al–(6.8–13) Si system melt at high temperature 577–613 °C (Figure 1, a) [20, 21] close to solidus temperature of alloys of 5000 (systems Al–Mg, alloy 5052 has  $T_s = 568$  °C) and 6000 (Al–Mg–Si, alloy A6061,  $T_s = 600$  °C) series [22] which has negative effect on base metal integrity and microstructure of  $\alpha$ -solid solution. For reduction of negative effect of temperature on base metal it is necessary to use elements decreasing melt-

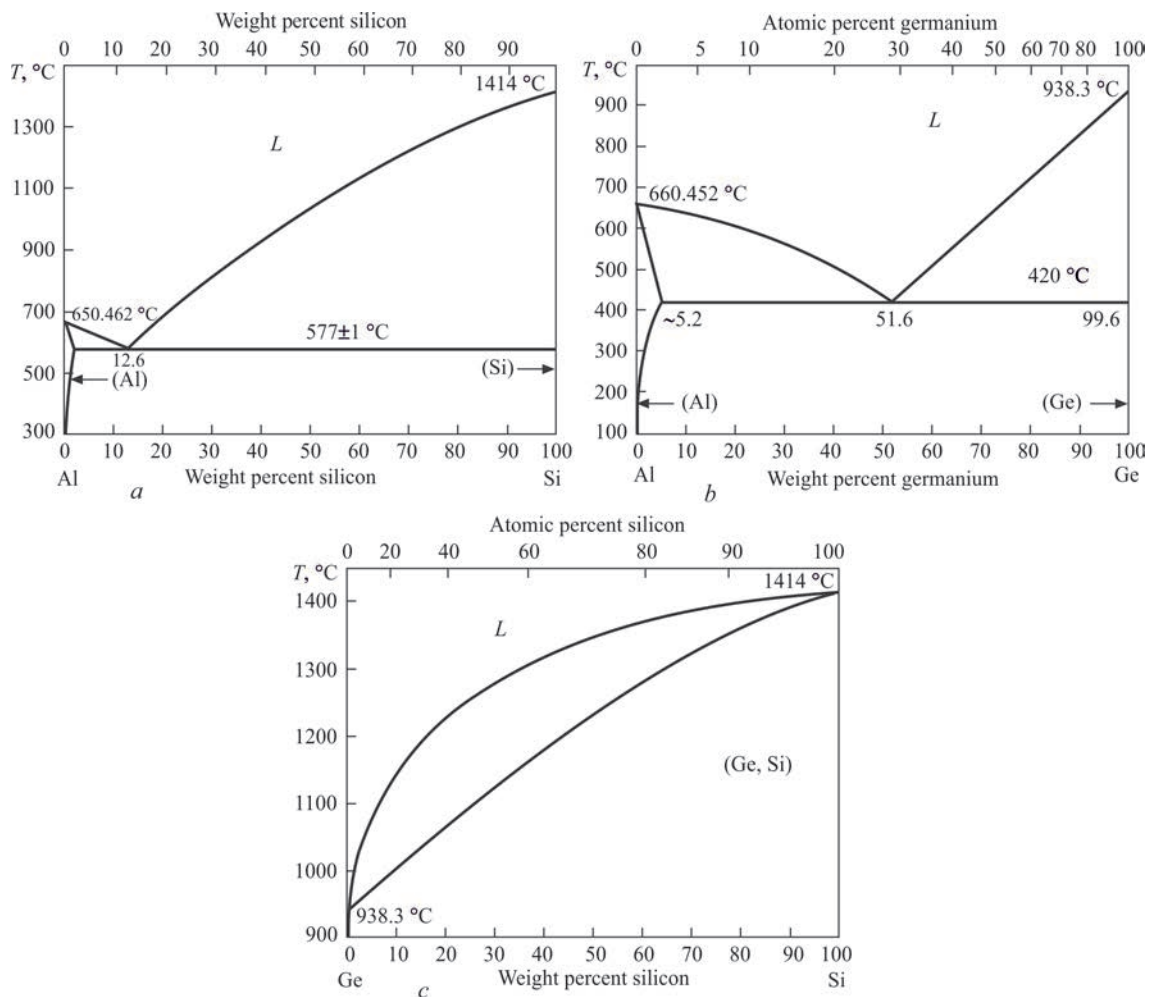


**Figure 1.** Binary diagrams of state of metallic systems: Al–Si (a); Al–Ge (b); Ge–Si (c) [20]

ing temperature of aluminium alloy to 450–550 °C (Figure 1, b).

Brazing filler metals with reduced temperature of melting are based on triple alloys of Al–Si–Me system with high content of metal-depressants (Me = Cu, Ge, Zn). In area reach with aluminium, Al–Cu–Si system contains combination of phases  $Al_2Cu$  and (Si) which are in equilibrium with solid solution based on  $\alpha$ -aluminium [23–25]. Triple eutectic Al–5Si–27Cu melts at 525 °C [23].

Volume and morphology of crystals of brittle phase  $Al_2Cu$  as a constituent of weld microstructure which is present in intergranular layer of  $\alpha$ -solid solution significantly effects a level of shear strength (40–60 MPa) of joint of alloy A6061 [26] brazed with Al–9.6Si–20Cu brazing filler metal (in vacuum at 570 °C temperature). Addition of nickel to brazing filler metal Al–9.6Si–20Cu narrows the temperature interval of melting of 73Al–20Cu–2Ni–5Si brazing filler metal, promotes enrichment of Al-solid solution with particles of phases  $Al_2Cu$ ,  $Al_6Cu_3Ni_6$  [27, 28],  $\delta$ - $Al_3CuNi(Al_3Ni_2)$  [29] and increase of shear strength.

Fluxless brazing in purified nitrogen using Al-sheet with double-layer coating Al–Si and Cu–Ni,

which at contact melting generates brazing filler metal 73Al–20Cu–2Ni–5Si, with simultaneous compression of parts at brazing temperature 540 °C rises (~ by 50 %) level of strength of brazed joints of alloys A3003, A6013, A7475 [27, 28]. However, application of compression is not always acceptable that is promoted by geometry and technological peculiarities of brazed assemblies. Flux brazing of alloy A6063 using 73Al–20Cu–2Ni–5Si brazing filler metal and chloride flux with next heat treatment (530 °C/3 h, 160 °C/3 h) promotes increase of strength (by 28 %) of joint in comparison with that using Al–6.5Si–20Cu brazing filler metal [29]. It should be noted that brazing filler metals of Al–Si–Cu system with high content of copper exceed allowable difference of potential of corrosion in relation to potential of aluminium alloys that intensifies corrosion failure of brazed joint in aggressive medium [27, 28, 30] and requires additional protective means.

Alloys of Al–Ge–Si system, studied experimentally [31] and by calculation methods [32, 33] are promising (from point of view of melting temperature) for brazing of aluminium materials. In the alloys of triple system Al–Ge–Si the areas of binary eutectic reac-

**Table 1.** Composition (wt.%) and melting temperature ( $T$ , °C) of aluminium alloys

Alloy	Si	Fe	Cu	Mn	Mg	Cr	Zn	Ti	$T_s$	$T_l$
AD1M	0.3	0.3	0.3	0.03	0.05	0.0	0.1	0.15	643	657
AMts	0.6	0.7	0.20	1.0–1.5	–	0.0	0.1	–	643	654
AD31	0.2–0.6	0.5	0.1	0.1	0.45–0.9	0.1	0.2	0.15	616	654

tions L (liquid) $\leftrightarrow$ (Al)+(Si) and L $\leftrightarrow$ (Al)+(Ge) join with the area L $\leftrightarrow$ (Al)+(SiGe) that results in decrease of melting temperature from 578 °C (~12.7 wt.% of Si) to 424 °C (~53 wt.% of Ge) [31].

Brazing filler metals of Al-Ge-Si system [34, 35] with high content of Ge (~25 %) are too expensive for most of the applications. A joint of alloy A6061 brazed with Al-12Si-(25, 35, 45)Ge-( $\leq 1$ )Mg-( $\leq 1$ )Cu brazing filler metals in vacuum at increase of temperature from 550 to 575 °C and long-term holding (~60 min) reaches strength making ~90 % of base metal strength [35]. As for alloy A5052 (Al-Si-2.2–2.8 % Mg), strength limit of joint dramatically decreases (~40 %) due to growth of available layer of brittle compound Mg<sub>2</sub>Ge in a reaction zone at interaction with Mg (from base metal) and Ge from the brazing filler material. Partial replacement of Ge by Zn in the brazing filler metal Al-9.5Si-10Ge-15Zn-0.75Sr and addition of Sr promoting refinement of  $\beta$ -(GeSi) contribute to increase of strength (by ~7 %) in the joint of alloy A6061 [36] in comparison with joint produced using the brazing filler metal Al-9.5Si-10Ge-15Zn [37] at brazing temperature 580 °C.

Acceptable melting temperature (525–565 °C) is typical for hypoeutectic alloys of Al-Si system containing zinc (10–50 wt.%) [38]. In the triple alloy Al-Si-Zn at silicon content > 1.6 wt.% it solidifies in form of acicular phase [39]. Microadditives of 0.09Sr [40], 0.06Ce and 0.08 wt.% Ti [41] refine primary crystals of (Si) phase in the brazing filler metal Al-6.5Si-42Zn. In flame flux brazing of the aluminium alloy A6061 with Al-6.5Si-42Zn-009Sr brazing filler metal at 580 °C temperature and using forced cooling of a joint in water the strength can reach ~90 % of strength limit of base metal [40]. A disadvantage of the brazing filler metals of Al-Si-Zn system is possibility to dissolve base metal (at  $T = 433$  °C ~70 wt.% of Zn [23] dissolves in Al) that can promote failure of brazed thin-walled elements of multilayer aluminium structure. Thus, development of the light-alloy brazing filler metals and methods of

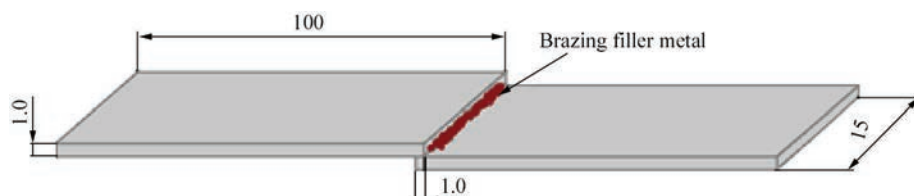
brazing at temperature lower than 550 °C is currently relevant and being in demand in manufacture of separate structures and brazed assemblies from aluminium alloys.

The aim of present work is investigation of formation of joints of aluminium alloys AD00, AMts, AD31 using light-alloy germanium brazing filler metal ( $T_1 = 500$  °C) under conditions of fluxless brazing in high-purity nitrogen medium.

## MATERIALS AND INVESTIGATION PROCEDURE

The samples for investigations were made from aluminium alloys AD1, AMts and profile of alloy AD31 of 1 mm thick (Table 1).

A brazing filler metal of Al-Ge-Si-Cu system with Mn and Ti additives was made using induction melting in pure argon medium of metals (99.95Al, 99.95Cu, Ge polycrystalline) and addition alloys (Al-12Si, Al-2Ti, Al-10Mn) at temperature 700 °C in a crucible from fine-graphite of MPG-7 grade. Obtained alloy was poured in a copper mould at 570–580 °C temperature. Temperatures of solidus ( $T_s$ ) and liquidus ( $T_l$ ) of the brazing filler metal was determined by thermal differential analysis (TDA) using VDTA-8M3 unit under heating-cooling conditions ( $V = 40$  °C/min) in helium medium. Preliminary an assembly (alloy of 1 g weight, thermal couple KhA of  $D = 0.1$  mm, alundum crucible) was calibrated at temperature of pure metals (Al, Zn, Sn) solidification. The aluminium samples were cleaned before brazing: degreasing in solution 15 % NaOH,  $R = 50$ –55 °C,  $t = 60$  s; etching in solution 20 vol.% of HNO<sub>3</sub>, 2 vol.% HF,  $t = 60$  s, rinsing between the operations in hot ( $T = 60$ –65 °C) and cold ( $T = 8$ –22 °C) water of double distillation. Brazing of the samples (Figure 2) with lap size 1 mm was carried out at  $550 \pm 5$  °C temperature and holding  $t \leq 2.5$  min in flow nitrogen (99.999 vol.% N<sub>2</sub>, 0.0005 vol.% O<sub>2</sub>, 0.0007 vol.% H<sub>2</sub>O) using a brazing paste (powder of brazing filler metal, coupling liquid — laprol 6003-2B-18).


**Figure 2.** Sketch of lap joint

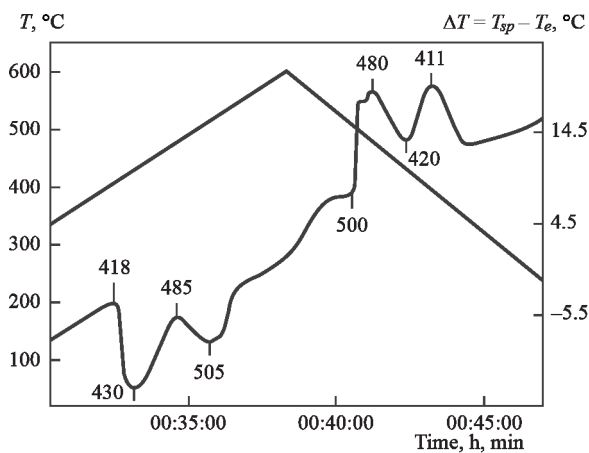


**Figure 3.** DTA thermogram of brazing filler metal Al-25Ge-5Si-5Cu-1.0Mn-0.15Ti

After heating turn down there was used a step-by-step cooling mode with holding at liquidus temperature of the brazing filler metal (500 °C) during 15 min.

Microstructure of the brazing filler metal in initial condition and in brazed joints of aluminium alloys was examined using scanning electron microscope JSM-840 with X-ray microprobe analyser Camebax SX50. Tensile tests were used in order to determine

shear strength of the brazed joints at room temperature with set speed ( $V = 1$  mm/s) of tensile machine grip travel.

## INVESTIGATION RESULTS AND DISCUSSION

The results of high-temperature differential thermal analysis showed the temperatures of solidus and liquidus of brazing filler metal Al-25Ge-5Si-5Cu-1.0Mn-0.15Ti (Figure 3). Heat effects on the obtained thermal curve indicate presence of three phases, temperature interval of melting of which lies in  $T = 418\text{--}505$  °C range.

It is necessary to note that a heat effect from eutectic component is weakly expressed that is caused by its amount. Microstructure investigations of Al-25Ge-5Si-5Cu-1.0Mn-0.15Ti brazing filler metal showed that the crystals of  $\beta$ -solid solution  $\text{Si}_x\text{Ge}_y$  are in equilibrium with  $\alpha$ -Al solid solution (grey colour) in a cast state. The solid solutions form separate areas with eutectic component which is a mesh from lamellar crystals of white colour precipitated on the boundaries of grains of solid solution based on al-

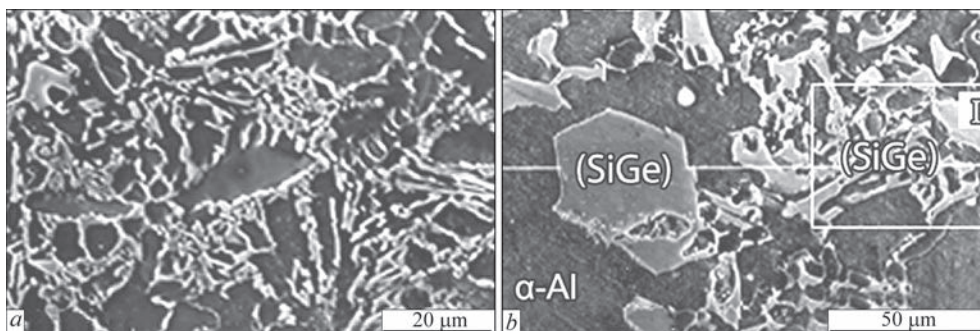


**Figure 4.** Microstructure of brazing filler metal 63.6Al-25Ge-5Si-5Cu-1.5Mn-0.15Ti: *a* — in cast state; *b* — in state of annealing by mode (400 °C/15 min)

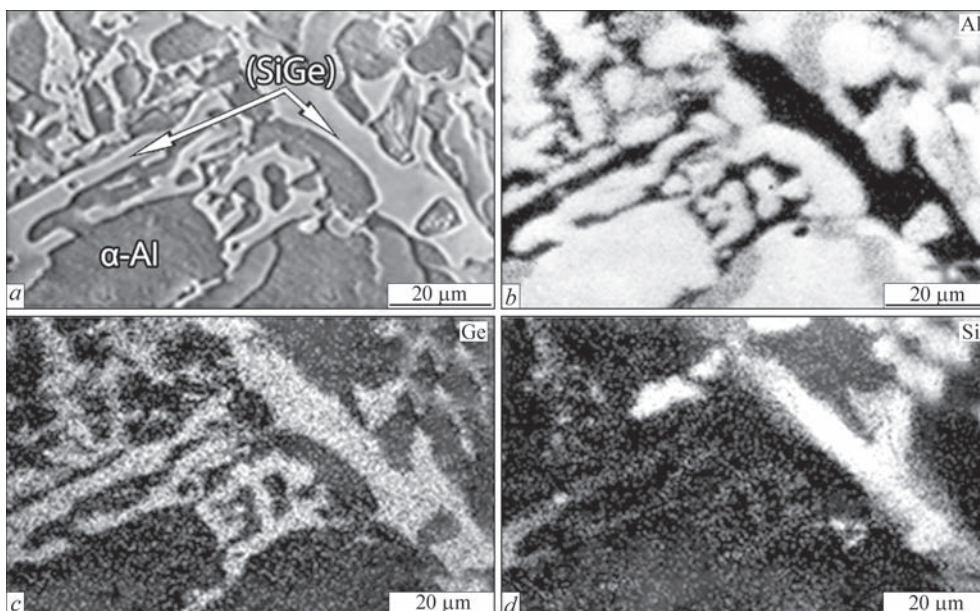


**Figure 5.** Electron image (*a*) of microstructure of brazing filler metal and maps of distributions of elements Al (*b*), Ge (*c*), Si (*d*)

uminium (Figure 4, *a*). Obtained data are well correlated with corresponding binary diagrams of state of metallic systems (Figure 1, *b, c*). Besides separate particles of germanium-based phase of  $\sim 40 \mu\text{m}$  size were found in the brazing filler metal: 6.65Al–87.65Ge–4.8Si–0.73Cu–0.17Mn–0.2Ti

The alloys of Al–Ge and Al–Si systems are characterized by minimum melting temperature in eutectic formation and the alloys of Si–Ge system differ by presence of the continuous solid solutions of alternating concentration (Figure 1, *c*) and higher melting temperature [20].

Content of aluminium, germanium and silicon in the brazing filler metal indicates the area of triple diagram Al–Si–Ge [31] with reaction  $L \leftrightarrow (\text{Al}) + (\text{Si}_x\text{Ge}_y)$  where the next constituents exist in equilibrium, namely liquid phase, aluminium solid solution,  $\beta$ -phase ( $\text{Si}_x\text{Ge}_y$ ). Cooling (4 K/min) of the alloys of Al–Ge–Si system promotes formation of lamellar crystals of  $\text{Si}_x\text{Ge}_y$  phase with different weight relationship of Si/Ge [31].

The results of X-ray microanalysis determined that annealing promotes the following phases in the brazing filler metal, namely solid solution based on

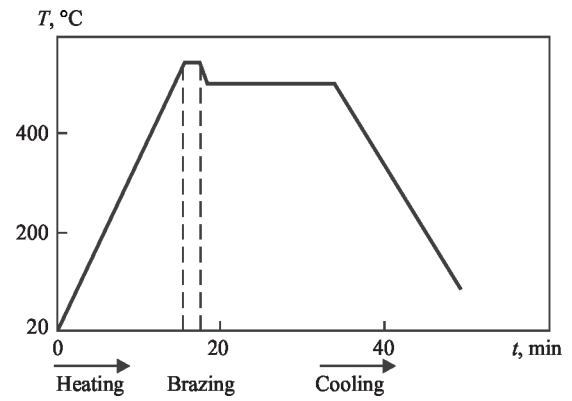


**Figure 6.** Thermal cycle of brazing by brazing filler metal of Al–Ge–Si–Cu system of aluminium alloys in nitrogen of high purity aluminium 93Al–4.6Ge–0.1Si–1.4Cu–0.07Mn–0.01Ti ( $\alpha$ -Al), crystals of phase  $\text{Si}_x\text{Ge}_y$  that contain 0.40Al–42.85Ge–56.58Si–0.17Cu (Mn, Ti traces), eutectic component and phase based on germanium 39.44Al–59.05Ge–0.67Si–0.84Cu (Mn, Ti traces) (Figure 4, *b*). After annealing it is possible to observe increase of sizes of the grains of  $\text{Si}_x\text{Ge}_y$  phase in comparison with initial condition. They are characterized by alternating concentration of component elements. Work [42] indicates that in the alloys of Al–18Si– $x$ Ge system at Ge content up to 60 % the grains of prima-

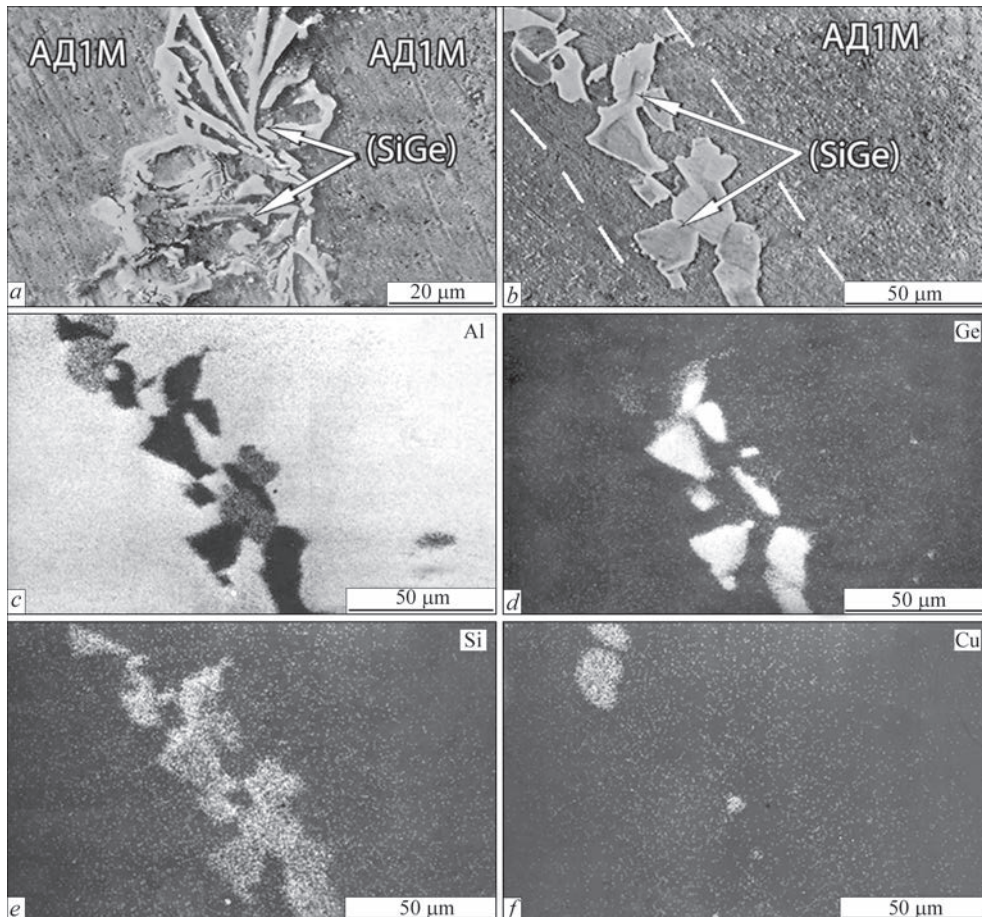


**Figure 7.** Electron image of microstructure of brazed weld of alloy AD1M in initial condition after brazing (*a*), after step-by-step cooling (*b*) and maps of distribution of chemical elements: aluminium (*c*), germanium (*d*), silicon (*e*) and copper (*f*) in application of Al–25Ge–5Si–5Cu–1Mn–0.15Ti brazing filler metal

ry phase ( $\text{Si}_x\text{Ge}_y$ ) become sufficiently coarse and can have size of several hundred micrometers.

Mapping of microstructure of brazing filler metal (Figure 5, *a*) allowed determining separate phases which contain increased concentration of aluminium (Figure 5, *b*), germanium (Figure 5, *c*) and silicon (Figure 5, *d*) that correlate with quantity determination of composition of separate phases.

Heating of the aluminium samples to temperature  $550 \pm 5$  °C that exceeds liquidus temperature of the brazing filler metal by 50 °C (with 1.5–2 min holding) in high purity nitrogen medium using germanium brazing filler metal provides its melting and wetting of base metal. Cooling in keeping with thermal cycle (Figure 6) provokes formation of the brazed joints of aluminium alloys AD1M, AMts, AD31 with full penetration.

Using X-ray microanalysis there was examined a structure of the joint from AD1M alloy after brazing (Figure 7, *a*) and after step-by-step cooling mode (Figure 7, *b*). It was determined that the structure of brazed weld from alloy AD1M contains  $\alpha$ -solid solution based on aluminium; lamellar crystals of  $\beta$ -phase ( $\text{Si}_x\text{Ge}_y$ ) and low melting eutectic component.

Obtained results of the investigation showed that composition of metal of the brazed weld has little difference from composition of the brazing filler metal in initial condition. Concentration of elements in  $\alpha$ -Al solid solution 94.22Al–3.79Ge–0.9Si–85Cu–0.02Ti–0.26Mn virtually does not change. In eutectic (39.44Al–59.05Ge–7.11Si–0.84Cu) there is insignificant increase of silicon concentration from 0.67 to 7.11 % and change of morphology of crystals of ( $\text{Si}_x\text{Ge}_y$ ) phase from lamellar to faceted and increase of their size (Figure 7, *b*).

Mechanical tensile tests (at room temperature) allowed determining that strength of the overlap brazed samples from alloy AD1M is higher than the strength of base metal, failure takes place on AD1M base metal, but not on the brazed weld. Short-term shear strength of the joint from alloy AMts makes 82 MPa. And shear strength of the brazed joint from alloy AD31 after step-by-step cooling with holding at brazing filler metal liquidus temperature (500 °C/15 min) rises from 84 to 102 MPa.

## CONCLUSIONS

There were determined the temperature-time modes ( $T_m = 550 \pm 5$  °C,  $t \leq 2$  min) of formation of quality joint from aluminium alloys AD1M, AMts and AD31 at fluxless brazing using brazing filler metal Al–25Ge–5Si–5Cu–1Mn–0.15Ti in high purity nitrogen.

X-ray microanalysis determined that after brazing the structure of brazed weld of joint from aluminium alloy (AD1M) contains two solid solutions, namely based on aluminium ( $\alpha$ -Al) and based on  $\beta$ -phase ( $\text{Si}_x\text{Ge}_y$ ) which form eutectic component.

The results of mechanical tests (at room temperature) proved that strength of the brazed weld from alloy AD1M is higher than the strength of base metal ( $\sigma_t = 60$  MPa). Shear strength of the brazed joint from alloy AMts makes 82 MPa.

Application of step-by-step cooling for the brazed joint from alloy AD31 promotes increase of shear strength from 84 to 102 MPa.

## REFERENCES

- Dudley, D.A., Perry, E.R. (1996) *Flux bath brazing — an engineering technique*. Park Thermal INT'L. Corp. 17.
- Storchay, E.I. (1980) *Flux brazing of aluminium*. Moscow: Mechanical engineering.
- Balashov, V.M., Pashkov, I.N., Kaplunov, A.A. (2009) High-temperature filler metal pastes for brazing complex waveguide structures. Questions of radio electronics. *General Technical Series*, **3**, 89–98.
- Balashov, V.M., Semenova, E.G., Liu, Ch.Ts. (2010) Resource-saving technologies for high-temperature brazing of complex-shaped antenna structures in electric furnaces. In: *Proc. of IV All-Russian Conf. on Radiolocation and Radio Communication — IRE RAS, November 29 – December 3, 2010, Moscow*, 826–838.
- Yoon, J.S., Lee, S.H., Kim, M.S. (2001) Fabrication and brazeability of three-layer 4343/3003/4343 aluminium clad sheet by rolling. *J. of Materials Processing Technology*, **111**, 85–89.
- Ohashi, Y., Gotou, A., Suzuki, Y., Yanagawa, Y. (2014) Flux-free brazing using brazing sheets with thin aluminium layer. *J. of the Japan Institute of Light Metals*, **64**(4), 137–141.
- Hattori, T., Sakai, S., Sakamoto, A., Fujiwara, C. (1994) Brazeability of aluminium in vacuum-nitrogen partial-pressure atmosphere brazing. *Welding Journal*, **10**, 233–240.
- Bernardi, C., Hazotte, A., Siredey-Schwaller, N. et al. (2014) Microstructure evolution in an aluminium clad sheet during vacuum brazing. *Vacuum Brazing Materials Science Forum*, 355–360. DOI: 10.4028/www.scientific.net/MSF.790-791.355
- Yiyu, T., Zhen, T., Jianqing, J. (2013) Effect of microstructure on diffusional solidification of 4343/3005/4343 multilayer aluminium brazing sheet. *Metallurgical and Materials Transactions A*, **44A**, 1760–1766. DOI: 10.1007/s11661-012-1550-5
- Bordo, K., Chakravarthy, V., Peguet, L., Afseth, A. (2018) Electrochemical and microstructural characterization of multi-clad aluminium brazing sheets. *Corrosion Science*, **131**, 28–37.
- Pech-Canul, M.A., Guía-Tello, J.C., Pech-Canul, M.I. et al. (2017) Electrochemical behavior of tube-fin assembly for an aluminium automotive condenser with improved corrosion resistance. *Results in Physics*, **7**, 1760–1777. DOI: 10.1016/j.rinp.2017.05.008
- Harksworth, D.K. (2013) Fluxless brazing of aluminium. *Advances in brazing. Science Technology and Applications*, Oxford, 566–585.
- Childree, D.L. (1996) A new Al–Si–Li filler metal that enhances brazeability of high-strength alloys in CAB and vacuum. *J. of Materials & Manufacturing*, **105**(5), 248–256.

14. Ohashi, Y., Gotou, A., Suzuki, Y., Yanagawa Y. (2014) Flux-free brazing using brazing sheets with thin aluminium layer. *J. of the Japan Institute of Light Metals*, **64**(4), 137–141.
15. Graham, M.E., Hoffman, R.A., Hoffman, M.A. (2005) *Fluxless brazing method and method for manufacturing layered material systems for fluxless brazing*. Pat. 6959853 US. B2K 31/02. Pub. Data: Nov. 01.2005.
16. Mooij, J.N., Wittebrood, A.J., Olga, J.H.J. (2002) *Brazing sheet product and method of its manufacture*. Pat. 6379818 US B32B 15/20; C25D 5/44; B32K 35/28. Pub. Data: Apr. 30 2002.
17. Swidersky, H.W. (2001) Aluminium brazing with non — corrosive fluxes — state of the art and trends in NOCOLOK flux technology. In: *Proc. of 6<sup>th</sup> Inter. Conf. on Brazing, High Temperature Brazing and Diffusion Bonding (LÖT 2001), May 2001, Aachen, Germany*, 164–169.
18. Yu, C.N., Hawksworth, D., Liu, W., Sekulic, D.P. (2012) Al brazing under severe alterations of the background atmosphere: A new vs. traditional brazing sheet. In: *Proc. of 5<sup>th</sup> Inter. Brazing and Soldering Conf., IBSC, April 22–25, 2012, Vegas, Nevada*. US, ASM International.
19. Shinoda1, T., Ozawa, S., Kawashima, K. et al. (2022) Flux-free brazing of aluminium alloys under ultra-low oxygen partial pressure through a zirconia oxygen pump. *Materials Transact.*, **63**(10), 1477–1483.
20. Massalski, T.B. (1990). *Binary alloy phase diagrams, american society for metals*. Ohio, Metals Park, ASM International, CD.
21. Schwartz, Mel. M. (2003) *Brazing*. Second Ed. ASM International® Materials Park, Ohio.
22. Mills, C.K. (2002) *Recommended values of thermophysical properties for selected commercial alloys*. Woodhead Publ. Ltd. and ASM International. Cambridge.
23. Mondolfo, L.F. (1976) *Aluminium alloys: Structure and properties*. London, UK.
24. Belov, N.A. (2009) *Phase composition of aluminium alloys*. Moscow.
25. Morandoa, C., Fornaro, O. (2018) Morphology and phase formation during the solidification of Al–Cu–Si and Al–Ag–Cu ternary eutectic systems. *Materials Research* **21**(2). DOI: <http://dx.doi.org/10.1590/1980-5373-MR-2017-0930>
26. Chang, S.Y., Tsao, L.C., Li, T.Y., T Chuang. H. (2009) Joining 6061 aluminium alloy with Al–Si–Cu filler metals. *J. of Alloys and Compounds*, **488**, 174–180.
27. Humpston, G., Sangha, S.P., Jacson, D.M. (1995) New fillet metals and process for fluxless brazing of aluminium engineering alloys. *Materials Science and Technology*, **11**, 1161–1167.
28. Jacobson, D.M., Humpston, G., Sangha, S.P. (1996) A new low-melting-point aluminium braze. *Welding J.*, **75**(8), 243–250.
29. Peng, C., Zhu, D., Li, K. et al. (2021) Research on a low melting point Al–Si–Cu(Ni) filler metal for 6063 aluminium alloy brazing. *Applied Sciences*, **11**, 4296. DOI: <https://doi.org/10.3390/app11094296>
30. Wang, S.S., Cheng, M.D., Tsao, L.C., Chuang, T.H. (2001) Corrosion behavior of Al–Si–Cu–(Sn, Zn) brazing filler metals. *Materials Characterization*, **47**, 401–409.
31. Song, H., Hellawell, A. (1990) Solidification in the system Al–Ge–Si. The phase diagram, coring patterns, eutectic growth, and modification. *Metallurgical Transact. A*, **21A**, 734–740.
32. Ohmiya, M., Ohsasa, K., Ohmi, T., Kudon, M. (1991) Calculation of equilibrium phase diagram of Al–Ge–Si ternary system. *Bulletin of the Faculty of Engineering Hokkaido University*, **156**, 11–19.
33. Hayes, F.H., Longbottom R.D., Ahmad, E., Chen G. (1993) On the Al–Si, Al–Ge, and Al–Ge–Si systems and their application to brazing in high power semiconductor devices. *J. Phase Equilibria*, **14**, 425–431.
34. Niu, Z., Huang, J., Chen, S., Zhao, X. (2016) Effects of germanium additions on microstructures and properties of Al–Si filler metals for brazing aluminium. *Transact. Non-ferrous Met. Soc. China*, **26**, 775–782. DOI: [10.1016/S1003-6326\(16\)64167-5](https://doi.org/10.1016/S1003-6326(16)64167-5)
35. Kayamoto, T., Kim, J.H., Saito, S., Onzawa, T. (1994) Brazing of Al–Mg Alloy and Al–Mg–Si Alloy with Al–Ge Based Filler Metals. *Proceedings of Workshop of the Japanese Welding Society*, **12**, 495–501.
36. Niu, Z., Huang, J., Chen, S., Zhao, X. (2017) Influence of Sr additions on microstructure and properties of Al–Si–Ge–Zn filler metal for brazing 6061 aluminium alloy. *J. of Materials Research*, **32**(4), 822–830. DOI: <https://doi.org/10.1557/jmr.2016.467>
37. Niu, Z., Huang, J., Yang, H. et al. (2015) Preparation and properties of a novel Al–Si–Ge–Zn filler metal for brazing aluminium. *J. of Materials Engineering and Performance*, **24**, 2327–2334.
38. Suzuki, K., Kagayama, M., Takeuchi, Y. (1993) Eutectic phase equilibrium of Al–Si–Zn system and its applicability for lower temperature brazing. *Light Metal*, **43**, 533–538.
39. Chen, R.Y., Willis, D.J. (2005) The behavior of silicon in the solidification of Zn–55Al–1.6Si coating on steel. *Metallurgical and Materials Transact.*, **36A**, 117–128.
40. Dai, W., Xue, S., Ji, F. et al. (2013) Brazing 6061 aluminium alloy with Al–Si–Zn filler metals containing Sr. *Inter. J. of Minerals, Metallurgy and Materials*, **20**(4), 365–370. DOI: [10.1007/s12613-013-0736-1](https://doi.org/10.1007/s12613-013-0736-1)
41. Yang, J., Xue, S., Dai, W., Xue, P. (2015) Saturation phenomenon of Ce and Ti in the modification of Al–Zn–Si filler metal. *Inter. J. of Minerals, Metallurgy and Materials*, **22**(2), 184–189. DOI: <http://dx.doi.org/10.1007/s12613-015-1059-1>
42. Zhang, Y., Gao, T., Liu, X. (2014) Influence of Ge content on the microstructure, phase formation and microhardness of hypereutectic Al–Si alloys. *J. of Alloys and Compounds*, **585**, 442–447. DOI: <http://dx.doi.org/10.1016/j.jallcom.2013.09.180>

#### ORCID

O.M. Sabadash: 0000-0002-9582-8673,  
S.V. Maksymova: 0000-0003-0158-5760

#### CONFLICT OF INTEREST

The Authors declare no conflict of interest

#### CORRESPONDING AUTHOR

S.V. Maksymova  
E.O. Paton Electric Welding Institute of the NASU  
11 Kazymyr Malevych Str., 03150, Kyiv, Ukraine.  
E-mail: maksymova.svitlana15@ukr.net

#### SUGGESTED CITATION

O.M. Sabadash, S.V. Maksymova (2023) Fluxless brazing of aluminium alloys by brazing filler metal of Al–Ge system. *The Paton Welding J.*, **5**, 35–41.

#### JOURNAL HOME PAGE

<https://patonpublishinghouse.com/eng/journals/tpwj>

Received: 18.04.2023

Accepted: 29.06.2023

DOI: <https://doi.org/10.37434/tpwj2023.05.07>

## 3D TECHNOLOGY OF GROWING SINGLE-CRYSTAL INGOTS IN THE FORM OF HOLLOW TUNGSTEN CYLINDERS

**Yu.O. Nykytenko, V.O. Shapovalov, V.V. Yakusha, O.M. Gnizdylo, O.V. Karuskevych**

E.O. Paton Electric Welding Institute of the NASU  
11 Kazymyr Malevych Str., 03150, Kyiv, Ukraine

### ABSTRACT

The paper presents the results of further development of the technology of growing superlarge single-crystals of refractory metals, developed at PWI of the NAS of Ukraine. Proceeding from the optimized technology and acquired experience, new generation equipment was manufactured, which allows growing single-crystals of refractory alloys in the form of a body of revolution. Experiments were performed on growing tungsten single-crystals in the form of a hollow cylinder, which can be used to manufacture such a product as a crucible. Technological parameters and energy modes were established, which allowed controlling the thickness of the wall being deposited. As a result of the experiments, an ingot with the deposited wall height of 68 mm, thickness of 20–22 mm and outer diameter of 85 mm was grown.

**KEYWORDS:** tungsten, single-crystal growing, hollow body of revolution, crucible, plasma-induction zone melting

### INTRODUCTION

Today in Ukraine and abroad, there is a need for single-crystals of refractory compounds ( $YAlO_3$ ,  $Y_2Al_5O_3$ ,  $LiCaF$ ,  $YLiF_4$  etc.), alloyed with rare earth elements (Nd, Ce etc.) for the production of powerful solid state lasers and hypersensitive scintillators. The LED industry is developing rapidly, in particular, the production of ultraviolet LEDs, which requires an expansion of production of single-crystals of aluminium nitride. Most of the abovementioned crystals are grown from the liquid phase with the use of crucibles [1, 2], which minimize melt contamination, provide high operating temperatures, etc. Quartz, alundum, graphite, platinum, molybdenum, tantalum or tungsten are predominantly used for the manufacture of crucibles. Taking into account the set of physico-chemical properties of the mentioned series of materials, tungsten most fully meets the requirements for high-temperature use when growing oxides and nitrides of certain metals with a melting point higher than 1800 °C. In addition, tungsten has the lowest coefficient of linear thermal expansion, which is very important when using crucibles in nonstationary thermal conditions [3, 4].

Traditionally, industrial production of crucibles from tungsten is associated with the technology of powder metallurgy. A significant disadvantage of such products is a low density of cermet tungsten (18.0–18.5 g/cm<sup>3</sup>) compared to the density of tungsten in a remelted state (19.20–19.25 g/cm<sup>3</sup>). The density of the crucible material determines its stability (amount of heat changes). Unlike density, more significant factor, affecting the stability of the crucible is its structure. During the technological process, in

the polycrystalline structure of the walls of a tungsten crucible, as a result of cyclic processes of heating (cooling), recrystallization processes acquire a significant development, that cause the appearance and development of crevices, which leads to the destruction of the inner part of the crucible, especially on the boundary melt-atmosphere. An even greater problem in a sintered cermet tungsten is the penetration of melt into the crevices. A melt that gets to the powder metal crevices leads to the destruction of the inner surface of the crucible. This process has an uncontrolled avalanche nature, after the destruction of the first layer, a crack arises that propagates rapidly in the wall of the crucible. In addition to mechanical destruction, there is a chemical interaction of highly-reactive elements of the melt with the material of the crucible, which leads to the contamination of the melt and a rapid wear of the crucible.

Solving the problem of improving the stability of tungsten crucibles lies in the direction of creating a defect-free, dense and homogeneous structure.

It is known that at thermocyclic loads, single-crystalline tungsten has a high stability of the structure and is accompanied by a much smaller change in shape than polycrystalline one. Compared to polycrystalline specimens, in the single-crystal, the processes of high-temperature grain boundary diffusion of defects of crystalline structure are inhibited. The stability of the geometric shape of single-crystalline parts is associated with a more improved structure, high purity and density, which affects the stability of the thermal field and temperature gradient on the crystallization front of the melt.

Tungsten single-crystals produced by plasma-arc technology, are up to 40 mm in diameter in the intersection and have large inner stresses, which sometimes

lead to the formation of crevices [5]. This makes it impossible to manufacture large-sized products from them, especially hollow cylinders.

In principle, the problem of growing large-sized tungsten single-crystals has been successfully solved at the PWI. A unique plasma-induction method of growing superlarge single-crystals of refractory metals (W, Mo) was offered. The latest technological equipment was developed and the technology of growing the largest in the world flat crystals of tungsten with the sizes 170x160x20 mm was optimized [6, 7].

Many years of experience became the basis for the creation of the latest 3D plasma-induction installation for growing tungsten single-crystals in the form of bodies of revolution (Figure 1) [8]. However, the technology of growing single-crystals in the form of bodies of revolution, especially hollow ones, has significant differences from the technology of growing profiled single-crystals in the form of plates. While growing single-crystal in the form of a plate, the inductor covers a single-crystal with a certain space and heats the surface of the single-crystal throughout the whole perimeter. In addition to heating, another important function of the inductor is maintaining a metal pool from leakage, i.e., providing its spatial stabilization. In the case with growing single-crystals in the form of hollow bodies, the inductor heats only the outer side surface of the crucible. The inner surface of the crucible is not heated by the inductor, and the metal pool is maintained by the surface tension forces. This imposes some complications in the technology development. Therefore, growing single-crystalline crucibles using 3D plasma-induction technology requires a comprehensive study.

In this sense, the aim of the work to create technological foundations for the production of single-crystals from tungsten is relevant.

### TECHNOLOGICAL EQUIPMENT, MATERIALS AND PROCEDURE OF EXPERIMENTS

The equipment created at PWI is the next generation of equipment, which is distinguished by a computerized system for control of mechanisms, sensors of movement for stepper motors, and monitoring the process of single-crystal growth. During the design, the possibility of growing single-crystals in the form of bodies of revolution is provided: an ingot or a hollow cylinder with an outer diameter of up to 100 mm (4 inches). Regarding the development of technological fundamentals, optimizing the technology of growing tungsten single-crystals will occur for the crucibles of 85 mm diameter. On the one hand, in the thermophysical aspect, the technology almost

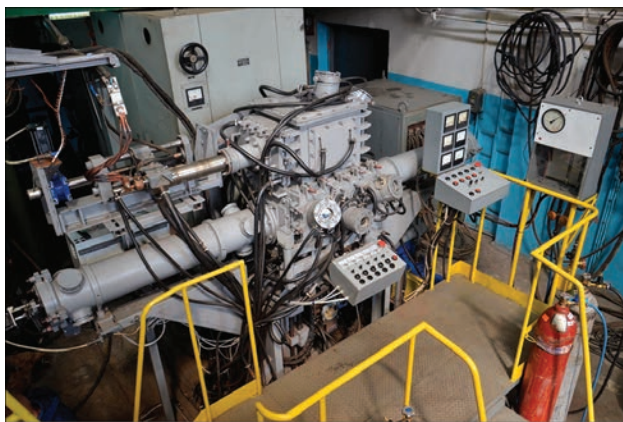


**Figure 1.** Equipment for growing tungsten single-crystals in the form of bodies of revolution

does not differ from the crucible with a diameter of 100 mm or more, and on the other hand, the resources in the form of consumables (tungsten, pure inert gases, etc.), power and time are saved.

In principle, 3D technology of growing hollow single-crystals in the form of bodies of revolution takes into account the basic technological approaches to the process of growing profiled single-crystals in the form of plates: layer-by-layer forming of a product on a single-crystalline embryonic crystal. The difference is the following. When growing single-crystalline plates, the layers are grown by a gradual movement of the plasmatron. The crystal is lowered down periodically after the formation of a layer is completed and in this case to form the next layer, the consumed rods are supplied alternately from each cassette. The difference in the work of the new installation while forming the crucible is the fact that the crucible rotates constantly around the vertical axis, the plasmatron is not moving, and the consumed rod is continuously supplied into the metal pool zone. In such a way, a gradual 3D surfacing by a local pool of layers on the embryonic crystal is carried out. Layer-by-layer forming of a single-crystal by moving the local pool has some advantages. The constant rate and direction of completion offsets the possible deviations of a set crystallographic axis of crystal growth, which is usually observed when growing axisymmetric crystals, when the pool is not local, but covers the whole horizontal section of the crystal. The cause of deviation of the axis of cylindrical crystals may be incomplete symmetry of the heat flux of the heating source and conditions of heat removal of the single-crystal surface.

When using 3D technology, the crystal is formed in a controlled way. The temperature field in the area of forming the crystal in the plasma-induction method of growing is determined by the total action of heat fluxes from the plasmatron and high-frequency inductor. The pattern of the temperature field in the body of the crystal depends on the ratio of power parameters

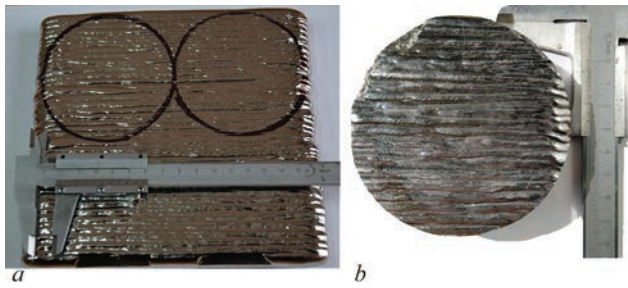


**Figure 2.** Tungsten single-crystal (a) and embryonic crystal that is cut out of it for growing crystals in the form of bodies of revolution with a diameter of 85 mm (b)

of heating sources and their spatial position relative to the grown single-crystal.

One of the determining factors in producing high-quality single-crystals without rough deviations from a set geometric shape is the invariance of liquid metal pool geometry in the process of growing. Based on these technological prerequisites, as a criterion that determines the ratio of capacities introduced by plasma-arc and induction sources of heating to the body of single-crystal, invariability of metal pool diameter was accepted.

As an embryonic crystal, a flat crystal with a set orientation of crystalline planes grown at PWI was used. From it discs were cut out (Figure 2). One of

the discs was fixed on the bottom-plate and centered relative to the inductor with a certain space.

## RESULTS OF EXPERIMENTS AND THEIR ANALYSIS

The first task when growing tungsten single-crystals in the form of hollow bodies of revolution was to establish the dependence of the influence of technological parameters on the diameter of the liquid pool, i.e., the wall thickness to be formed. While conducting experiments with the determination of the parameters of the plasmatron work, the effect of the current on the width of the pool was investigated, which had to form a wall of the crucible during a continuous rotation of the embryonic crystal (Figure 3).

Changing the power of the plasma-arc heating source, the diameter of the metal pool on the embryonic crystal was visually fixed, which continuously rotated in the horizontal plane. With the help of photographing, all stages of forming concentric circles were recorded. After a full revolution, the current was changed, which allowed a clear measurement of the pool width. The rate of revolution of the embryonic crystal was 30 deg/min, which was approximately the linear speed of the pool center of 14 mm/min. The power parameters of the experiment: current change from 300 to 600 A, arc voltage — 38–42 V, power of additional induction heating — 105–110 kW (anode power of the HF tube). As the experiments showed, the pool began to form at the plasmatron current of only 400 A. The displacement of the plasmatron from the axis of rotation of the embryonic crystal was 24 mm. The effect of the current on the width of the liquid pool on the embryonic crystal was investigated and, as a result, a dependence was obtained (Figure 4). However, at a further growing of the wall of the hollow cylinder and an increase in the height of the ingot, power parameters (arc current and induction heating) should rise. This is associated with an increase in the mass of the crystal to be maintained in a heated state and an increase in the radiation surface and heat losses.

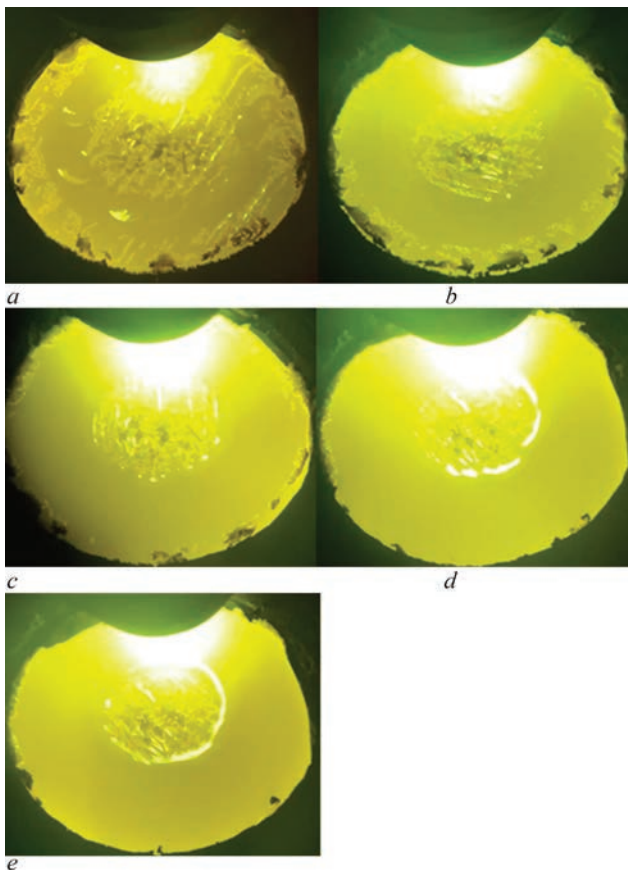


**Figure 3.** General appearance of the liquid tungsten pool, depending on current, A: a — 400; b — 450; c — 500; d — 550; e — 575

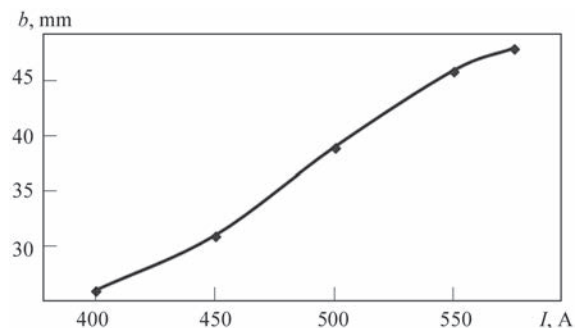


**Figure 4.** Effect of plasmatron current on the width of a metal pool

The final appearance of the surface of the embryonic crystal after the experiments and melting of the central part to align the entire upper part is shown in Figure 5.

Based on the experience of growing flat and cylindrical tungsten single-crystals, the diameter of the local pool was maintained at 22 mm. The formation of a single-crystalline crucible was carried out as a result of scanning by a local pool along the concentric trajectories in the plane of growing with an average radius of 30–31 mm. Calibrated tungsten rods with a diameter of 8 and 800 mm long (about 650 mm is remelted), with the purity of 99.95 wt.% were used to power the pool (Table 1). Previous studies have shown that refining and contamination of tungsten during plasma-induction zonal melting does not occur. Melting modes were optimized on the condition of stability of the ratio of the linear speed of the local pool and the rate of rod feed.

The process of growing ingots in the form of hollow cylinders was performed for the first time, so its study was divided into three stages. At each stage, a set quantity of single-crystal layers were grown. After completing the task of the stage, the process was stopped, the crystal was investigated and then mounted on the bottom-plate and growing of the following layers was continued. This approach made it possible to study in detail the processes of forming individual layers, to optimize the technology of positioning ingot and plasmatron during stops, to investigate the heredity of the crystalline structure and defect arising. The crystal was removed between the melts, etching by



**Figure 5.** Outer surface of the embryonic crystal before the experiments on growing the walls of the hollow single-crystalline cylinder

chemical reagents of the upper, outer and inner surfaces was performed.

After the first tests, two consumable rods were remelted, which made approximately six cylindrical layers. As a result, when optimizing the process of growing a hollow cylinder, a wall of 20–22 mm thick was produced and approximately 13–15 mm high. The technological scheme and the process of drop transfer of the melt is shown in Figure 6.

The peculiarity of the latest technology is the fact that when growing the outer side of the crucible, which is formed from a liquid state in the field of high-frequency electromagnetic field, is subjected to a strong effect of the field that maintains the metal pool and forms, practically, a perfect cylindrical shape.

**Table 1.** Chemical composition of tungsten rods of 8 mm diameter, wt.%

Si	Mg	Sn	Ni	Al	Mo	N	C
<0.001	<0.0001	<0.0001	0.0002	0.0002	0.017	0.002	0.001
As	Sb	Pb	Fe	Bi	Ca	P	O
<0.0001	<0.0001	<0.0001	0.0013	<0.0001	<0.001	<0.001	0.0046

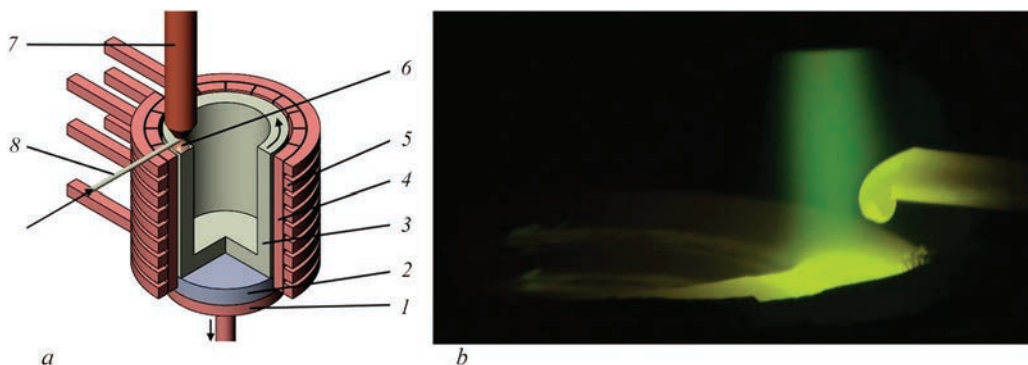


**Figure 6.** Scheme (a) and the process of remelting the consumed rod (b) during growing the ingot in the form of a hollow cylinder: 1 — bottom-plate; 2 — support; 3 — single-crystal; 4 — sectional wall; 5 — inductor; 6 — heat flux from plasmatron; 7 — consumed rod; 8 — plasmatron



**Figure 7.** Tungsten single-crystal: *a* — after the first stage of deposition of 6 layers and surface etching; *b* — after the second stage of growing, the height of the wall is 35–37 mm

The metal pool on the inner side of the crucible is not maintained by the electromagnetic field, which can lead to a leakage of the melt. Therefore, when growing a crystal in the form of a hollow cylinder, a layer formation scheme is used when the plasma heating source is shifted from the middle of the pool closer to the inductor. The pool acquires a rather complicated front of crystallization, which is formed by certain factors — absence of heating of the inner side of the wall of the crucible with a significant overheating of the outer one. As a result, slightly different conditions of crystal growth in the vertical plane arise that passes through the axis and radius. Due to this feature of thermal field, the inner surface of the crucible will be colder with relative to the outer one. This will create different conditions of solidification tungsten and the formation of dislocations in different parts of the crucible. In our opinion, in such circumstances, on the inner surface of the crucible, subboundaries, subgrains and exits of the edges of the crystal lattice will be more noticeable.

After melting, the sample of the crystal was etched with a chemical solution  $H_2SO_4:HNO_3:H_2O$  in a ratio of 2:2:4, which allowed identifying the boundaries of subgrains and the features of the structure formation and its orientation. Depending on the orientation of the crystal lattice, the rate of etching metal is different, so it is possible to monitor the formation and he-



**Figure 8.** Appearance of tungsten single-crystal in the form of a hollow body of revolution of 85 mm diameter

redity of the single-crystalline structure. As a result of etching, the sample acquires a matt tint (Figure 7, *a*).

At the second stage, further studies of the process of remelting and forming were carried out when growing tungsten single-crystal in the form of a hollow body of revolution. While setting the same modes as in the first experiment, nine horizontal layers were deposited. The experiment showed that the process is stable, the thickness of the wall does not change, no leakages from the outside and inner sides occur. On the outer side, the solidified layers formed some waves, which is associated with the hydrodynamics of the liquid metal pool in the electromagnetic field of a high-frequency inductor. However, it did not lead to a large leakage of metal, also there were no electrical short-circuits. The total height of the welded wall was approximately 35–37 mm, the weight of the sample was 5.23 kg (Figure 7, *b*).

The third stage confirmed the stability and regularities of selected parameters for growing a crystal in the form of a 3D object. The overall height of the wall of the deposited crystal was approximately 68 mm, the weight was 7.635 kg with an outer diameter of 85 mm and the wall thickness of 20–22 mm (Figure 8). The final mode of growing crystal: plasma arc current is 415–550 A, the total power of a high-frequency generator is 170 kW, the dependence is shown in Figure 9. Taking into account the efficiency of the generator, the design of the thermal unit, the load of

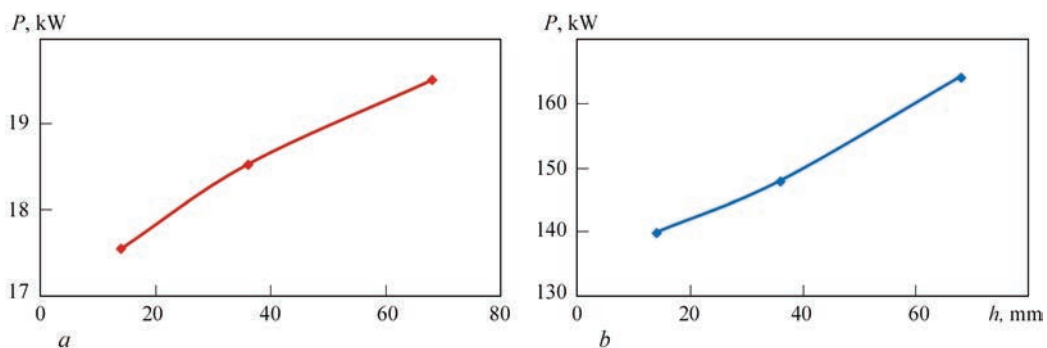


**Figure 9.** Dependences of change in power parameters on an increase in height while growing a hollow tungsten single-crystal of 85 mm diameter: *a* — change of power of the plasma arc; *b* — change of total power of high-frequency generator

the inductor with a crystal, the efficient power transmitted by the crystal may be 60–70 % [9]. At the speed of movement of the pool within 15–16 mm/min, the mass of drops that are formed and moved to the local pool, ranges from 1.3 to 1.4 g. The mass rate of growing is 14–15 g/min. The surface of the single-crystal is characterized by a slight ribbing, which is associated with a layer-by-layer formation. The thickness of the grown single layer is 2.3–2.4 mm.

During visual inspection on the surface of the ingot, it is possible to see vertical bands, which differ in the reflective capacity of light. These bands correspond to the structure of the elementary crystalline lattice (BCC) of tungsten, which is hereditary distributed throughout the whole ingot, forming a single-crystalline structure. In the adjacent bands, the reflective capacity changes, which corresponds to the planes or faces of the crystalline lattice, which indicates the heredity of the single-crystalline structure throughout the whole volume. In addition, these bands correspond to a part of the embryonic crystal that was subjected to melting.

## CONCLUSIONS

For the first time in the world based on the latest technology developed at PWI of the NAS of Ukraine, a tungsten ingot in the form of a hollow cylinder on a solid single-crystalline embryonic crystal with a diameter of 85 mm was grown. The grown crystal has 68 mm of the deposited wall with a thickness of 20–22 mm. The surface inspection after etching of the ingot by chemical reagents showed the heredity of the structure from the single-crystalline embryonic crystal and all the signs of the monocrystalline structure throughout the crystal.

*This work was supported and completed with the assistance of the Ministry of Education and Science of Ukraine. Order of 02.02.2021 No. 134 “On financing of scientific and technical works in the framework of the execution of the state order for scientific and technical (experimental) development and scientific and technological products in 2021”, according to the contract No. DZ/103-2021 of 09.03.2021: “Development of innovative 3D technology of growing single-crystalline crucibles from tungsten”.*

## REFERENCES

1. Winsch, I.O., Kyle, M.L., Pierce, R.D., Burris, Jr.L. (1967) Tungsten crucibles in pyrochemical processing of nuclear fuels. *Nuclear Applications*, 3(4), 245–251. DOI: <https://doi.org/10.13182/NT67-A27764>.
2. Junhyuk Jang, Seungyoub Han, Tack-Jin Kim et al. (2019) Stability of tungsten crucible against uranium, rare earth, cadmium, and chlorides for cathode process in pyroprocessing. *Sci. and Technol. of Nuclear Installations*, 31 July, 1–7. DOI: <https://doi.org/10.1155/2019/4121285>.
3. Kofanov, D., Gerasymov, Ia., Sidletskiy, O. et al. (2022) LuAG:Ce and LuYAG:Ce scintillation crystals grown under reducing conditions from W crucibles. *Optical Materials*, 134, Pt A, 113176.
4. Takahiro Suda, Yuui Yokota, Takahiko Horiai et al. (2022) Crystal growth of La<sub>2</sub>Hf<sub>2</sub>O<sub>7</sub> by micro-pulling-down method using W crucible. *J. of Crystal Growth*, 583(1), 126547.
5. Savitsky, E., Burkhanov, G., Kirillova, V. (1982) *Single-crystals of refractory and rare metals, alloys, and compounds. Analytical methods high-melting metals*. Springer-Verlag, 107–148. DOI: <https://doi.org/10.1007/978-3-642-68731-0>
6. Shapovalov, V.A., Yakusha, V.V., Gnizdylo, A.N., Nikitenko, Yu.A. (2016) Application of additive technologies for growing large profiled single-crystals of tungsten and molybdenum. *The Paton Welding J.*, 5–6, 134–136.
7. Shapovalov, V.O., Gnizdylo, O.M., Yakusha, V.V. et al. (2022) Intensification of the process of plasma-induction growing of large profiled tungsten single-crystals. *PAST*, 137(1), 40–45.
8. Shapovalov, V.O., Nikitenko, Yu.O., Yakusha, V.V. et al. (2020) Manufacture of super large tungsten single-crystals in the form of rotation bodies. *Ibid.*, 125(1), 60–63.
9. Shapovalov, V.O., Nykytenko, Yu.O., Gnizdylo, O.M. et al. (2022) Investigation of energy balance in the system of the crystal-high-frequency heating module at plasma-induction growing of refractory metal single-crystals. *Suchasna Elektrometal.*, 4, 27–33 [in Ukrainian]. DOI: <https://doi.org/10.37434/sem2022.04.05>

## ORCID

Yu.O. Nykytenko: 0000-0002-3603-2333,  
V.O. Shapovalov: 0000-0003-1339-3089,  
V.V. Yakusha: 0000-0001-5962-9194,  
O.M. Gnizdylo: 0000-0001-7537-6481,  
O.V. Karuskevych: 0000-0002-7037-5903

## CONFLICT OF INTEREST

The Authors declare no conflict of interest

## CORRESPONDING AUTHOR

Yu.O. Nykytenko  
E.O. Paton Electric Welding Institute of the NASU  
11 Kazymyr Malevych Str., 03150, Kyiv, Ukraine.  
E-mail: [nikyu80@gmail.com](mailto:nikyu80@gmail.com)

## SUGGESTED CITATION

Yu.O. Nykytenko, V.O. Shapovalov, V.V. Yakusha, O.M. Gnizdylo, O.V. Karuskevych (2023) 3D technology of growing single-crystal ingots in the form of hollow tungsten cylinders. *The Paton Welding J.*, 5, 42–47.

## JOURNAL HOME PAGE

<https://patonpublishinghouse.com/eng/journals/tpwj>

Received: 01.03.2023

Accepted: 29.06.2023

DOI: <https://doi.org/10.37434/tpwj2023.05.08>

# AUTOMATED EDDY CURRENT INSPECTION SYSTEMS WITH SURFACE PROBE OF DOUBLE-DIFFERENTIAL TYPE

V.N. Uchanin<sup>1</sup>, G.G. Lutcenko<sup>2</sup>, A.V. Opanasenko<sup>2</sup>

<sup>1</sup>Karpenko Physico-Mechanical Institute of the NASU

5 Naukova Str., 79060, Lviv, Ukraine

<sup>2</sup>Ukrainian Scientific Institute for Non-Destructive Testing

8 Naberezhno-Lugova Str., 04070 Kiev, Ukraine

## ABSTRACT

The prospects and state-of-the-art related to the development of automated non-destructive testing systems are considered. The formation of the tendency concerned with creation of the adaptive automated systems for complex testing based on the application of various physical principles to obtain a synergistic effect is indicated. The factors affecting the variability of eddy current probe signals during the manual and automated eddy current testing were analyzed. The advantages of selective probes of double-differential type for automated systems development are indicated. Features of the design and characteristics of multi-channel automated systems based on the eddy current method application developed in Ukraine are presented, in particular: a robotic eddy current testing system for detection and identifying of in-service defects in the tubes of secondary reforming furnaces; the eddy current unit of the multi-channel system of complex testing of railway axles during their production; automated system of complex testing of wheel pairs in the conditions of repair plants; eddy current block of the system for complex inspection of railway rails during their production.

**KEYWORDS:** automated system, complex non-destructive testing, eddy current defect detection, eddy current probe of double-differential type

## INTRODUCTION

Rebuilding of industry in scope of the Fourth Industrial Revolution results in formation of the new approaches in non-destructive testing (NDT) using NDE 4.0 abbreviation (Non-destructive Evaluation 4.0), where the issues of automation of testing operations (including with robots application) take a leading place [1, 2]. Let's consider automation as a complex of technical and program means providing NDT performance without direct human participation. It is impossible to provide large scopes of NDT in many spheres of industry without partial or complete automation. Automated NDT is not only used during manufacture where it is easy to provide testing of products of simple shape in form of rotation bodies (pipes, rods, wires, balls etc.) that can be considered a common phenomenon long ago. This testing during operation of products creates the unique possibilities for NDT without human participation in the dangerous and harmful for health environments [3, 4]. At the first stages of NDT development the methods of manual NDT were mainly implemented. At that all procedures from equipment preparation and scanning of surface of tested object (TO) to making a decision on quality or defectiveness of products were made by operator. Such an approach resulted in significant limitation of reliability and validity of testing due to dependence of the obtained results on operator qualification. In order to get rid of effect of this factor there were implement-

ed the rigid requirements as for training and certification of personnel by NDT methods and commercial sectors, accreditation of laboratories and verification of NDT procedures. Ukraine in particular to realize these requirements has the acting standard DSTU EN "Non-destructive testing — Qualification and certification of NDT personnel". It in full corresponds to international reference documents. Therefore, the most important positive effect from implementation of automated NDT is the increase of its reliability. At the same time scientific literature contains warnings as for possible risks and production losses that can accompany automatic NDT due to its inappropriate application and widespread (and not always grounded) trust in its reliability [5, 6].

Increase of NDT efficiency can be considered other by value effect of automation, which is in particular important under conditions of continuous manufacture. It is necessary to note that NDT automation does not detract a value of operator or engineer who makes a decision on product quality or structure operational integrity. Implementation of automated NDT systems require from them knowledge of higher level necessary for determination of rejection criteria, introduction of changes in algorithm of product testing depending on reference documents (standards) corresponding to the requirements of specific client etc.

The aim of this work is the analysis of peculiarities of automation of eddy current (EC) testing and presentation of domestic automated system (AS) of eddy

current testing with surface selective double-differential eddy current probes (ECP).

### STATE OF THE ISSUE

A separate methodology for development of automated NDT systems (ASNDT) has not been developed yet. At this stage the logical step is application of methodological principles and approaches developed for information-measuring systems (IMS) which are sufficiently developed [7–9] as well as consideration of existing works on general theory of automation [10–12]. At that it is necessary to take into account the peculiarities of functioning of specific NDT method. It is also necessary to note that the purpose of testing systems (including NDT) in contrast to IMS is determination of correspondence of technical condition of TO to standard requirements and registration of deviations in the parameters characterizing TO technical condition from determined norms. For ASNDT, the purpose of which is technical diagnostics of TO in operation (in foreign scientific literature this direction is abbreviated as SHM — structural health monitoring), it is also necessary to determine the reasons of non-conformity of TO technical condition (in particular, presence of defects, degradation of materials, wear out of operating surfaces etc.) with evaluation of reliability and prediction of its further service life.

It is necessary to note that very often existing ASNDT not only generate a protocol by the results of performed NDT, but also have in their content the means for formation of the signals based on obtained results for regulation of executing mechanisms, to which in particular the mechanisms of presorting and marking of defective zones can be referred. Such ASNDTs have already the features of automated systems for regulation of technological processes [13].

It should be noted that there is no accurate terminology for the issues of NDT automation. In the literature such terms as “mechanized”, “automated”, “semi-automated” and “automatic” [14] can be found. NDT means, in which operations of scanning are completely or partially (by one of the coordinates) performed automatically, can be referred to mechanized ones. Operator at that usually checks workability and calibrates unit on a standard specimen (SS), makes a decision on defect presence and forms testing protocol. Automated NDT systems mostly foresee automation of operations of TO delivery on testing position and scanning of TO surface, check of workability on SS and formation of protocol about defects presence and their coordinates. However, a decision on product quality is made by operator of the highest level of qualification based on analysis of testing protocol and, if necessary, results of additional test operations. To automatic ones it is pos-

sible to refer the NDT systems, in which all operations including taking decisions on product quality and correspondence to normative documents and reject of poor products are made without operator participation. Does such classification reflect the modern level of technological development? Probably not, since there are, in particular, AS based on application of robots which carry various NDT equipment. Lifting and underwater types of robots or pilotless vehicles [4] are used for NDT of difficult-to-reach zones of structures. Besides, there were developed technical solutions as for creation of adaptive AS, in particular, based on application of technical vision devices [15] (see Kuts Yu.V., Shapovalov E.V., Uchanin V.M. et al. Method of adaptive eddy current testing. Patent of Ukraine 140906, 2020, Bul. No. 5 and Uchanin V.M., Vertiy O.O., Yatsenko O.Yu. et al. Adaptive method of scanning eddy current testing. Patent of Ukraine 149803, 2021, Bul. No. 49), AS of complex NDT using different physical methods (for example, ultrasonic and EC) and AS using tomography principles [16–18]. Therefore, there is a need in development of up-to-date classification of ASNDT based on expansion of a list of classification features.

In total it can be told that there is a formation of a tendency of development of multi-functional adaptive AS for solution of several tasks, including based on realization of complex NDT built on application of different physical principles for production of synergy effect related with limitations of each separate NDT method and different probability of defect detection depending on type and place of location [19, 20].

In recent years the spheres of application of EC NDT methods using the reaction of TO material on probing action of alternating electromagnetic field have significantly expanded [21–23]. It is related with a series of advantages of this method in comparison with other NDT methods. It is a well-grounded statement that the EC method has high sensitivity to different type defects and sensitivity to a series of electrophysical and geometry parameters of TO (multi-parameter). However, for automation the most important is a factor of contactless of EC method, i.e. possibility to provide sufficient sensitivity to defects at certain distance between ECP and TO surface or even through dielectric coating. At that the basic importance is the possibility of reduction of interferences from a gap change, i.e. distance between ECP and TO surface during scanning. Double-differential ECPs providing high sensitivity in testing with large gap [24] correspond to such requirements.

A Table 1 shows an attempt to compare automatic and manual eddy current NDT analysing the factors affecting variability of ECP signals, and, respectively, testing reliability.

**Table 1.** Factors affecting variability of ECP signals during manual and automated EC testing

Automated testing	Manual testing
1. Violation of ECP positioning 2. Violation of scanning rate	1. ECP positioning (gap, inclination, orientation) by operator. 2. Parameters of scanning of TO surface (step, rate etc.). 3. Adjustment of device (selection of operating frequency, amplification, level of signalization of defects etc.). 4. Correspondence of SS for adjustment to TO characteristics. 5. Selection of method of interpretation of ECP signals (for example, using a complex plane) 6. Selection of parameters of high frequency filter for suppression of effect of interferences related with changes of electrophysical and geometry parameters of TO, effect of edge etc. 7. Selection of parameters of filters of low frequencies for suppression of effect of electronic interferences respectively to scanning frequency. 8. State of operator health and environment.

The right part of the table provides sufficiently large list of operations which should be realized by operator during manual testing for its reliability. Obviously, that inaccuracy of performance of each operation can result in violation of optimum scanning of TO surface, wrong adjustment of equipment and, as a result, defect skipping. In AS most of the procedures of the right part of the table are selected at the stage of preliminary investigations and being realized in correspondence with the set algorithms of operation of AS constituents. To provide testing selectivity it is important to choose such informative signs of ECP signals which allow reliably finding the defects under conditions of interferences action. AS functioning virtually has no dependence on operator qualification, state of health and working conditions. The left part of the table determines importance of the requirements to quality operation of scanners and AS positioning devices. Presented table proves the perspectives of automation of EC testing as for increase of testing reliability under conditions of creation of reliable scanners and positioning devices.

#### **ROBOTIC SYSTEM OF EDDY CURRENT NDT FOR DETECTION AND IDENTIFICATION OF SERVICE DEFECTS OF PIPES OF FURNACE OF SECONDARY REFORMING**

A relevant problem of chemical industry is a detection of service cracks on inner and outer surfaces of pipes of furnaces of secondary reforming. Pipes of 102 mm diameter with 15 mm wall thickness are manufactured using the method of centrifugal casting from stainless steel 40Kh25N20. Testing should be carried out from outside without excess to pipe inner surface with high sensitivity to defects lying at 7–8 mm depth (around 50 % of pipe thickness). The task is complicated by large structural inhomogeneity of pipe material, which significantly decreases efficiency of ultrasonic method. Therefore, leaving no alternative solution of the problem is application of EC method using low operating frequencies. Besides, means

of EC testing should identify found defects by their division for several classes, namely inner and outer relative to pipe surface on which they are initiated as well as longitudinal and transverse relatively to pipe axis. Besides, it is necessary to evaluate defect depth (in percent from pipe thickness) independent on the fact on which surface they were found. All these tasks should be solved under conditions of high level of interferences appearing due to structural inhomogeneity of material and roughness of pipe surface.

When designing ECP the attention was paid on sufficient sensitivity to defects on inner pipe surface, level of signal of which shall exceed the level of structural noise. In ECP design there were used sufficiently large coils located on ferrite cores of 10 mm diameter that provided a possibility due to integration properties to reduce the level of structural noise with conservation of necessary sensitivity to the defects. The best sensitivity to inner defects was provided by ECP of MDF 3301 type with diameter of operating area 33 mm. It allows EC testing in a range of operating frequencies 50 Hz – 150 kHz. ECPs were investigated using EDDYMAX type EC board on operating frequency 1.5 KHz, which provided the sensitivity to the defects on inner pipe surface during testing from pipe outer surface. There was used a fragment of pipe on inner surface of which three semi-elliptical longitudinal defects of 0.2 mm thickness were milled. The latter simulate a crack of 35 mm thick and 7.5 mm depth (D1); 9.0 mm (D2) and 10.0 mm (D3) that corresponds to lying depth 50; 40 and 33.3 % from pipe wall thickness (15 mm) in testing from outer pipe surface [27].

Figure 1, *a, b* provides signals from three defects on inner pipe surface (D1, D2, D3) in a complex plane (after demodulation) as well as vertical and horizontal components of ECP signal in mode of time-base sweep.

Figure 1, *c, d* for evaluation of the possibility of detection of inner defects provides the corresponding signals from structural noise which were obtained by means of scanning of defect-free zone of the pipe as well as the signals from change of a gap which were

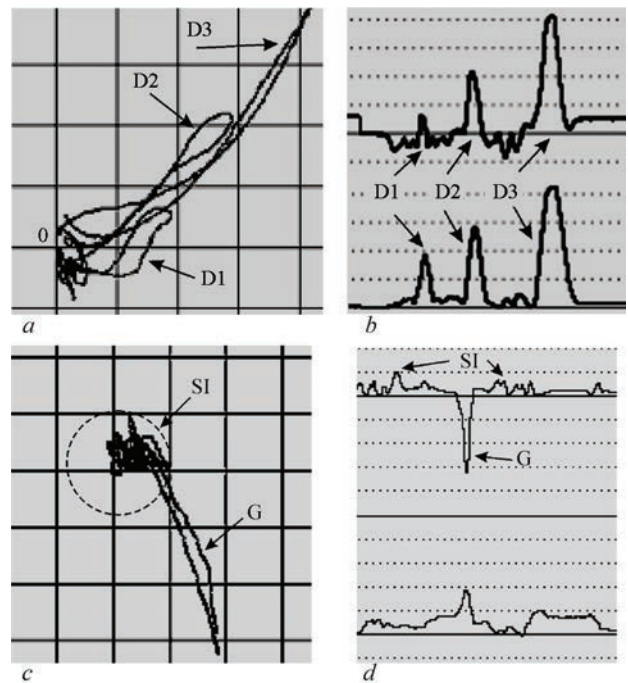
obtained by withdrawal of ECP from pipe surface at a distance more than 3 mm. The signals from structural noise can be observed in a complex plane (on Figure 1, *c* shown by dashed circle) or in a mode of time-base sweep of signal components (Figure 1, *b*). It can be seen that the signals from inner defect of crack type (D1) with lying depth 7.5 mm (50 % of pipe wall thickness) are more than for 6 dB higher than the signals from structural noises.

Figure 2 shows the ECP signals from surface cracks of different orientation on operating frequency 1.5 kHz at sensitivity by 18 dB lower than during registration of signals on inner pipe surface (Figure 1). Figure 2 *a, b* provides the ECP signals in a complex plane and in a mode of time-base sweep from longitudinal relatively to pipe axis surface crack of 5.0 mm depth. Figure 2, *c, d* gives corresponding signals from transverse crack. Data on Figure 2 indicate the peculiarity of the signals of double-differential ECP when the signals from longitudinal and transverse cracks have opposite direction of hodographs and, respectively, different sign of vertical component. This peculiarity can be used for identification of detected cracks respectively to their direction.

Comparison of the signals from inner (Figure 1, *a, b*) and surface (Figure 2) defects and signals from gap change (Figure 1, *c, d*) indicates the possibility of differentiation of the signals from the defects and the signals from gap change and identification of detected defects as for surface of their location by direction of hodograph (phase angle) of the signal. In particular, a hodograph of the signal from defects on inner pipe surface differs from the signal caused by a gap by  $\sim 90^\circ$  angle that gives the possibility to mark it out effectively by rotation of complex plane.

The results of the investigations were used by SPC "Promprylad" for development of a system of robotic EC testing of pipes of secondary reforming of CRAB type [25]. The CRAB system provides 4-channel double-frequency testing of pipes under service conditions. It consists of 4 ECPs connected to 4 identical EC channels, mechanical scanner-robot with control block, that provide independent scanning of pipe surface by all ECPs, and commercial computer. Specially developed scanner-robot (Figure 3) provides simultaneous movement of four ECPs each of which scans separate sector of the pipe on meander type trajectory. After testing of one section of the pipe from all sides the scanner together with ECP automatically moves to the next area. Original pneumatic mechanisms are used for scanner construction. This allows reducing the level of electric noise due to absence of electric drives in ECP zones.

Rate of movement along the pipe is 1 m/min. A scanner can be installed on the pipe not only from the edge,



**Figure 1.** Signals of ECP of MDF 3301 type from inner defects of pipes lying at 7.5 depth (D1); 6.0 (D2) and 5.0 mm (D3) as well as signals of structural noises (SI) and gap change (G) in complex plane (*a, c*) and components of ECP signal in a mode of time-base sweep (*b, d*)

but also from its cylindrical surface that provides the possibility to test built-in pipes during their repair.

A block for scanner regulation forms six control signals, takes four signals from executing mechanisms of scanning device as well as takes and processes signals from angular movement sensor. Each eddy current channel processes signals from one ECP on two operating frequencies 1.4 and 5.0 kHz necessary for detection

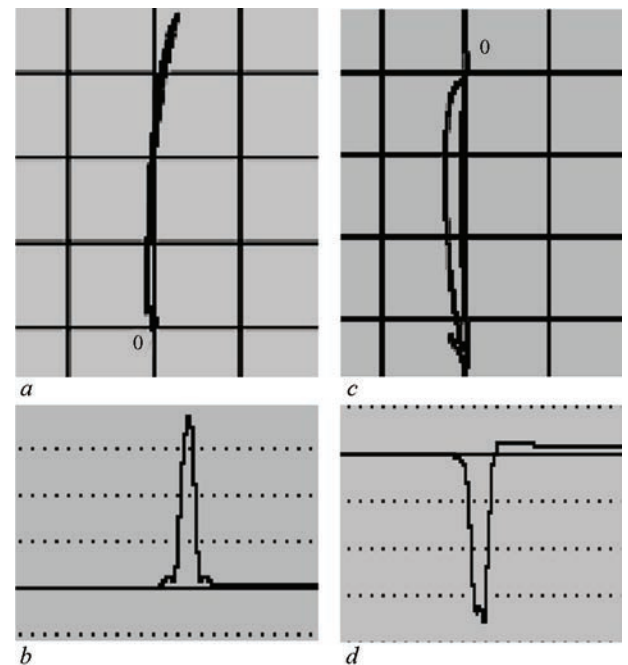


**Figure 2.** Signals of ECP of MDF 3301 type from longitudinal (*a, b*) and transverse (*c, d*) defects in complex plane (*a, c*) and in mode of time-base sweep (*b, d*)



**Figure 3.** EC scanner of CRAB system installed on pipe of secondary reforming furnace

and identification of defects on different pipe surfaces. Registration of signals on different operating frequencies from each ECP separately allows identification of defects by surface of their location. During testing it is possible to observe and register the signals from all four ECPs on operating frequencies 1.4 and 5 kHz simultaneously (Figure 4). Inner defects form a signal only on frequency 1.4 kHz and outer ones on frequency 1.4 kHz as well as on 5 kHz frequency. The system has a possibility to register hodograph of ECP signal from defect in a complex plane or its components in a time-base sweep mode. To realize an automatic defect signalling (ADS) on each of channels it is possible to mark out up to four zones of defect registration in a complex plane. The possibility is stipulated to build a sweep of selected sector of the pipe for separate channel as well as sweep of whole pipe for inner or outer defects. CRAB system provides for storage of all collected data for their further analysis and documenting and possibility of evaluation of depth of detected defect in percent relative to pipe wall thickness independent on its location.

The investigations showed that the CRAB system detects defects of more than 20 % depth on outer surface and more that 50 % from pipe wall thickness on inner one. The CRAB system identifies detected defects by

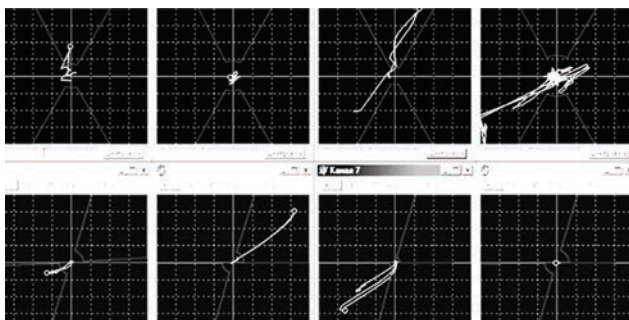


**Figure 4.** Signals from four ECP on operating frequencies 1.4 (top) and 5 kHz (bottom)

their location (on inner and outer surfaces of pipe) and orientation (longitudinal or transverse) as well as evaluates their depth in percent relative to pipe wall thickness.

### EDDY CURRENT BLOCK OF MULTI-CHANNEL AUTOMATED SYSTEM FOR COMPLEX TESTING RAILWAY AXES

Manual testing of railway axles with formation of test results protocol for each axle has low productivity that limits their testing on zones of possible defect nucleation. Significant increase of productivity and reliability of axles testing can be achieved by application of complex NDT that is caused by different sensitivity of selected NDT methods to separate groups of defects. Defects of railway axles can be divided on two main groups, namely 1) inner which are sufficiently well identified by ultrasonic method; 2) surface, sensitivity to which during ultrasonic testing is not enough high. In some AS during NDT of axles the ultrasonic method is combined with magnetic-particle testing which provides high sensitivity to surface defects, but at the same time it has a series of significant disadvantages. Therefore, EC method is more perspective for complex automated NDT of axles. Ukrainian SRI for Non-destructive testing (Kyiv) created an automated system of complex NDT of railway axles SANK-3, in which EC method was added to ultrasonic testing [26]. Railway axles of RU1Sh and RU1 type from axle steel subjected to NDT have sufficiently complex shape (Figure 5).

Total length of RU1Sh makes 2216 mm and RU1 axle is 2294 mm. Diameters of neck, near-hub part, hub and middle part of the axle make 130; 165; 194 and 172 mm, respectively. Length of areas of axle along the neck, near-hub part and hub of axle is 190 (for RU1 — 176), 76 and 250 mm, respectively.

Due to its complex shape, sufficiently large area of testing, and necessity to provide high productivity the axle surface is divided into separate zones being tested in parallel in multi-channel mode. In whole there were marked 16 testing zones (Figure 5). At that zones 1, 3, 5, 6 and 8 are tested with two ECPs and zone seven with four ECPs. Zones 2 and 4 of fillets should be tested in a separate mode since the tested surface in this case have small curvature radius. Therefore, ECP with a smaller radius of the working area is used for these zones. For testing of different zones of railway axles, ECPs of two types were used:

- MFD 0701 with working area diameter 7 mm for testing of cylinder surfaces, fillets of middle part and axle edges (all zones, except for second and fourth);



**Figure 5.** Scheme of division of railway axles on separate test zones

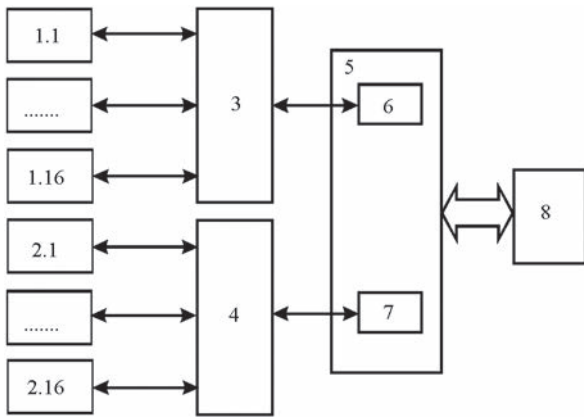


**Figure 6.** Scheme of EC block of SANK-3 type system for complex NDT of axles: 1.1-1.16 and 2.1-2.16 — ECP; 3 and 4 — multiplexers; 5 — electronic module OKO-13, 6 and 7 — eddy current blocks; 8 — central computer

- MDF 0602 with 6 mm diameter for testing of small radius fillets (zones 2 and 5 on Figure 5).

A structural scheme of eddy current block of automated system SANK-3 (Figure 6) contains 32 ECPs divided on two groups 1.1-1.16 and 2.1-2.16. Each group of 16 ECPs is served by two multiplexers 3 and 4 which in turn interrogate ECP. Each of multiplexers can switch up to 32 ECPs which are fixed in the mandrels with possibility to scan surfaces of axles with 0.2 mm gap. The mandrels with ECP in start position are shown on Figure 7.

Electronic module 5 of previous collection and processing of the information OKO-13 consists of two eddy current blocks (ECB) 6 and 7 (Figure 6), each of which serves one multiplexer. Module OKO-13 is improved central block of multi-channel flaw detector OKO-01 with no display and control elements. It can have up to four ECB. Electronic module 5 and ECPs 6 and 7 connected to it are located in one body. Module 5 is equipped with field-bus module WizNet for connection with PC 8, which is carried out using standard protocol TCP/IP 4.0. ECB sends a signal from generator of sine oscillations and code to multiplexer that corresponds to current ECP and channel. The multiplexer activates channel corresponding to obtained code and signals from selected ECP come to ECB where their primary processing and accumulation take place. After testing completion these data are transferred to the central computer 8 which processes them and stores information on defective areas in a data base. The inserts with artificial defects mounted on SS in form of special control axle are provided for verification of workability and calibration.

The results of experiments and operation of SANK-3 system showed that EC testing using double-differential ECP of MDF type provides sufficiently high sensitivity to defects. This provided the possi-



**Figure 7.** Automated SANK-3 system with ECP on start position possibility to replace magnetic-particle NDT and increase productivity of AS testing of railway axles.

### AUTOMATED SYSTEM OF COMPLEX NON-DESTRUCTIVE TESTING OF WHEEL PAIRS

Automated system SNK KP-8 (Figure 8) of complex (ultrasonic, electromagnetic-acoustic and EC) testing of wheel pairs of RU1 and RU1Sh-957 type was developed at Ukrainian SRI for Non-destructive testing (Kyiv) after long-term operation [27].

Eddy current tract AS SNK KP-8 provides multi-channel testing of different zones of wheel pairs that guarantees high testing productivity. One of the variants of AS for different zones of wheel pair applies the following amount of EC channels, namely 16 channels for testing of side surfaces of wheel rim; 6 channels for testing of wheel rolling surface; 9 channels for testing of wheel flange; 24 channels for testing of near-rim zone of disk; 8 channels for middle part of axle; 8 channels for testing of axle neck and 10 channels for testing of inner racers. Double-differential ECPs are used for testing of rim (MDF 1201), fillets (MDF 0601), flange (MDF 0901) and rolling surface (MDF 1201) of wheel, middle part (MDF 1201) and necks (MDF 0601) of axle as well as inner racers (MDF 0901). Figure 9 demonstrates scanners of AS SNK KP-8 for testing of different zones of wheel pair.

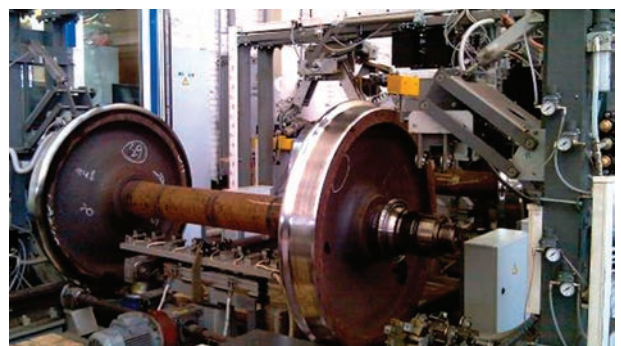


**Figure 8.** Automated system of complex testing SNK KP-8 with tested wheel pair

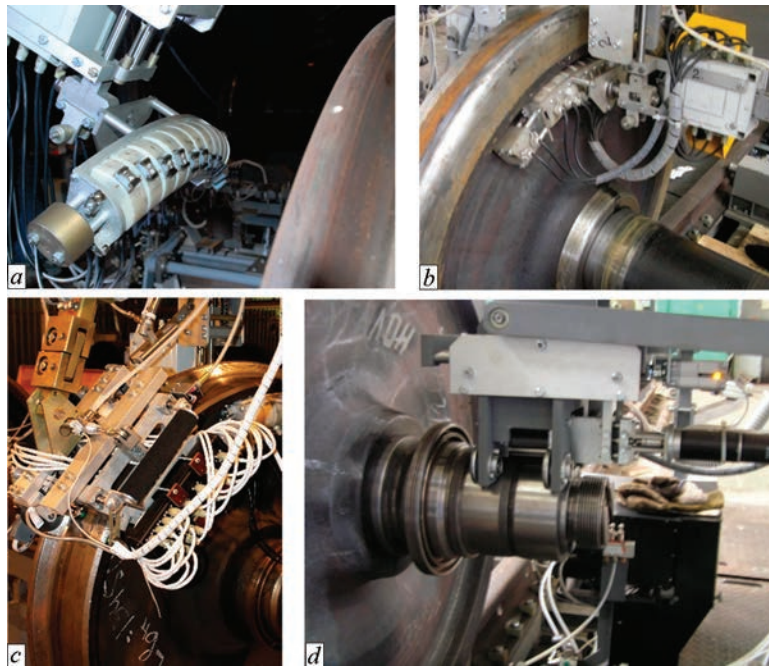


**Figure 9.** AS SNK KP-8 scanners for testing of fillets of wheel rim in start (a) and operating positions (b), for testing of rim (c) and racers zone (d)

The system provides complex testing of not less than ten wheel pairs per hour under condition of their uninterrupted supply on testing position. During commercial experiments and operation of automated system SNK KP-8 the eddy current method detected the defects in middle parts of axles, inner racers as well as rims, flanges, rolling surfaces and in near-rim zones of wheels.

#### **EDDY CURRENT BLOCK OF AUTOMATED SYSTEM OF COMPLEX TESTING OF RAILWAY RAILS**

Complex NDT of rails at the stage of their manufacture is provided by series of standards as an important

factor of reliable and trouble-free operation of railway transportation. Ultrasonic and EC methods of NDT are often combined for reliable detection of rails defects. In this case synergy effect of such an approach is reached by their orientation on different groups of defects [19, 20]. For development of selective EC system under condition of effect of strong interferences there are used different variants of the method including application of rotation ECPs [28]. Such an approach can significantly limit productivity of EC testing and disturb the synchrony of operation cycles that can result in decrease of productivity of rail manufacture in whole. Multi-channel AS using selective ECP are prospective for increase of NDT productivity. They can carry out testing under conditions of effect of large interferences including connected with inhomogeneity of magnetic properties of steels and instability of gap between ECP and TO surface [29].

Automated system for complex (ultrasonic, electromagnetic-acoustic and EC) testing of railway rails after their rolling was developed by SPC “Promprylad” (Figure 10) [30].

Let’s consider in details EC block of this AS which provides testing of rails with productivity to 2 m/s due to application of 56 channels [30]. Main requirements to ECP of such AS stipulated high sensitivity to longitudinal and transverse cracks, possibility of testing under conditions of distance between operating surface of ECP and rail surface not less than 1 mm to prevent ECP damage and high level of noise suppression related with changes of this distance (gap) during scanning. Preliminary tests showed that double-differential ECPs of MDF 1201 type with working sur-

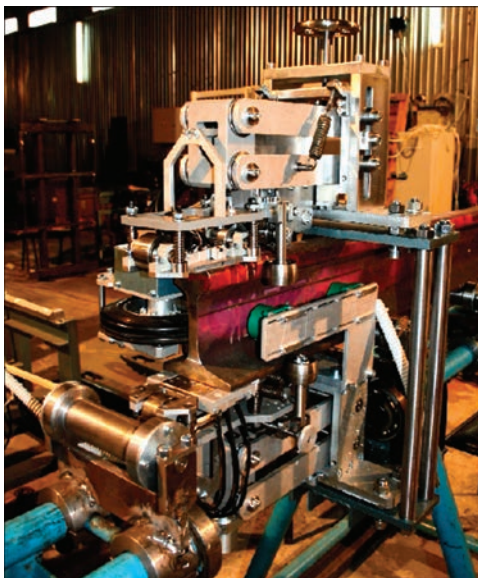


**Figure 10.** General view of AS of complex NDT of rails after their rolling

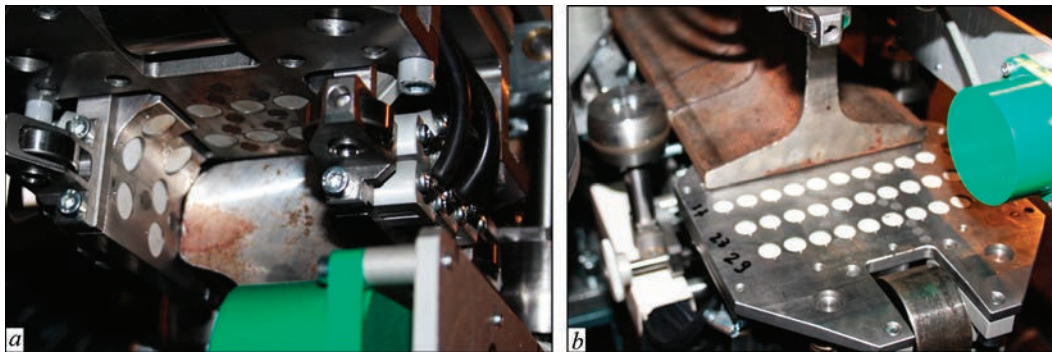


Figure 11. Sets of ECP for testing of head (a) and base (b) of rail

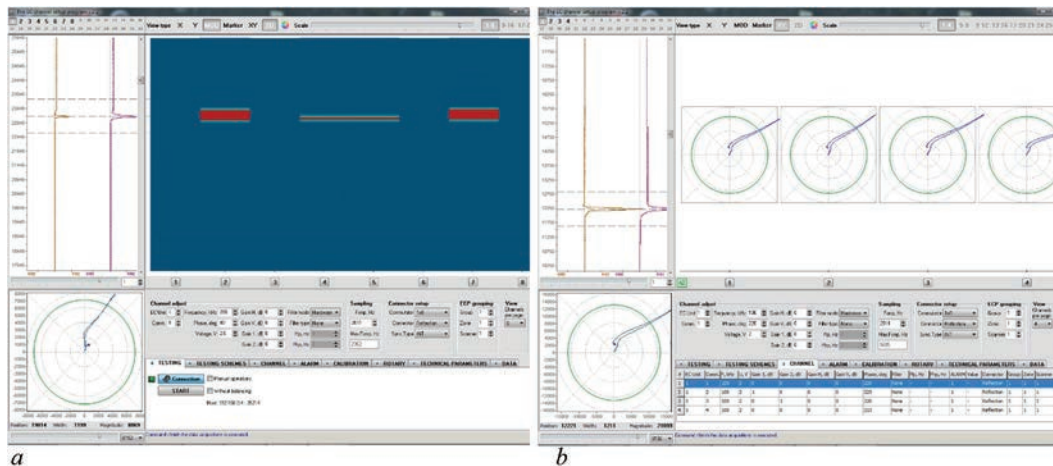


Figure 12. Display of EC block of AS with signals from defects in rail head in mode of 2D presentation (a) and in mode of complex plane (b)

face diameter 12.5 mm fulfil these requirements. They provided maximum sensitivity to defects in ferromagnetic steel on operating frequency 100 kHz. In total there were used 25 ECPs for testing of rail head including with side surfaces (Figure 11, a) and 31 ECPs for testing of rail base (Figure 11, b). EC block of AS provides detection of longitudinal and transverse cracks of depth more than 1.0 or 1.5 mm and length more than 20 or 10 mm, respectively.

Appearance of display of EC module of AS with visualization of the testing results in modes of 2D visualization (a) and complex plane (b) is given on Figure 12.

## CONCLUSIONS

The state of the problem of ASNDT development is considered. It was noted a tendency to development of adaptive AS for complex NDT built on application of different physical principles for provision of synergy effect. There were analysed the reasons affecting variability of ECP signals during manual and automated EC testing. The advantages of selective double-differential ECPs for development of EC testing systems was noted.

There were presented the peculiarities of design and characteristics of developed in Ukraine (SPC “Prom-

prylad” and Ukrainian SRI for Non-destructive testing) multi-channel AS using EC method, in particular:

- robotic four-channel EC testing system for detection and identification of operation defects of pipes of second reforming furnaces on two operating frequencies 1.4 and 5.0 kHz with rate of movement of ECP block along the pipe 1 m/min;

- eddy current block of multi-channel (32 channels) AS of complex testing of railway axles in their manufacture;

- automated system for complex NDT testing of wheel pair under conditions of repair enterprises (different variants have at least 98 EC channels), which provides the possibility of NDT of not less than ten wheel pairs per hour;

- eddy current AS block for testing of railway rails in their manufacture with productivity to 2 m/s due to application of 56 channels, sensitivity of which allows detection of longitudinal and transverse cracks of depth more than 1.0 or 1.5 mm and length more than 20 or 10 mm, respectively.

## REFERENCES

1. Meyendorf, N., Heilmann, P., Bond, L. (2020) NDE 4.0 in manufacturing: Challenges and opportunities for NDE in the 21<sup>st</sup> Century. *Materials Evaluation*, 78(7), 794–803. DOI: <https://doi.org/10.32548/2020.me-04144>

2. *Handbook of Nondestructive Evaluation 4.0*. (2021) Eds by N. Meyendorf, N. Ida, R. Singh, J. Vrana. Springer, Cham. DOI: <https://doi.org/10.1007/978-3-030-48200-8> 43-1
3. Vajpayee, A., Russell, D. (2019) Inspection of boiler water wall tubes using electromagnetic inspection technique. Yesterday (manual) and Today (automated). *Industrial Eye*, 5(6), 39–43.
4. Bridge, B., Sattar, T., Chen, S., Khalid, A. (1997) On the design of multi-task, compact, climbing robotic NDT systems for remote operation on large surfaces and in hazardous environments. *Nondestructive Testing and Evaluation*, 13(2), 85–111. DOI: <https://doi.org/10.1080/02780899708953021>
5. Bertovic, M. (2016) A Human Factors Perspective on the Use of Automated Aids in the Evaluation of NDT Data. In: *Proc. of 42<sup>nd</sup> Annual Conf. on Review of Progress in Quantitative Nondestructive Evaluation*, 1706, 020003, 1–16. DOI: <https://doi.org/10.1063/1.4940449>
6. Bertovic, M. (2015) *Human factors in non-destructive testing (NDT): Risks and challenges of mechanised NDT*, Dr. Dissertation, Technical University, Berlin.
7. Ornatsky, P.P. (1983) Theoretical fundamentals of information-measurement technique. Kyiv, Vyshcha Shkola [in Russian].
8. Babak, V.P., Babak, S.V., Ieremenko, V.S. et al. (2017) *Theoretical fundamentals of information-measurement systems*. Ed. by V.P. Babak, 2<sup>nd</sup> Ed. Kyiv, NAU [in Ukrainian].
9. Zashchepkina, N.M., Shulga, O.V., Nakonechnyi, O.A. (2021) *Metrological support of information-measurement systems*. Kyiv, KPI [in Ukrainian].
10. Parasuraman, R., Sheridan, T.B., Wickens, C.D. (2000) A model for types and levels of human interaction with automation. *IEEE Transact. on Systems, Man, and Cybernetics. Pt A: Systems and Humans*, 30(3), 286–297. DOI: <https://doi.org/10.1109/3468.844354>
11. Le Liu (2018) The process to design an automation system. *J. of Physics: Conference Series*, 1087(4). DOI: <https://doi.org/10.1088/1742-6596/1087/4/042001>
12. Calhoun, G. (2022) Adaptable (not adaptive) automation: Forefront of human-automation teaming. *Human Factors*, 64(2), 269–277. DOI: <https://doi.org/10.1177/00187208211037457>
13. Bobukh, A.O. (2006) *Automated systems of control of technological processes*. Kharkiv, KhNAMG [in Ukrainian].
14. Gurvich, A.K., Shcherbinsky, V.G. (2006) Automated NDT of metal products. *V Mire Nerazrushayushchego Kontrol'ya*, 33(3), 4–5 [in Russian].
15. Dolinenko, V., Shapovalov, E., Skuba, T. et al. (2017) Robotic system of non-destructive eddy-current testing of complex geometry products. *The Paton Welding J.*, 5–6, 51–57. DOI: <https://doi.org/10.15407/as2017.06.10>
16. Koshovyy, V.V., Nazarchuk, Z.T. (2001) Estimating the predefective state of a material using methods of ultrasonic computerized tomography. *Mater. Sci.*, 37(2), 279–293. DOI: <https://doi.org/10.1023/A:1013219011254>
17. Vertiy, O., Uchanin, V. (2021) Three-dimensional visualization of the detected defects by eddy current computing tomography. *The Paton Welding J.*, 9, 49–55. DOI: <http://doi.org/10.37434/tpwj2021.09.08>
18. Tamburrino, A., Rubinacci, G. (2006) Fast methods for quantitative eddy-current tomography of conductive materials. *IEEE Transact. on Magnetism*, 42(8), 2017–2028. DOI: <http://doi.org/10.1109/TMAG.2006.877542>
19. Thomas, H.M., Heckel, T., Hanspach, G. (2006) Advantage of a combined ultrasonic and eddy current examination for railway inspection trains. In: *Proc. of 9<sup>th</sup> Europ. Conf. on Non-destructive Testing*, Berlin, www.ndt.com.
20. Rockstroh, B., Kappes, W., Walte, F. (2008) Ultrasonic and Eddy-Current Inspection of Rail Wheels and Wheel Set Axles. In: *Proc. of 17<sup>th</sup> World Conf. on Nondestructive Testing*, Shanghai, www.ndt.com.
21. Libby, H.L. (1971) *Introduction to electromagnetic nondestructive test methods*. Wiley-Interscience New York.
22. Teterko, A.Ya., Nazarchuk, Z.T. (2004) *Selective eddy current flaw detection*. Lviv, PMI [in Ukrainian].
23. García-Martín, J., Gómez-Gil, J., Vázquez-Sánchez, E. (2011) Non-destructive techniques based on eddy current testing. *Sensors*, 11, 2525–2565. DOI: <https://doi.org/10.3390/s110302525>
24. Uchanin, V.M. (2023) Surface eddy current probes of double-differential type as an effective tool to solve non-destructive inspection problems. *The Paton Welding J.*, 2, 46–55. DOI: <https://doi.org/10.37434/tpwj2023.02.07>
25. Uchanin, V., Lutcenko, G., Nikonenko, A. (2006) Automated Eddy Current System for Flaw Detection and Sizing during In-service Stainless Steel Tube Inspection. In: *Proc. of 9<sup>th</sup> Europ. Conf. on Nondestructive Testing*, Berlin, www.ndt.net.
26. Uchanin, V., Lutcenko, G. et al. (2010) The system of automated complex testing of rail axles in their manufacture. In: *Proc. of 10<sup>th</sup> Europ. Conf. on Nondestructive Testing*, Moscow, www.ndt.net.
27. Lutcenko, G., Uchanin, V., Mischenko, V., Opanasenko A. (2012) Eddy Currents Versus Magnetic Particles. In: *Proc. of 18<sup>th</sup> World Conf. on Nondestructive Testing*, Durban, www.ndt.com.
28. Raj, M., Mallik, D., Bansal, S. et al. (2012) Non-Destructive Testing and Inspection of Rails at JSPL – Ensuring Safety and Reliability. In: *Proc. of 18<sup>th</sup> World Conf. on Nondestructive Testing*, Durban, www.ndt.net.
29. Song, Z., Yamada, T., Shitara, H., Takemura, Y. (2011) Detection of damage and crack in railhead by using eddy current testing. *J. of Electromagnetic Analysis and Applications*, 12(3), 546–550. DOI: <https://doi.org/10.4236/jemaa.2011.312082>
30. Opanasenko, A., Iurchenko, A., Lutcenko, G., Uchanin, V. (2016) Eddy current multi-channel module for in-line high-speed inspection of railroad rails. In: *Proc. of 19<sup>th</sup> World Conf. on Nondestructive Testing*, Munich, www.ndt.net.

## ORCID

V.N. Uchanin: 0000-0001-9664-2101

## CONFLICT OF INTEREST

The Authors declare no conflict of interest

## CORRESPONDING AUTHOR

V.N. Uchanin

Karpenko Physico-Mechanical Institute of the NASU  
5 Naukova Str., 79060, Lviv, Ukraine.

E-mail: vuchanin@gmail.com

## SUGGESTED CITATION

V.N. Uchanin, G.G. Lutcenko, A.V. Opanasenko (2023) Automated eddy current inspection systems with surface probe of double-differential type. *The Paton Welding J.*, 5, 48–56.

## JOURNAL HOME PAGE

<https://patonpublishinghouse.com/eng/journals/tpwj>

Received: 04.02.2023

Accepted: 29.06.2023